NEURAL CORRELATES OF SENSATION AND NAVIGATION IN THE RETROSPLENIAL CORTEX

DUN MAO
B.E. Biomedical Engineering
Zhejiang University, 2010

A Dissertation
Submitted to the School of Graduate Studies
of the University of Lethbridge
in Partial Fulfillment of the
Requirements for the Degree of

DOCTOR OF PHILOSOPHY

Canadian Centre for Behavioural Neuroscience
Department of Neuroscience
University of Lethbridge
LETHBRIDGE, ALBERTA, CANADA

NEURAL CORRELATES OF SENSATION AND NAVIGATION IN THE RETROSPLENIAL CORTEX

DUN MAO

Date of Defence: December 16, 2016

Bruce L. McNaughton Supervisor	Professor	Ph.D.
Masami Tatsuno Thesis Examination Committee Member	Associate Professor	Ph.D.
Artur Luczak Thesis Examination Committee Member	Associate Professor	Ph.D.
Majid Mohajerani Internal External Examiner	Assistant Professor	Ph.D.
James J. Knierim External Examiner Johns Hopkins University Baltimore, MD, USA	Professor	Ph.D.
David Euston Chair, Thesis Examination Committee	Associate Professor	Ph.D.

ABSTRACT

By virtue of its anatomical connections, the retrosplenial cortex (RSC) is well suited to mediate bidirectional communication between the hippocampal formation and the neocortex. However, what information is encoded in the firing of RSC neurons is largely unclear. I used 2-photon calcium imaging to measure RSC population activity during a goal-directed virtual spatial task that was sometimes complemented by drifting gratings visual stimuli. Over 10% of RSC neurons, mainly in superficial layers, showed place fields with properties similar to CA1 place cells measured in the same task. A distinct subset of neurons (~15%), predominantly in agranular RSC, showed pronounced responses to the visual stimuli. Some of these RSC visual neurons were specifically selective for the speed and direction of visual motion. The results suggest that RSC contains multiple functional cell types distributed differentially across depths and subregions showing responses to external sensory stimulation and internal navigational signals.

PREFACE

This thesis project has been a collaboration between the laboratories of Drs. Bruce McNaughton, Vincent Bonin, and Majid Mohajerani. The data presented in Chapters 3, 4, and 5 were collected in the laboratory of Dr. Vincent Bonin from February 2012 to June 2015 at the Neuro-Electronics Research Flanders in Leuven, Belgium. The data presented in Chapter 6 were collected at the University of Lethbridge.

Experiments in Chapter 3 were performed in close collaboration with Dr. Steffen Kandler who did the imaging part. Results in Chapter 3 have been presented in the format of conference abstracts and proceedings (Mao, Kandler et al. 2014 Areadne; Mao, Kandler et al. 2014 FENS; Kandler, Mao et al. 2014 SfN; Kandler, Mao et al. 2015 SfN). A manuscript representing Chapter 3 is under preparation on which I am a co-first author. A manuscript representing Chapter 4 is under preparation and to be submitted. A manuscript representing Chapter 5 is currently in revision. I am the sole first author on the latter two manuscripts.

ACKNOWLEDGEMENTS

I am indebted to many people who have made my PhD journey a rewarding and unforgettable experience.

First and foremost, I would like to thank my advisors, Drs. Bruce McNaughton and Vincent Bonin. I am fortunate enough to have such a unique and complementary combination of advisor team. Bruce has provided me with great training opportunities and has allowed me much freedom in pursuing my own research interests. His confidence in me, his vision of the field, and his invaluable advice have trained me to become an independent scientist. Vincent has provided me with great daily supervision. His scientific rigor, his great analytical and scientific insights, and his patient guidance have equipped me with multifaceted skills and scholarships.

Secondly, I would like to thank Dr. Majid Mohajerani for his insightful advice and helpful discussions as well as for providing research resources. I would also like to thank my supervisory committee members Drs. Artur Luczak and Masami Tatsuno for their time and encouragement throughout my PhD journey.

I have collaborated closely with Dr. Steffen Kandler on the first chapter of the results section (Chapter 3). Steffen has been a great teammate and friend and our collaboration has been fruitful. I am grateful to Dr. Jianjun Sun for his excellent surgical assistance. His unique skills and patience have made the final steps of the thesis project much smoother. Adam Neumann has been a close friend and he has provided great assistance and helped expedite the final

progress. Thanks to Dr. Fabian Kloosterman, Dr. Zaneta Navratilova, Dr. Samsoon Inayat, Xu Han, and Javad Karimi for helpful comments and discussions on the manuscripts. I also want to thank Amanda Mauthe-Kaddoura, Ilse Eyckmans, Frederique Ooms, Jake Jordan, Jessica Mitchell, Molly Kirk, Valerie Lapointe, Aubrey Demchuk, Jennifer Tarnowsky, Di Shao, Dr. Maurice Needham, and Leo Molina for their technical and administrative help.

I am indebted to my parents and my sister for their unconditional and continuous support and encouragement.

Lastly, the Alberta Innovates Health Solutions has provided generous financial support throughout my PhD study.

TABLE OF CONTENTS

LIST OF FIGURES

LIST OF ABBREVIATIONS

RSC – Retrosplenial cortex

Sup. agr. – Superficial agranular retrosplenial cortex

Sup. gr. – Superficial granular retrosplenial cortex

Rga – Retrosplenial granular a cortex

Rgb – Retrosplenial granular b cortex

CA1 – Cornu Ammonis area 1

AChE – Acetylcholinesterase

PCC – Posterior cingulate cortex

PER – Perirhinal cortex

POR – Postrhinal cortex

LEC – Lateral entorhinal cortex

MEC – Medial entorhinal cortex

PPC – Posterior parietal cortex

HF – Hippocampal formation

PHR – Parahippocampal region

V1 – Primary visual cortex

LGN – Lateral geniculate nucleus

PM – Posteromedial visual area

AL – Anterolateral visual area

LFPs – Local field potentials

DI – Discrimination index

MI – Mutual information

SI – Spatial information

SF – Spatial frequency

TF – Temporal frequency

OSI – Orientation selectivity index

DSI – Direction selectivity index

1. General Introduction

In rodents, the retrosplenial cortex (RSC) is an extended cortical region that sits along the midline of the posterior brain. RSC is involved in a number of cognitive functions, including learning, memory, and spatial navigation in both rodents and primates (Vann et al 2009). In this general introduction chapter, I first go over the anatomy of rodent RSC and its connections with other brain regions, including the hippocampal formation, the neocortex, and the thalamus. I then introduce what is known about the functions of RSC followed by its functional cell types. I also provide an overview of important theories of hippocampal-neocortical interactions. In the last section, this chapter covers the motivation and aims of the thesis.

1.1. Anatomy and Connections of the Retrosplenial Cortex

Localization and Subregions of the Retrosplenial Cortex

In earlier literature, rodent RSC is sometimes referred to as the posterior cingulate region (van Groen & Wyss 1990, Vogt & Peters 1981). RSC is one of the largest neocortical areas and extends approximately half of the length of the entire cortical mantle along the anterior-posterior axis (Figure 1.1). In general, it consists of two subregions, granular (Brodmann area 29) and agranular (Brodmann area 30, or dysgranular) parts (Figure 1.1). The division of granular and agranular parts is based on the transitional lamination of 4- or 5-layered granular region and 6-layered agranular region. The border between granular and agranular regions can be identified by Nissl or acetylcholinesterase (AChE) staining (van Groen & Wyss 1992). The granular RSC can be further divided into

two subregions, retrosplenial granular a cortex (Rga) and retrosplenial granular b cortex (Rgb). Some researchers divide RSC into four subregions, Brodmann areas 29a, b, c, and d (Vogt & Peters 1981). Rga corresponds to 29a and 29b. Rgb corresponds to 29c (van Groen & Wyss 1992). Agranular part corresponds to 29d. Agranular part has wider layers II-IV while granular layer II neurons are more densely packed (Jones et al 2005, van Groen & Wyss 1992, Vogt & Peters 1981). I will use the nomenclature of Rga, Rgb, and agranular RSC adapted from (van Groen & Wyss 1992).

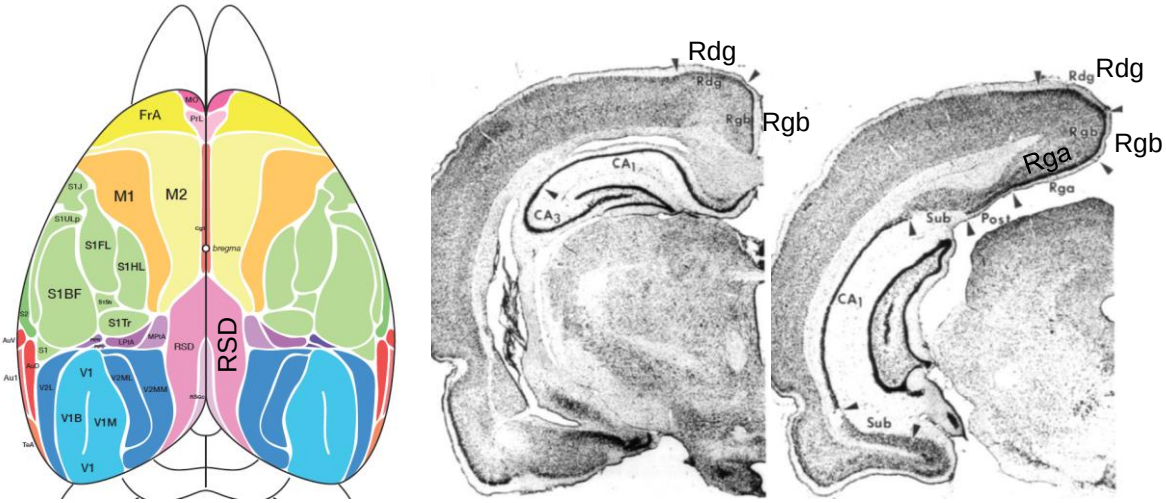

Figure 1.1 Location and subdivisions of RSC
Left, overhead view of regions of mouse neocortex. RSC is located in posteromedial part of the neocortex as colored in pink (denoted as RSD – dysgranular RSC and RSG – granular RSC). Middle and right, coronal view of RSC. Rdg, dysgranular RSC; Rgb – Retrosplenial granular b cortex; Rga – Retrosplenial granular a cortex; CA1, *Cornu Ammonis* area 1; CA3, *Cornu Ammonis* area 3; Sub, subiculum; Post, postsubiculum. Adapted from (Kirkcaldie 2012) and (van Groen & Wyss 1992).

The visual cortex is laterally adjacent to the agranular RSC. The border is characterized by the density of granule cells in layer IV that agranular RSC has few but the visual cortex has many granule cells (van Groen & Wyss 1992). It is also worth noting that the distribution of acetylcholine is throughout layer I-IV of

agranular RSC but only in layer I of PM, as revealed by AChE staining (van Groen & Wyss 1992). This may explain the movement-related activity in RSC that will be discussed later. Rgb differentiates from Rga in that it has a wider layer II which contains smaller cell bodies (van Groen & Wyss 1990). Rgb also differs from Rga in that it has a wider layer IV as densely stained by AChE. Rga is ventrally adjacent to the subiculum and the presubiculum. Layer IV of Rga contains granule cells which are not evident in the subiculum. With AChE staining, layer I of Rga exhibits patches of AChE while the layer I of the subiculum and presubiculum is more uniformly stained. Moreover, deep layers of the subicular structure are stained by AChE more extensively than that of the granular RSC (van Groen & Wyss 1990).

Retrograde and anterograde tracing studies further identified distinct interconnections within RSC subregions and connections between RSC subregions and other brain regions. RSC subregions are densely connected and the connections are also topographically organized (Shibata et al 2009, Shibata & Naito 2008). Each subregion has distinct set of intrinsic connections (Shibata et al 2009). Compared to ipsilateral connections, contralateral RSC connections are sparser (Shibata et al 2009, van Groen & Wyss 1992).

The columnar structure is a prominent feature of the functional organization across many neocortical areas (Mountcastle 1997). It is hypothesized that the columnar organization underlies the fundamental computing unit in sensory cortices (Buxhoeveden & Casanova 2002, Hubel & Wiesel 1962, Mountcastle 1997). Each column consists of many minicolumn

structures, which contain tens to hundreds of neurons each. Neurons within the same minicolumn have many more interconnections than neurons in different minicolumns. Like some other areas of the cortex, the granular RSC also shows a minicolumnar structure (Michael et al 1990). The apical dendrites of layer II pyramidal cells form bundles in layer I that are 30-100 um from adjacent bundles (Ichinohe & Rockland 2002, Michael et al 1990). Interestingly, these columnar dendritic bundles and thalamic projections in layer I of granular RSC are spatially matched (Ichinohe 2012, Michael et al 1990).

RSC Connections with other Brain Regions

RSC has strong connections with multiple cortical and subcortical regions, including sensory and motor cortices, the hippocampal/parahippocampal formation, and the thalamus. These anatomical connections suggest RSC may be involved in sensory-motor integration, spatial navigation and memory. Notably, RSC connects the hippocampal formation (HF) and the neocortex (Figure 1.2), potentially conveying hippocampal information to neocortical areas, and vice versa.

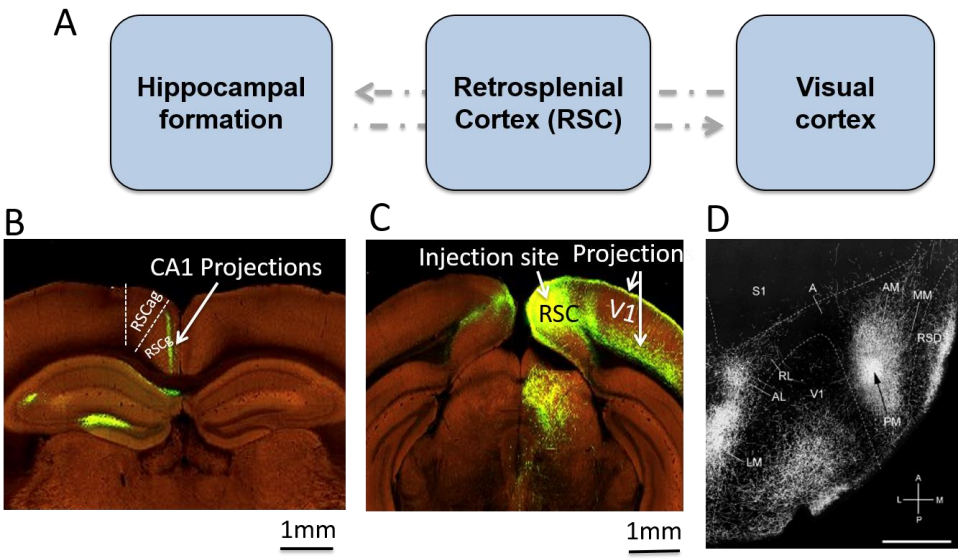

Figure 1.2 RSC connects the hippocampal formation and the visual cortex
(A) Schematic diagram showing RSC connections with the hippocampal formation and the visual cortex. (B) CA1 projections in layer II of the granular RSC. RSCag, agranular RSC; RSCg, granular RSC. (C) RSC projections in layer I and layer VI of the visual cortex. (D) Projections from the higher visual area PM to agranular RSC (RSD). Adapted from Allen Brain Atlas: Mouse connectivity and (Wang et al 2012).

RSC Connections with the Visual and Motor Cortices

A major stream of afferents to RSC originates in the visual cortex, mostly the postero-medial (PM) higher visual area (Figure 1.2) (Vogt & Miller 1983, Wang et al 2012). Compared to extensive monosynaptic axons from the visual cortex to layer I of agranular RSC, granular RSC receives little direct visual outputs (van Groen & Wyss 1992, Van Groen & Wyss 2003). Furthermore, visual information could reach RSC via indirect pathways. One such route involves the claustrum, which projects to RSC and receives direct visual afferents (Vogt & Miller 1983). The RSC to visual projections mainly originate in layer V of the caudal agranular RSC neurons and superficial Rgb neurons, which project to layer I and deep layers of PM (van Groen & Wyss 1992, Van Groen & Wyss 2003, Vogt & Miller 1983) (Allen Mouse Brain Atlas). The RSC-visual connections may subserve a

role of RSC in feature extraction from sensory stimuli. It may also underlie a pathway by which sensory information could reach the hippocampal network. RSC is also highly connected with the secondary motor cortex (M2) (Yamawaki et al 2016). The direct connections with both the motor and visual cortices suggest a role of RSC in sensorimotor integration.

RSC-Hippocampal Connections

RSC has dense connections with the hippocampal formation which is involved in spatial navigation and memory (Figure 1.2). RSC is one of the only neocortical regions (others include the entorhinal cortex, the perirhinal cortex, etc) that directly connect the subiculum and CA1 with the neocortex (Cenquizca & Swanson 2007). Layers II and III of the granular RSC receive direct inputs from dorsal hippocampal CA1 and subiculum (Cenquizca & Swanson 2007, Miyashita & Rockland 2007, van Groen & Wyss 1990, Van Groen & Wyss 2003, Vogt & Miller 1983) (Figure 1.2). Interestingly, the HF-RSC projections are different along the proximal-distal and septal-temporal axes. The proximal-septal subiculum targets the rostral part of the granular RSC while the distal subiculum targets the caudal part (Miyashita & Rockland 2007, Naber & Witter 1998, Van Groen & Wyss 2003, Vogt & Miller 1983). CA1-RSC projections also include those from CA1 GABAergic neurons that are mostly located between the stratum radiatum and stratum lacunosum-moleculare (Jinno 2009, Miyashita & Rockland 2007). Compared with the granular RSC, the agranular RSC receives only subicular axons that end in layers I and II (Finch et al 1984, Vogt & Miller 1983, Witter et al

1990). RSC-subiculum projections are also topographically organized and layer-specific (Shibata 1994, van Groen & Wyss 1990, Van Groen & Wyss 2003). Specifically, the rostral RSC innervates the stratum pyramidale of the mid-level septal-temporal subiculum while the caudal RSC mainly innervates the temporal subiculum.

RSC-Parahippocampal Connections

RSC also has reciprocal connections with the parahippocampal region (PHR) which is involved in spatial navigation. The granular RSC has extensive projections to PHR (Shibata 1994, van Groen & Wyss 1990). These projections are topographically organized such that the rostral-caudal RSC maps onto the septal-temporal presubiculum (Jones & Witter 2007, Shibata 1994, van Groen & Wyss 1990, Vogt & Miller 1983). Granular RSC also targets the parasubiculum, the perirhinal cortex (PER), the postrhinal cortex (POR), the lateral entorhinal cortex (LEC), and the medial entorhinal cortex (MEC) (Czajkowski et al 2013, Jones & Witter 2007, Kononenko & Witter 2012, Shibata 1994). These projections are confined to certain layers. For example, retrosplenial efferents target principal neurons in layer V of MEC, which also receive hippocampal output and project to superficial neurons within MEC (Czajkowski et al 2013, Jones & Witter 2007). Similarly, agranular RSC also projects to the entire PHR. One topographical and layer-specific projection worth noting is that the caudal agranular RSC projects only to the deep layers of the entorhinal cortex and more rostral part to the superficial layers of the entorhinal cortex (Burwell & Amaral

1998, Jones & Witter 2007, Shibata 1994, van Groen & Wyss 1992). There are developmental processes of the RSC-PHR projections in that the RSC projections are seen in PHR from postnatal day 1 but reach adult-like density only in postnatal day 12 (Sugar & Witter 2016). Back projections from PHR to RSC are strong and topographically organized (Agster & Burwell 2009, van Groen & Wyss 1990, Vogt & Miller 1983). See Sugar et al. 2011 for a review (Sugar et al 2011).

RSC Connections with the Thalamus

Thalamic innervations to the agranular RSC mainly originate in the anterior, laterodorsal, and reuniens nuclei (Shibata 1993, van Groen & Wyss 1992). Rga mainly receives axons from anterodorsal and laterodorsal thalamic nuclei (van Groen & Wyss 1990). Rgb is mostly innervated by anterior thalamic nuclei (Van Groen & Wyss 2003). The thalamic-RSC projections are layer-specific. Although Rga is several synapses away from the visual cortex, it could receive direct visual information from the anterior thalamic nuclei, which is shown to be innervated by retinal ganglion cells (Itaya et al 1981). The granular RSC also receives efferents from the claustrum and the locus coeruleus (van Groen & Wyss 1990, Van Groen & Wyss 2003).

1.2. Spatial Representations in the Hippocampus and Beyond

Spatial Representations in the Hippocampal and Parahippocampal Regions

Place cells in the hippocampus and grid cells in the medial entorhinal cortex are two of the most prominent functional cell types in the hippocampal formation (HF)

and the parahippocampal region (PHR). Place cells fire at one or a few specific locations when animals move in an environment (O'Keefe & Dostrovsky 1971). Grid cells fire at multiple specific locations that are organized in a hexagonal grid pattern (Hafting et al 2005). The formation of firing fields is governed by path integration that arises from self-motion signals (McNaughton et al 1996, McNaughton et al 2006, Samsonovich & McNaughton 1997). Sensory inputs and contextual information can exert modulatory influence on the firing rates within the firing fields. The spacing between adjacent grids and the size of grid fields increase progressively along the entire dorsoventral axis of MEC (Hafting et al 2005, Stensola et al 2012). Hippocampal place fields also scale along the dorsoventral axis. Besides grid cells, MEC also contains head-direction cells, border cells, speed cells, and conjunctive spatial and behavioral signals (Kropff et al 2015, Sargolini et al 2006, Solstad et al 2008). The firings of MEC grid cells require both inputs from the hippocampal place cells and thalamic head-direction network (Bonnevie et al 2013, Winter et al 2015). Grid cells and head-direction cells also exist in the pre- and parahippocampal regions (Ranck Jr 1984, Taube et al 1990a, Taube et al 1990b). As the major output region of the hippocampal formation, some subicular neurons also exhibit localized firing patterns but the firing fields are more expanded (Sharp & Green 1994). Subiculum also contains boundary vector cells which encode distance and head-direction relative to the environmental boundaries (Lever et al 2009).

Position Representation Beyond the Hippocampal System

Neural correlates of positional information have been long sought in the brain regions that are immediately connected with HF and PHR. Most notably, the claustrum exhibits positional signals that are somewhat comparable to hippocampal place cells, although the mechanisms underlying the formation of the firing fields between the two are likely different (Jankowski & O'Mara 2015). Positional signals have also been identified in POR. These positional signals are different from hippocampal place cells in that they reflect visual objects at different locations in the environment or object-location conjunctions (Burwell & Hafeman 2003, Furtak et al 2012).

1.3. Functions of the Retrosplenial Cortex

RSC in Spatial Learning and Memory

Earlier studies have mainly used lesion and then assessed its effect on behavior or certain tasks to probe the functions of RSC. Given its extensive connections with HF, many researchers have focused on the role of RSC in spatial learning and memory. One of the first lesion studies examines the role of RSC in Morris-water maze - a spatial navigation and memory task (Sutherland et al 1988). They use a visible or a sub-merged platform to test how the animals use visual cues and allocentric representation to navigate to a fixed location. Rats with bilateral RSC lesions show impairment in using allocentric information in the Morris-water maze task. Rats with lesioned RSC show similar impairment even with extensive pre-training. It is possible that RSC lesion disrupts the spatially-guided behavior by disconnecting the hippocampus and the neocortex. Rats with RSC lesions have difficulty in learning new platform locations, while rats with intact RSC learn

it in one trial. Some studies also show subicular damage abolishes learning-related discriminative responses in an active avoidance task (Gabriel & Sparenborg 1986), likely by disconnecting the hippocampal-neocortical connections.

Human fMRI studies have pinpointed the role of RSC in learning to encode the most permanent landmarks in a visual environment (Auger et al 2012, Auger et al 2015). PHR also codes for permanent landmarks, but with less selectivity than RSC (Auger & Maguire 2013).

RSC in Path Integration

Animals can rely purely on self-movement information to track their location in an environment. In a homing task (Mittelstaedt & Mittelstaedt 1980), animals integrate translational and rotational movement along the outward journey to estimate the distance and direction of the current position relative to the home location, which allows them to return home along a straight line. The process that integrates self-motion cues is called path integration. Path integration could rely on several cues: vestibular signals, proprioception, motor efference, and optic flow. Certain animals can use the earth's magnetic field to path integrate (Kimchi et al 2004). Previous studies have shown the involvement of RSC in path integration (Cooper et al 2001b, Whishaw et al 2001b). Some studies show that RSC is important for path integration only in darkness (Cooper et al 2001a, Elduayen & Save 2014). When visual cues are available, RSC-lesioned animals show path integration performance comparable to control animals (Elduayen &

Save 2014). It is likely that the lack of visual information in darkness impairs accurate path integration due to incapability of the path integration system to correct cumulative errors from self-motion. Why do RSC-lesioned animals show normal path integration performance in light conditions? It is possible that different circuits required path integration are recruited in light and dark conditions. In light conditions, a complementary circuit, involving the visual cortex - parietal/postrhinal cortex - entorhinal cortex - hippocampus, may fulfill the function.

The neural circuits that are sufficient for path integration have not been precisely identified. With few exceptions, hippocampal place cells and entorhinal grid cells reflect a phenomenon of path integration. Hippocampal place cells could generate ensemble sequences encoding running distance without using any external cues (Villette et al 2015). On the other hand, the persistent capability of path integration in hippocampus-lesioned animals suggests that the neural substrates required for path integration reside outside of the hippocampal proper (Alyan & McNaughton 1999). It is possible that RSC is one of them.

Thus, RSC is important for both allothetic and ideothetic types of spatial navigation. Some earlier studies failed to observe deficits in spatial navigation in animals with RSC lesions (Aggleton et al 1995, Neave et al 1994, Warburton et al 1998). However, such discrepancies likely result from the differences in animal strains, spatial task demands, and/or lesion size (Harker & Whishaw 2002, Harker & Whishaw 2004, Vann & Aggleton 2002a). The impairment in spatial memory with RSC lesion tends to be less significant than that with hippocampus

lesions, suggesting RSC damage does not abolish memory of external cues, but rather the ability to coordinate self-motion with mnemonic information of the environment.

RSC in Contextual Fear Memory

Aside from spatial memory, RSC is also important for the consolidation, storage, and

retrieval of other memories, such as contextual fear memory (Keene & Bucci 2008a). Animals with RSC damage prior to training have less of an effect on fear memory recall than RSC damage after training, indicating RSC is a preferred candidate for the storage and/or retrieval phase in an intact brain while other brain regions can compensate when RSC is damaged (Keene & Bucci 2008b). NMDA but not AMPA receptors are necessary during this process (Corcoran et al 2011). Inactivating RSC also somewhat impairs the retrieval of inhibitory avoidance memories (Bouton & Todd 2014). It is hypothesized that RSC contributes to memory processing by forming associations among multiple stimuli that are present in the environment (Robinson et al 2011). While the hippocampus is not necessary in this initial stimulus-stimulus association, it is likely that RSC feed-forwards this information to the hippocampus, where spatial representations are formed (Iordanova et al 2011, Wimmer & Shohamy 2012). Inactivating the hippocampus does not affect the recall of contextual fear memories in RSC, indicating a functionally dissociable role of RSC and hippocampus in contextual memory retrieval. It is likely that the hippocampus is

primarily for recent memories while RSC is more responsible for remote memories (Cowansage et al 2014).

RSC in Memory Deficits

Human studies have implicated RSC in various neurological disorders. For example, the

retrosplenial glucose metabolic deficit is among the earliest signs of cortical abnormality in patients with Alzheimer's disease (Minoshima et al 1997, Nestor et al 2003). RSC metabolic deficit is significantly greater than that in the hippocampal region. It is hypothesized that RSC metabolic deficit contributes to memory deficit by disconnecting hippocampal mnemonic indexing and cortical memory storage. Bilateral RSC pathology has also been linked to both retrograde amnesia and anterograde amnesia (Maguire 2001, Vann & Albasser 2009).

1.4. Spatial, Behavioral and Sensory Signals in the Retrosplenial Cortex

Very limited single-unit recordings and cellular imaging have been done in RSC despite its pivotal role in spatial navigation and memory. RSC has been shown to encode various spatial, behavioral and sensory correlates (Alexander & Nitz 2015, Chen et al 1994a, Chen et al 1994b, Cho & Sharp 2001, Murakami et al 2015, Smith et al 2012). About 10% of RSC neurons show head-direction tuning, that is, they fire predominantly when animal's head points to a certain direction (Chen et al 1994b). The vast majority of these head-direction cells do not need visual cues to maintain head-direction preference. Their preferred direction does not change with rotation of salient visual landmarks or their head-direction tuning

persists in darkness. Most of the RSC head-direction cells require ideothetic rotation to form directional firing. Interestingly, some RSC head-direction cells show position-dependent direction preference, that is, at distinct locations in the environment, they have distinct tuned directions (Cho & Sharp 2001). RSC and the anterior thalamic nuclei forms a head-direction network. Damaging RSC disrupts head-direction representation in the other (Clark et al 2010). This head-direction network is needed for the formation of grid cell activity in MEC (Winter et al 2015). Some RSC neurons also show highly correlated firings with linear or angular movement speed (Cho & Sharp 2001).

Regarding the spatial aspect of RSC neuronal activity, a more recent electrophysiology study has shown some RSC neurons exhibit spatially modulated firings that reflect a combination of reference frames including allocentric, route-centered, and egocentric frames (Alexander & Nitz 2015). A subset of those neurons is specifically selective for the locations of reward obtainment (Smith et al 2012, Vedder et al 2016). Imaging studies identify repetitive activation of a subset of RSC neurons during spatial learning in the Morris water task (Czajkowski et al 2014). Manipulating the transcription factor CREB (known important for memory consolidation) in RSC can enhance spatial memory. This provides one of the first evidence from cellular imaging in support of RSC's role in the formation and storage of spatial memory. Nonetheless, all these studies failed to observe hippocampal place cell-like firing patterns in RSC, which exhibit single, isolated place fields with little background activity.

Another study employing wide-field and 2-photon calcium imaging identifies visual responses in RSC (Murakami et al 2015). A minority of RSC neurons are visually responsive and some of them are selective for the orientation and direction of grating stimuli. This result adds evidence to the role of RSC in transferring visual information from the visual cortex to other connected regions.

1.5. Functional Relationships between the Hippocampus and the Retrosplenial Cortex

Pharmacological and behavioral studies have shown that long-term fear memory storage requires a functional interplay between the anterior RSC and dorsal hippocampus, in that impairing the function of one can be rescued by enhancing the other (Katche et al 2013a, Katche et al 2013b). Hippocampal lesions significantly reduce the expression of immediate-early gene c-fos and zif268 in RSC, without affecting the physical properties of RSC neurons (Albasser et al 2007). Human fMRI studies have also shown evidence of the link between RSC and the hippocampus in the formation and retrieval of spatial memories (Iaria et al 2007). RSC and POR are hypothesized to form the ‘where’ pathway which contains information about the spatial and/or temporal context of objects and/or events (Bucci & Robinson 2014, Ranganath & Ritchey 2012). Together with the ‘what’ pathway that is consisted of PER and LEC, they feedforward complementary information that is integrated in the hippocampal CA3 and dentate gyrus (Ranganath & Ritchey 2012).

Recent electrophysiological studies have identified complementary and distinct response properties of hippocampal and RSC neurons. On a plus maze with reward being switched between east and west arms in blocks, place fields of hippocampal neurons emerge rapidly and they globally remap in a learning-dependent manner (Smith et al 2012). Simultaneous recordings in RSC show spatially-modulated firings but they do not remap when the reward is shifted. However, a subset of RSC neurons codes for the most prominent cue in the environment, in this particular case, the reward cue. This is somewhat consistent with human fMRI studies that show RSC encodes the most permanent landmarks. Thus, it is likely that the hippocampus makes use of this information from RSC, identifying manipulations and stability of the environment. Indeed, inactivating RSC causes rearrangement of but does not abolish hippocampal place fields (Cooper & Mizumori 2001). On the other hand, information flow from the hippocampus to RSC is also very important, particularly considering that the cues in an environment are normally embedded in a spatial context. Consistent with this, disconnecting the hippocampus and RSC diminishes RSC neurons' responses to the salient cues in different environments (Smith et al 2004). Taken together, the hippocampal system and RSC work in concert to support cognitive functions.

1.6. Theories of Hippocampal-Neocortical Interactions

Perhaps one of the most influential models on hippocampal-neocortical interactions is the hippocampal indexing theory (Marr et al 1991, McClelland et al 1995, Teyler & DiScenna 1986, Teyler & Rudy 2007). During the encoding

phase, feedforwarding information from the neocortex to the hippocampus enables an indexing code in the hippocampus that is formed through recurrent connections in CA3. Partial neocortical information (of the same memory, can be spontaneous) reactivates the hippocampal indexing code which then back-projects to the neocortex to enable the retrieval of the entire memory (Marr et al 1991, Teyler & DiScenna 1986). Such reactivation of neuronal activity after behavioral tasks, presumably helpful for memory consolidation, has been observed in the hippocampus and the neocortex (Euston et al 2007, Ji & Wilson 2007, Wilson & McNaughton 1994). Reactivation of hippocampal place cell sequences happens in sharp-wave ripples during slow-wave sleep and even awake still states (Carr et al 2011, Karlsson & Frank 2009). Such replay of activity sequences also happens in the neocortex, which happens during cortical up-down state transitions. Whether neocortical memory reactivation depends on hippocampal reactivation is largely unknown. Some hint that these two are linked lies in the coordinated activity between hippocampal ripples and neocortical up-down transitions (Battaglia et al 2004a) and the coordinated replay between the hippocampus and the neocortex (Ji & Wilson 2007). It is also likely that hippocampal output is required only for initial reactivation in the neocortex, after which memory can be sustained through strengthened interconnections in a hippocampus-independent manner (Schwindel & McNaughton 2011).

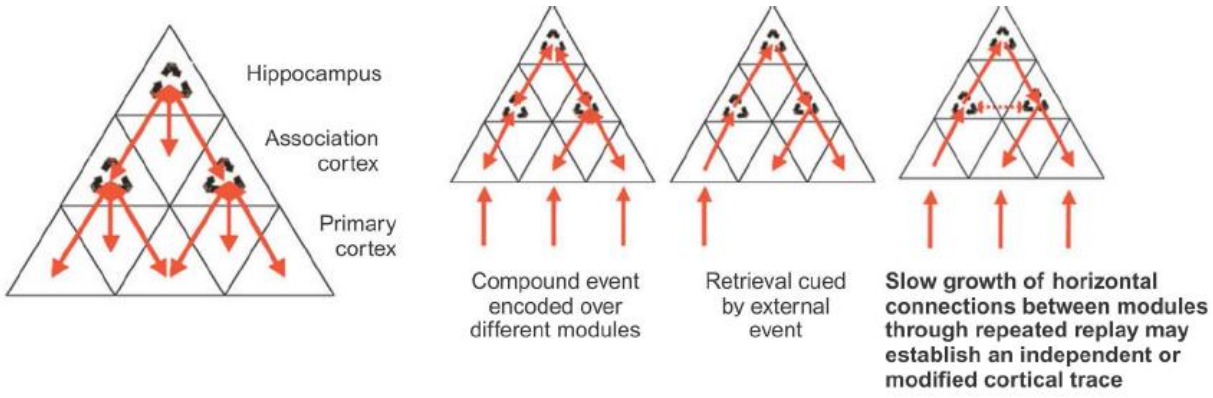

Figure 1.3 Generic model of hippocampal-neocortical interactions
Left, hippocampal outflow reaches primary cortex via association cortex. Right, during encoding phase, information from different neocortical modalities converges in the hippocampus, which also back-projects to the neocortex. During retrieval phase, partial external information reinstates the entire event through hippocampal back-projections to the neocortex. Repeated retrieval strengthens connections between neocortical modalities, enabling hippocampus-independent reinstatement.
Adapted from (Schwindel & McNaughton 2011).

The hippocampus indexing code provides a solution for how information across neocortical modalities can be linked together, which is required for an intact memory. This generic hippocampal-neocortical model is illustrated in Figure 1.3. The question is what information this indexing code contains. The first thought would be related to the spatial representation (place cells) in the hippocampus. The spatial representation provides a spatial context (allocentric representation) of an event/episode/experience, with which sensory perception across modalities can be associated. That is, for example, “what happens” and “what I see” at this particular location in this environment. Based on this theoretical ground and the direct hippocampus - RSC connections, I hypothesize RSC contains place cell-like spatial information.

1.7. Roadmap of the Thesis

With the motivation of questing spatial information in the neocortex, I started with the investigation of position encoding in the primary visual cortex (V1). I adapted a head-fixed virtual spatial task to enable well-controlled external stimulation and accurate monitoring of behavioral variables. Hippocampal CA1 neurons exhibited robust place cell activity. V1 neurons showed ‘position-related’ response modulations. However, this effect originated from cross-modal tactile inputs. I next studied position encoding and visual processing in RSC which connects the hippocampus and the visual cortex. I identified a subset of RSC neurons exhibiting CA1 place cell-like responses. Unlike hippocampal neurons, many RSC neurons did not show place fields but showed clear visual responses. Some RSC visual neurons specifically encoded the speed of visual motion. RSC place cells and visual neurons formed distinct neuronal populations. The results of this thesis advanced our understanding of V1 in multisensory processing and RSC in processing internal and external information.

2. General Methods

To study neuronal encoding of sensory and spatial information in a well-controlled way, I developed a head-fixed linear treadmill assay and combined it with silicon probe recording and 2-photon calcium imaging in awake mice moving on the treadmill. In this methods chapter, I introduce the experimental procedures, the treadmill setup, simultaneous silicon probe recordings in CA1 and V1, and imaging preparations in RSC (with and without a prism) and in CA1 (with a cannula window). I also include some example data and highlight the virtual spatial task.

2.1. Treadmill Apparatus, Electrophysiology and Imaging Methods

I adapted a treadmill apparatus in which mice were head-fixed and voluntarily moved a treadmill belt (Figure 2.1) (Royer et al 2012). The treadmill belt was covered with various tactile textures. Belt motion was monitored by a rotation encoder attached to the wheel that guided the belt movement. Mice were rewarded at a fixed position on the belt for every completed lap running. A visual stimulation screen was placed in front of the right eye and silicon probe recordings were performed in the left V1. Eye movement and pupil size were monitored.

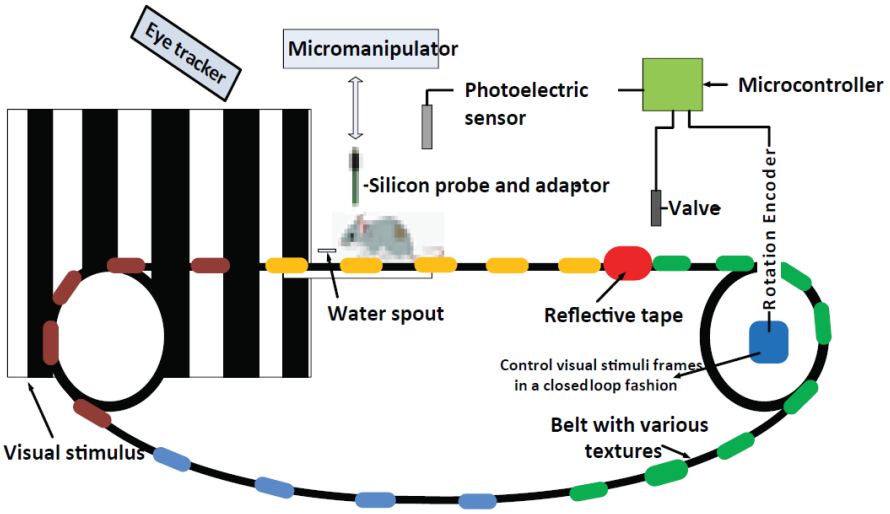

Figure 2.1 Diagram of the treadmill setup
The belt was covered with various tactile cues (indicated as colored stripes).

Figure 2.2 shows a snapshot of the front view and an example movement speed profile when the animal is well trained.

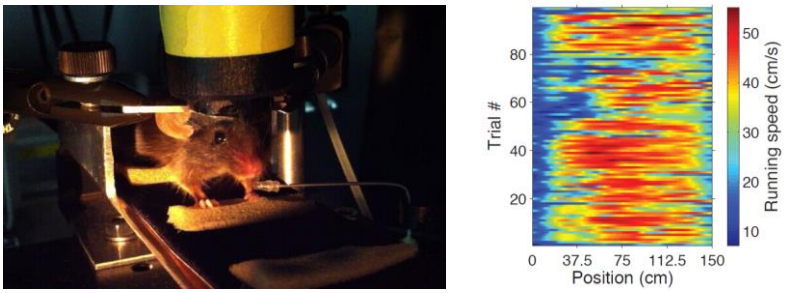

Figure 2.2 Front view of the treadmill apparatus with a mouse being head-fixed and typical behavior profile after training

I first used simultaneous silicon probe recordings in dorsal hippocampal CA1 and V1 (Figure 2.3) to study position encoding in V1 and CA1-V1 interactions.

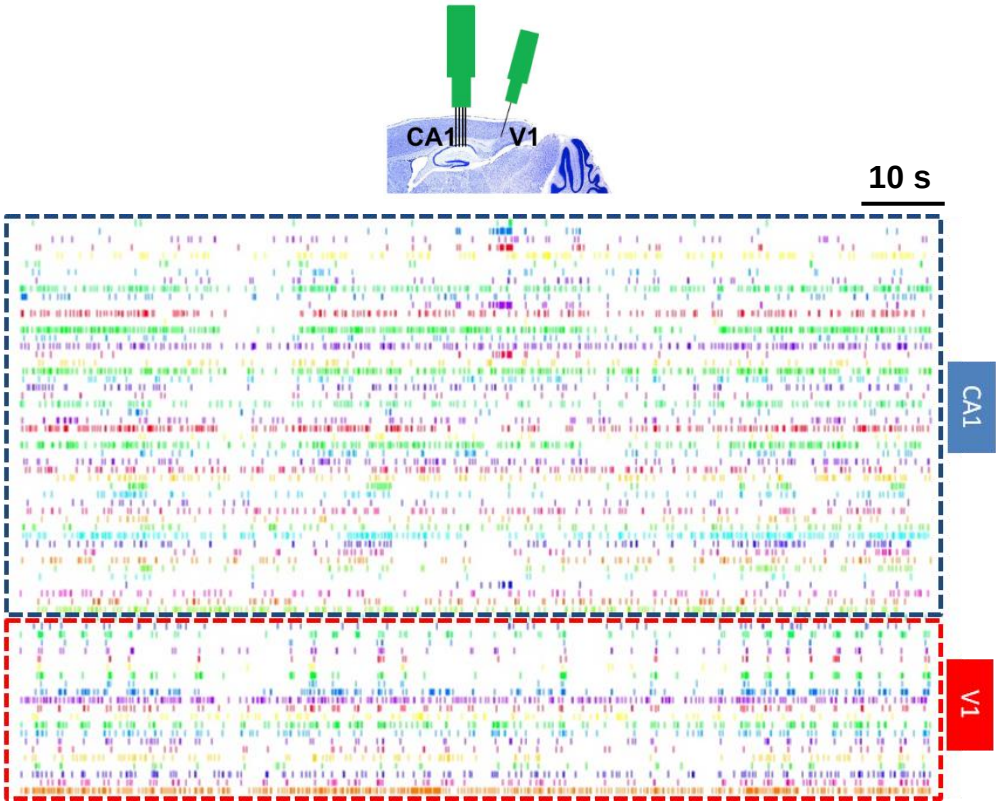

Figure 2.3 Simultaneous probe recordings in CA1 and V1
A four-shank silicon probe was used for CA1 recording and a single shank probe was used for V1 recording. Raster plot shows simultaneously recorded CA1 and V1 units. Each row represents a single unit and each tick represents a spike. The periodicity of V1 responses was due to periodic visual stimulation.

Behavioral variables were monitored, including movement speed, position on the track, and eye position (e.g. Figure 2.4).

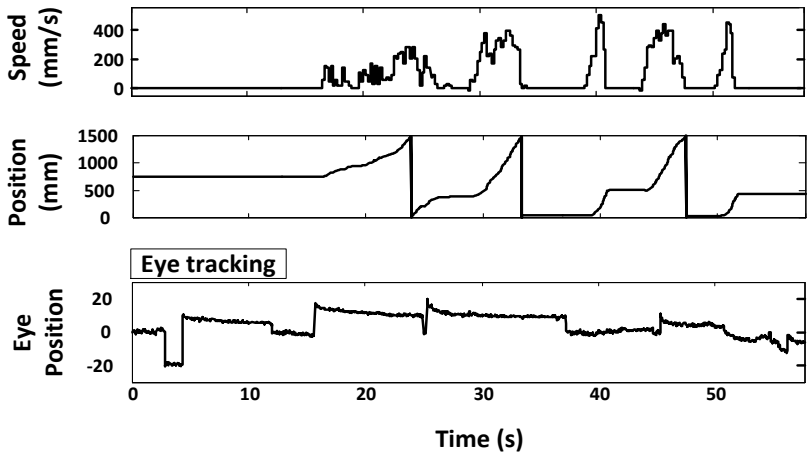

Figure 2.4 Monitoring of behavioral variables
Movement speed, position on the belt, and eye position (in degree) were simultaneously monitored.

The general experimental and surgery workflow for long-term cellular imaging in awake mice is outlined below (Figure 2.5):

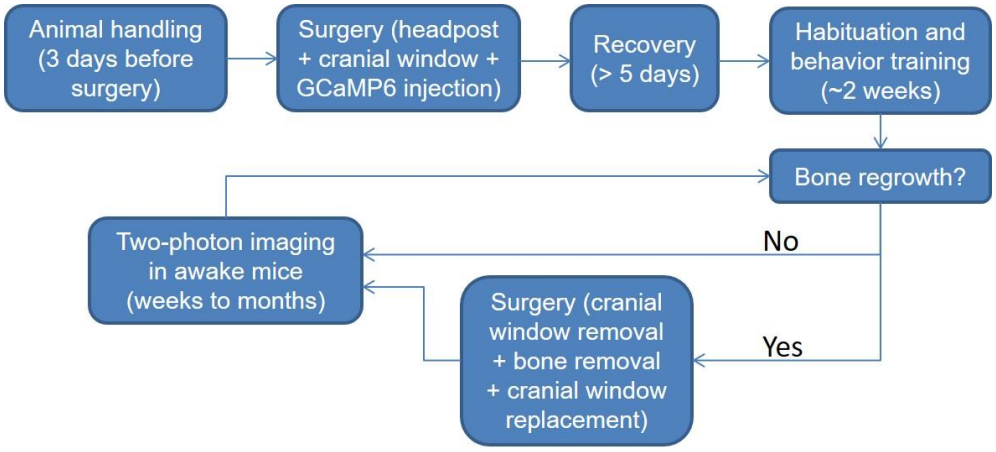

Figure 2.5 Workflow of experiment and surgery for chronic calcium imaging in awake mice

Habituation and behavior training are performed in a gradual manner. By the end of training, mice could be head-restrained for more than one hour on the treadmill. Bone regrowth underneath the cranial window is common. When it happens, regrown bone needs to be removed (Goldey et al 2014) because it can

obscure the imaging window. Two-photon imaging of the same population of hundreds to thousands of neurons could be performed for weeks to months.

For imaging in RSC, a cranial window composed of 3 coverslips was implanted above RSC, crossing the midline (Figure 2.6) (Goldey et al 2014).

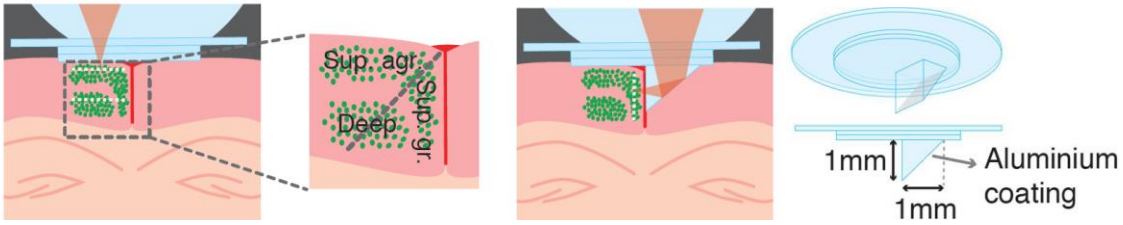

Figure 2.6 Diagrams of imaging in RSC

Sup. agr., superficial agranular RSC; Sup. gr., superficial granular RSC; Deep, deep layers of agranular and granular RSC. To image many neurons in the superficial granular RSC of the left hemisphere, a prism window was implanted in the right hemisphere (right 2 panels). The prism window was composed of a 3-layered coverslip and a right-angle prism. Green dots indicate neurons labeled with GCaMP6m. White dashed lines indicate imaging depths.

Representative imaging plane and time-courses of example RSC neurons are shown in Figure 2.7. The Galvo-Resonant X-Y scanners combined with piezoelectric Z scanning enables fast imaging of multiple depths, resulting in simultaneous monitoring of hundreds to thousands of neurons in superficial RSC.

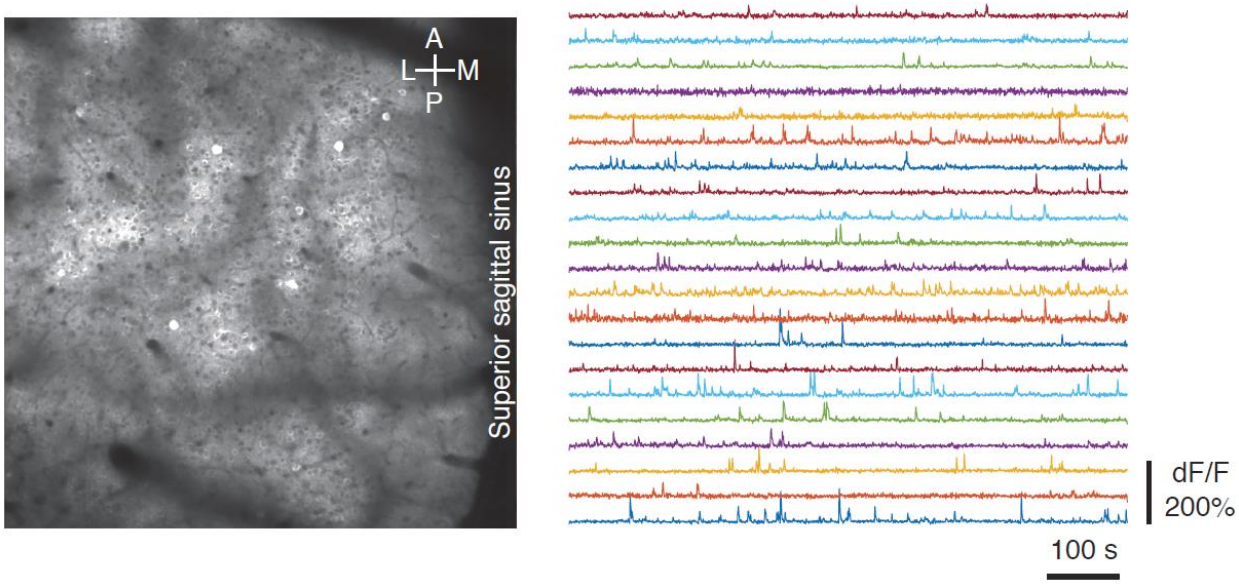

Figure 2.7 Example imaging plane and neuronal activity in RSC

2.2. Goal-directed Virtual Spatial Task

I also adapted a chronic imaging preparation in dorsal hippocampal CA1 (Figure 2.8) (Dombeck et al 2010).

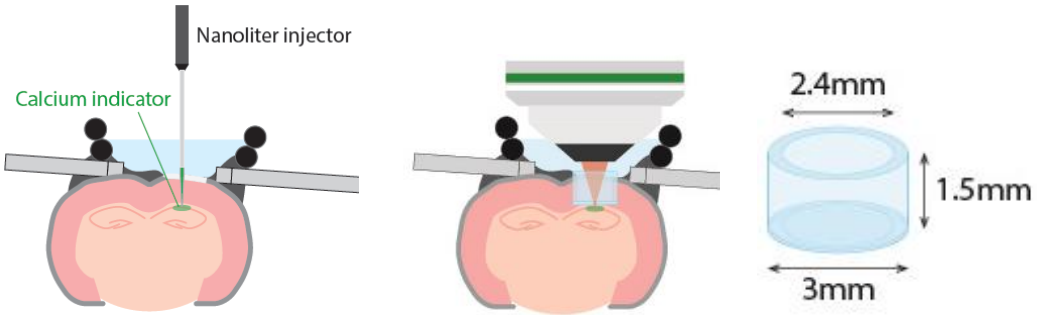

Figure 2.8 Chronic imaging preparation in dorsal hippocampal CA1
A ~1 mm thick cortex trunk was aspired to expose the white matter (medial-lateral travelling corpus callosum) above the dorsal hippocampus. A cannula window composed of a glass cylinder (1.5 mm long, 3 mm outer diameter, 2.4 mm inner diameter) and a coverslip (3 mm in diameter) was used as the cranial window. The head plate was sometimes tilted so that the vertical axis of the cannula window was parallel to the laser path.

The combination of the cannula window and transgenic GCaMP6 mouse lines (e.g. Thy1-GCaMP6, (Dana et al 2014)) enables simultaneous

monitoring of thousands of excitatory neurons in the pyramidal layer of dorsal CA1 (Figure 2.9).

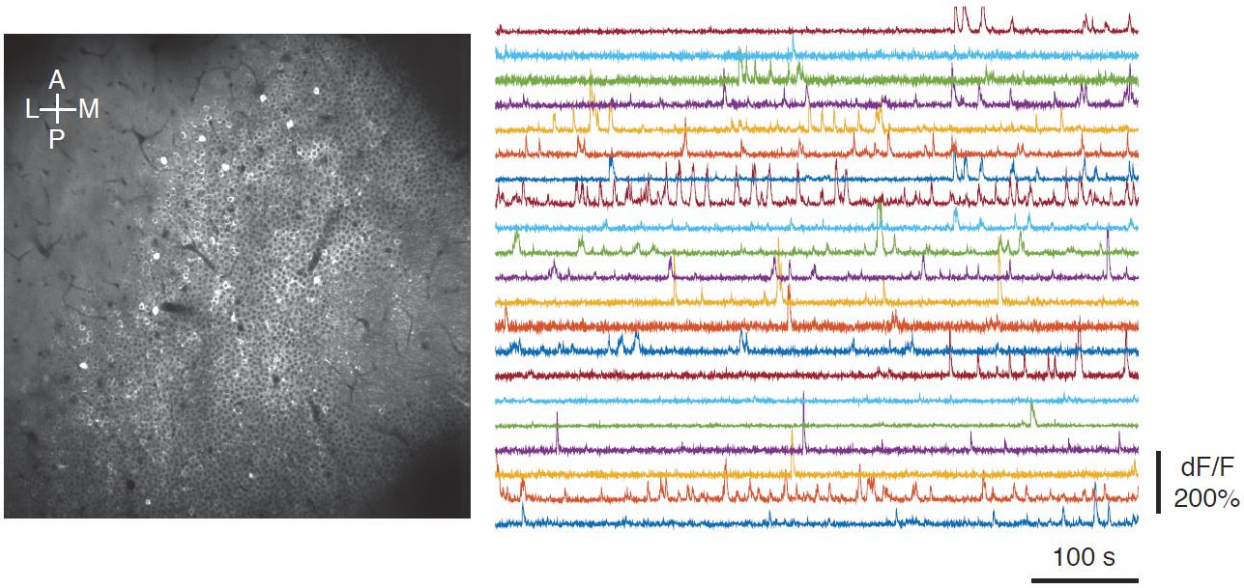

Figure 2.9 Example imaging plane and neuronal activity in dorsal CA1
The left panel shows an average imaging plane in CA1 pyramidal layer with each neuron shown as a donut. More than 2000 active neurons were identified. The right panel shows the fluorescence signals of some example CA1 neurons.

CA1 neurons in head-fixed mice exhibited place cell activity as seen in freely behaving rodents (Figure 2.10). Ensemble activity exhibited sequential activation during running on the treadmill (Figure 2.10). Tactile cues were not required for forming robust place fields (Figure 2.11), likely reflecting a dominant role of path integration in generating place cell activity which was reset by the reward site after each lap running. I refer to the treadmill lap running as a goal (reward)-directed virtual spatial task. In freely behaving rodents, switching environments can induce remapping of hippocampal place fields (i.e. distinct place cell representations in different environments). In the head-fixed treadmill

apparatus, global remapping in the hippocampal CA1 can be evoked by changing the treadmill belts (Figure 2.12).

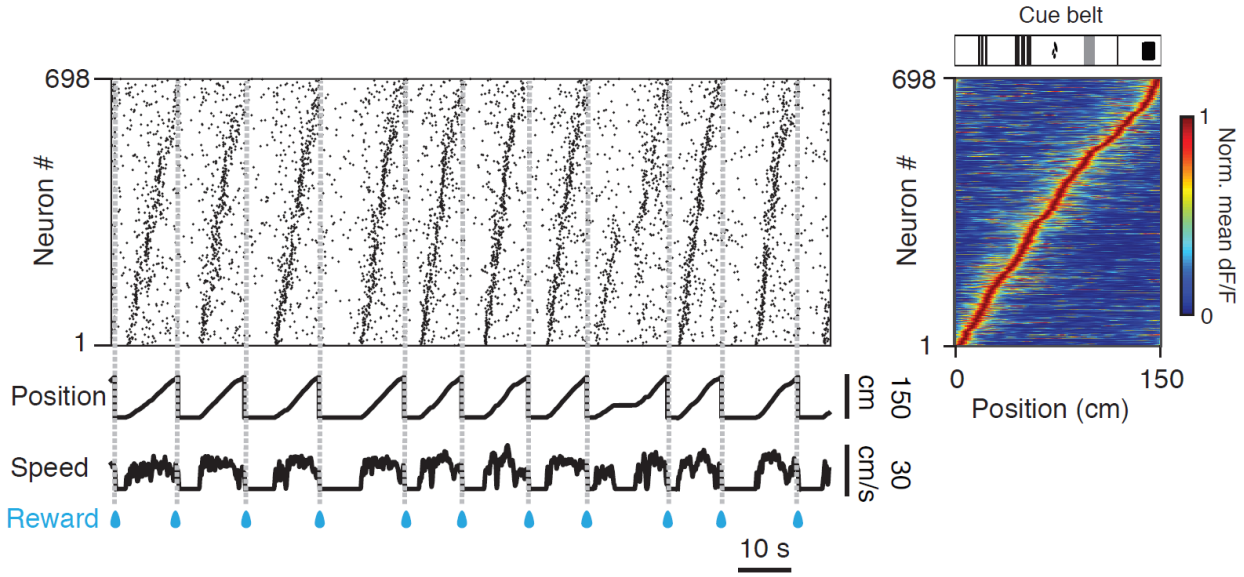

Figure 2.10 Hippocampal place cells and sequential activity during running on a tactile belt (belt covered with various tactile patches)
Left, raster plot of neuronal activation of 698 simultaneously imaged CA1 place cells on a tactile cue-rich belt. Neurons were ordered by their peak response positions; bottom two traces show position and movement speed. Grey dashed lines and blue drops indicate reward. Right, average position activity map for the 698 CA1 place cells. Belt diagram is shown at the top.

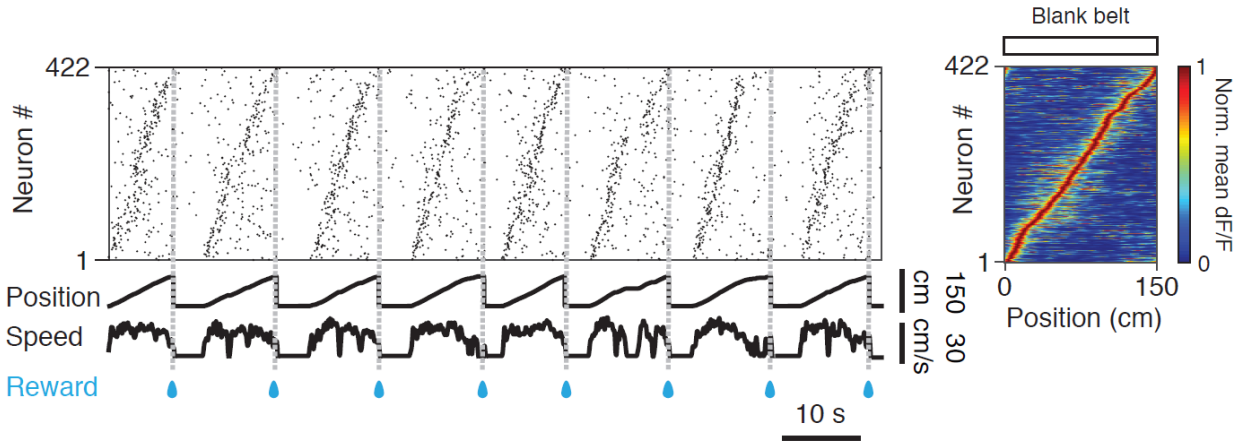

Figure 2.11 Hippocampal place cells and sequential activity during running on a blank belt (no tactile cues)

Left, raster plot of neuronal activation of 422 simultaneously imaged CA1 place cells on a blank belt (no tactile cues). Neurons were ordered by their peak response positions; bottom two traces show position and movement speed. Grey dashed lines and blue drops indicate reward. Right, average position activity map for the 422 CA1 place cells. Belt diagram is shown at the top.

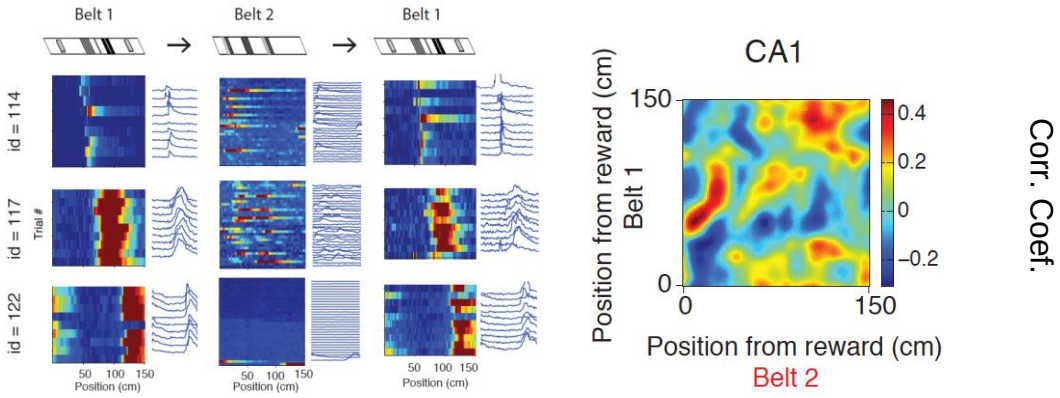

Figure 2.12 Hippocampal global remapping on two distinct tactile belts

Left, three example CA1 place cells that showed robust place fields on belt 1 but not on belt 2. Right, population vector correlation matrix for CA1 place cell activity on the 2 distinct belts. The 2 belts had distinct tactile cues at distinct locations.

3. Contextual Response Modulations in the Primary Visual Cortex

We started the thesis project with the motivation to test the hypothesis that the primary visual cortex (V1) encodes spatial information. This was done in collaboration with Steffen Kandler at the Neuro-electronics Research Flanders. In order to study this, we adapted a virtual spatial assay in which mice were head-fixed and actively moved a treadmill belt enriched with tactile cues. This assay reliably drove spatial representation in the dorsal hippocampal CA1. V1 neurons showed 'position-related' response modulations. The origins of these response modulations arose from whisker-mediated tactile influences.

3.1. SUMMARY

We studied the encoding of visual and contextual information in the mouse primary visual cortex (V1) in a virtual spatial paradigm comprised of both path integration and local tactile cues. The assay reliably drove place cell activity in the hippocampus and allowed for precise control of visual inputs. We studied how visual responses of V1 populations to brief noise stimuli presented in a closed-loop manner were influenced by contextual variables. Consistent with previous reports (Niell and Stryker 2010; Saleem, Ayaz et al. 2013), V1 responses to visual stimulation were modulated by movement. Surprisingly, V1 neurons also showed position-related response modulations that could not be explained by behavioral variables. Based on this groundwork, our collaborator, Steffen Kandler at the Neuro-Electronics Research Flanders has demonstrated the tactile origins of the position-related V1 response modulations we observed here.

3.2. RESULTS

Neurons in the rodent primary visual cortex (V1) convey nonvisual signals that may reflect information about the task, behavior, and internal processing (Fu et al 2014, Keller et al 2012, Niell & Stryker 2010, Saleem et al 2013, Shuler & Bear 2006). We used a head-restrained treadmill assay to probe spatial modulations in mouse V1 during a virtual spatial task. Using acute silicon probe recordings, we studied the neuronal encoding of position in hippocampal CA1 and V1 when the animals actively moved along the treadmill belt.

3.2.1. Place Cells in the Hippocampus during the Virtual Spatial Task

To investigate spatial modulations in the visual cortex, we adapted a spatial paradigm encompassing both path integration and local cues (Royer et al 2012) (see Materials and Methods). We trained head-restrained mice to move a low-friction circular treadmill apparatus and to interrupt their movement at regular distance intervals for a drop of sucrose water reward (Figures 3.1A and 3.1B; also see Materials and Methods). The treadmill belt was covered with texture patches hidden from the animals' eyesight but accessible to their lower limbs and whiskers (Figures 3.1A and 3.1B; also see Materials and Methods). These local cues along with movement feedback gave animals information about position on the belt. This assay formed a tightly controlled 'virtual' environment, which the animals traversed repeatedly by 'moving' laps along a single direction. Belt position, movement speed, and eye position were monitored and provided precise behavioral readout.

After 2–3 weeks of habituation to head fixation and training, the animals

behaved consistently on the treadmill apparatus for experimental sessions lasting 30-50 laps (30 laps in 621.5 ± 77.1s; 30 to 50 laps per recording session; N = 5 animals, 14 sessions). The behavior consisted of periods of high-speed movement interspersed with short periods of stillness mostly around the reward site. Movement speed changed with position on the virtual track, with the animals speeding up after reward consumption and slowing down when approaching the reward position (Figure 3.1B). Movement speed ranged from 9.5 ± 0.3 cm/s at the reward position to 31.0 ± 0.3 cm/s (N = 527 laps) in the middle of the track. Movement speed patterns were highly correlated across laps (r = 0.91 ± 0.02, N = 5 animals, 14 sessions).

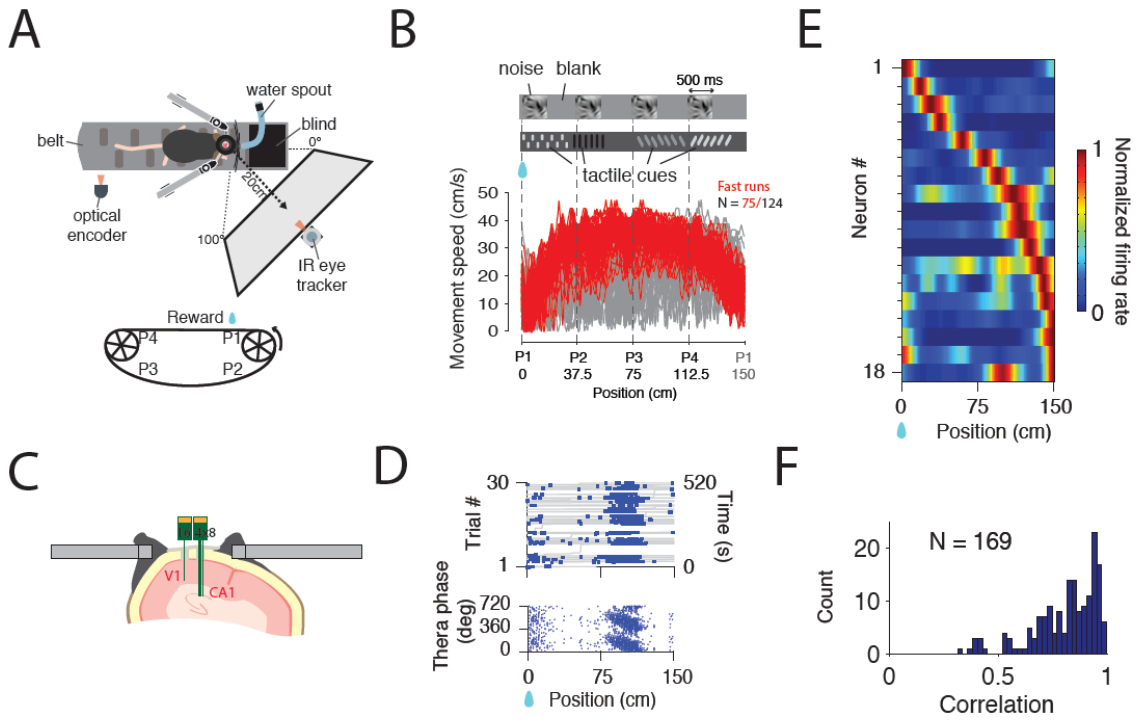

Figure 3.1 Experimental setup, behavior, and hippocampal place cells

(A) Upper panel, top view of the treadmill setup. Mouse sat on a fabric belt with head being restrained. Visual stimulation screen and eye tracker were positioned in front of the right eye. Recordings were made in the left hemisphere. Running speed and position on the belt were monitored by a rotation encoder. Belt sight was blocked from the mouse by putting a black fabric piece in the lower visual field. Bottom, side view of the treadmill belt. Mouse moved the belt in one direction and got a drop of sucrose water reward at a fixed position on the belt.

(B) Upper panel, experimental design and belt diagram. Identical wavelet noise stimulus with 500 ms duration was triggered by four fixed positions on the belt in a closed-loop way. The belt was covered with various tactile cues. The belt was 150 cm in length. Bottom, representative lap running behavior. Running speed was plotted as a function of position on the belt for one training session with 124 laps. Red traces indicate trials in which the animal only stopped at the reward position (0 cm). Blue drop indicates reward delivery.

(C) Diagram of simultaneous silicon probe recordings in the dorsal hippocampal CA1 and the primary visual cortex (V1).

(D) The activity of an example hippocampal place cell. Upper panel, raster plot in time and position for 30 trials. Grey traces represent running trace. Bottom, raster plot of theta phase precession. Two theta cycles were shown for visualization purpose.

(E) Normalized firing map of 18 simultaneously recorded place cells from one example session. The firing map was normalized by occupancy in each position bin. Neurons were ordered by their peak firing positions.

(F) Distribution of correlation coefficients between the position firing vectors of the first half session and the second half session for all CA1 place cells (n = 169).

The stereotyped behavior suggested the animals acquire an internal

representation of the track position. To test this hypothesis, we performed acute multi-site silicon probe recordings in the dorsal hippocampal CA1 (Figures 3.1C and 3.2). We measured local field potentials (LFPs, Figure 3.2) and single units in CA1 (N = 264 pyramidal neurons, 9 - 40 per session, 24 ± 2.5, mean ± s.e.m.) during the task and studied how LFPs and single unit activity varied with movement and position on the virtual track.

Consistent with past work in freely-moving (O'Keefe & Recce 1993) and head-fixed animals (Royer et al 2012), hippocampal LFPs showed characteristic network patterns, including theta and ripple oscillations (Figure 3.2). CA1 neurons fired at specific positions on the virtual track. Out of 264 well-isolated CA1 pyramidal neurons, 169 neurons (15.4 ± 2.1, mean ± s.e.m.) showed significant position-locked activity (Figures 3.1D, 3.1E and 3.2). As observed in freely-moving animals (O'Keefe & Recce 1993, Skaggs et al 1996), the timing of place cell action potentials was synchronized to theta oscillations and showed a characteristic theta phase precession with position within the place field (Figure 3.1D). This activity-defined place fields were stable within running sessions (Figure 3.1F). Hippocampal place cells formed a population representation of the animal’s position on the linear track. Place fields were distributed over the entire track (Figure 3.2) ($p = 0.15$, Rayleigh test).

Thus, LFPs and single-units in the hippocampal CA1 in our head-fixed assay showed activity patterns that are comparable to those seen in freely-moving animals, allowing us to study V1 visual responses at distinct hippocampal output states in a well-controlled way.

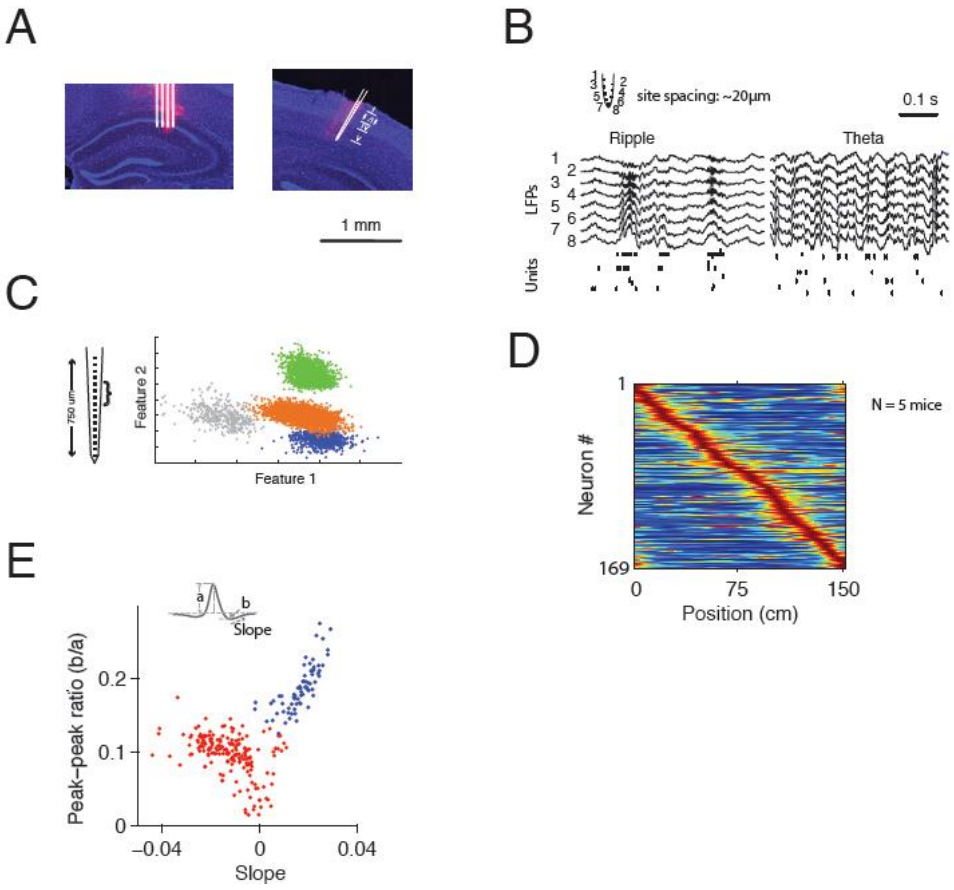

Figure 3.2 Hippocampal single-unit and LFPs activity during the task

(A) Example histology showing probe tracks in the dorsal hippocampal CA1 (left) and the primary visual cortex (right). Blue, DAPI staining; red, DiO labeling of the silicon probe track. Silicon probes were coated with DiO before insertion. A 4-shank 32-channel probe was used for recording in CA1. A linear probe with 16 channels was used for recording in V1 across all layers.

(B) Representative CA1 LFPs from one shank showing ripple and theta oscillations. LFPs were anatomically ordered from dorsal to ventral. Raster plots at the bottom show simultaneous unit activity from the same shank.

(C) Example sorted neurons from 4 adjacent recording sites on the linear probe in V1. The 16 sites were grouped into 4 groups (each group contained 4 sites), and clustering was performed for each group.

(D) Trial-averaged normalized activity of 169 place cells from 5 mice. Neurons were ordered by the positions of peak responses.

(E) Putative clustering of CA1 pyramidal cells and interneurons (also see Materials and Methods), with red dots indicating putative pyramidal cells, blue dots indicating putative interneurons.

3.2.2. Contextual Modulations in V1 Neurons

We next investigated how V1 responses to the identical stimulus varied as the animals moved along the track. Whether V1 neurons convey information about the animal's location in the environment is, however, not known.

To address this question, we used silicon probes to record single-unit responses in V1 while the animal moved on the track (Figure 3.1C). We studied V1 responses to a brief stimulus presented to the contralateral eye (Figure 3.3A) and triggered as the animal passed four equidistant positions on the track (P1–P4), with the first position (P1) corresponding to reward delivery (Figure 3.3B). Since the stimulus was identical at the four locations, changes in firing rates with location may be closely linked to the local task context.

Many V1 neurons showed pronounced contextual response modulations. We studied the firing rate responses of 146 well-isolated V1 neurons (10 ± 1 neurons per session, N = 5 mice, 14 sessions). Of the 146 neurons, 98 neurons (67%) increased their firing rates in response to the visual stimulus whereas 20 neurons (14%) showed a reduction in firing rate. While the time courses of responses were repeatable across trials/laps (Figure 3.3A), the responses strengths varied with the animal's positions on the track (Figure 3.3B). Across the population, 65 neurons (44.5%) showed a significant difference in evoked firing rate at least one position on the track ($p < 0.05$, shuffling analysis).

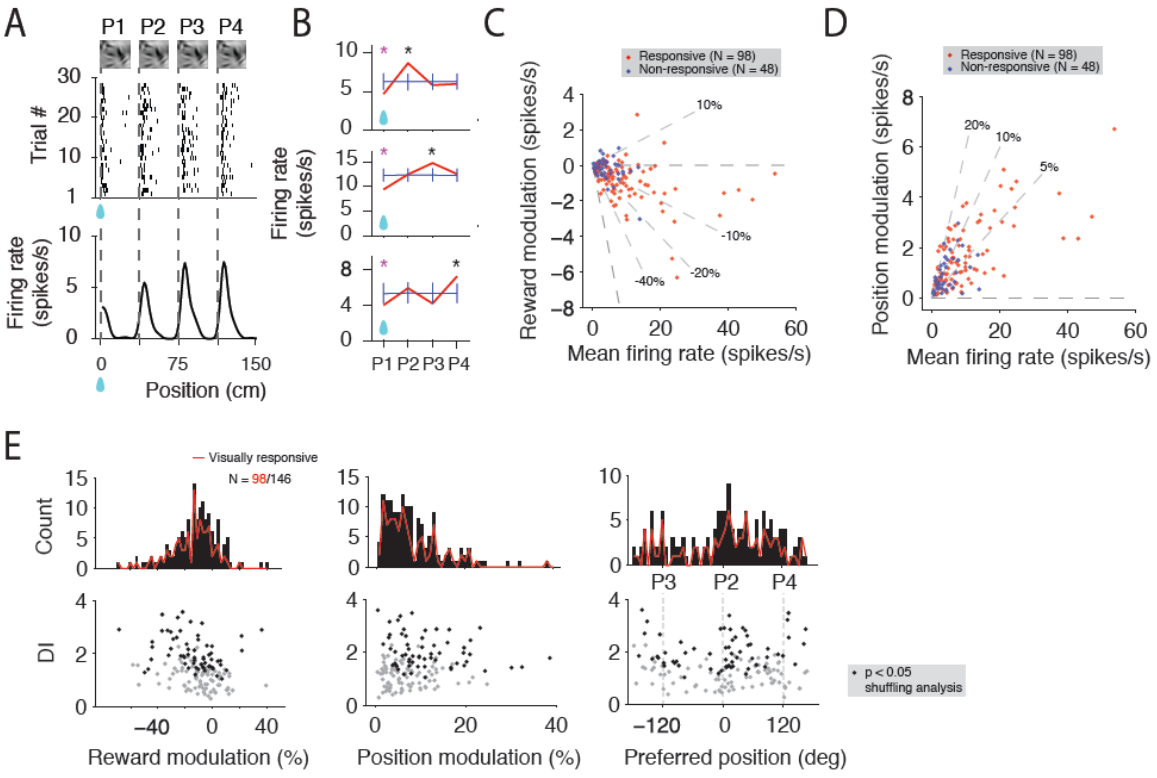

Figure 3.3 Contextual modulations in V1 neurons

(A) Raster plot of one example V1 neuron in position for many trials/laps. Top panel shows the diagram of the stimulus at the four equidistant positions (P1-P4). Bottom panel shows the occupancy-normalized firing curve. Blue drop indicates reward delivery.

(B) Three example V1 neurons in one session showing diverse contextual modulations. Red lines are original tuning curves at the four positions. Blue lines are position-shuffled tuning curves with 95% confidence intervals. Magenta and black asterisks indicate significantly suppressed and enhanced responses at corresponding positions, respectively.

(C) and (D) Scatters of the mean firing rate and reward and position modulated firing rate in spikes/s. Visually responsive neurons are indicated as red dots. Dashed lines indicate the degree of reward and position modulations.

(E) Distributions and significance measures of reward and position modulations. Upper panel, distributions of reward modulation (%), position modulation (%), and preferred tuned position (in degree). Visually responsive population is indicated as the red lines. Bottom panel, scatters of discrimination index (DI) and reward and position modulations. Black dots show the significantly modulated neurons identified by position-shuffling analysis as shown in (B). Right, Distribution of preferred modulated positions. Note a slight bias toward P2.

At the reward position (P1), V1 neurons showed a general reduction in firing rates (Figures 3.3B and 3.3C). To quantify the effect, we calculated for each neuron a reward modulation index, defined as the ratio of the firing rate to the stimulus at

the reward position (P1) over the average firing rate across the four track positions (Figure 3.4, also see Materials and Methods). Across the population, 30.1% of the neurons showed a significant reduction in response at the reward position (Figure 3.3E, left) ($p < 0.05$, shuffling analysis) and the average reduction was -11.9 ± 1.4% (N = 146). Non-visually responsive neurons showed a similar level of reward modulation as visually evoked activity (Figures 3.3C and 3.3E).

At positions away from reward (P2-P4), neurons showed preferences for specific positions on the track (Figures 3.3B, 3.3D and 3.3E). To quantify the strength of position modulations, we calculated a position modulation index, defined as the circular variance (Ringach et al 2002) of responses at P2–P4, a fractional measure of modulation depth (Figure 3.4, also see Materials and Methods). The effects varied in strength, with 22 neurons (15.1%) showing changes in firing rates greater than 15% (N = 146). We estimated for each neuron the preferred position defined as the position eliciting the largest firing rate (Figure 3.4). Over the population, the neurons' preferred positions were broadly distributed over the 3 non-reward positions. However, the strongest and most significant modulations clustered near the 3 positions (Figure 3.3E, right), indicating that neurons often responded strongly to one of the positions.

The modulations were robust in the face of trial-to-trial variability of responses. To quantify signal–to–noise across trials, we calculated the normalized distance (Figure 3.4, discrimination index, DI or d-prime) between the distributions of average responses across trials estimated from resampled data (average of half of the trials, n = 1000 permutations). 110 neurons (75.3%) had a DI of position-

related modulations greater than one. DI and significance measures from position-shuffling analysis (Figure 3.3B) were in close agreement (Figure 3.3E).

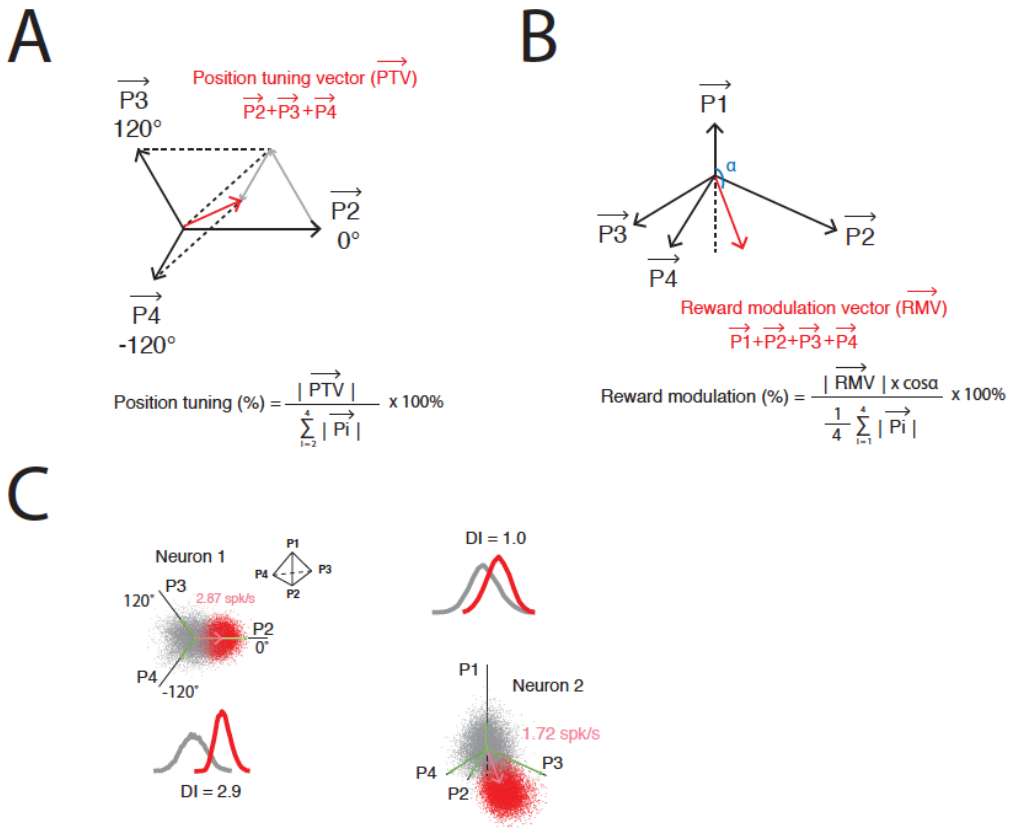

Figure 3.4 Quantification of position tuning and reward modulation

(A) Position tuning vector was calculated by summing the response vectors at P2, P3, and P4 between which the angles were 120°. Position tuning (%) was the ratio between the magnitude of the position tuning vector and the summed responses at P2, P3, and P4.

(B) Reward modulation vector was calculated by summing the response vectors at P1-P4 between which the angles were 120° in 3D space. Reward modulation (%) was the projection of the reward modulation vector onto the response vector at P1 divided by the average response across P1-P4. Negative means reward suppression.

(C) Left, one example neuron showing quantification of position tuning; right, one example neuron showing quantification of reward modulation. Grey cloud, each point represents one position tuning vector from one shuffling across P1-P4. Red cloud, each point represents one position tuning vector from one bootstrapping that performed at each of P1-P4. 1000 times shuffling and bootstrapping were performed. The multi-dimensional gray and red clouds were projected 2D and discrimination index (DI) was used to measure the discriminability between the two clouds.

Pronounced and weak modulations were observed at both low and high firing rates (Figures 3.3C and 3.3D). While the modulations were correlated with

firing rates, these alone could not account for the cell-to-cell variations of the effects. This was particularly the case for modulations at P2-P4 where effect size was only weakly correlated with modulation strength (Figure 3.3E, middle). These findings held for both visually responsive and nonresponsive neurons (Figure 3.3E, red vs. black). When accounting for dependence on the mean firing rates (Figures 3.3C and 3.3D), the two measures of modulations were only weakly correlated (partial correlation r = -0.21). Thus, response modulations at P1 and P2-P4 seem to be shaped by cell-specific and independent mechanisms.

To further investigate cell specificity, we studied how modulations were distributed amongst physiological cell classes and across cortical layers (Figure 3.5). We studied the response properties of putative excitatory and inhibitory neurons in superficial and deep layers in the cortex. Despite the clear separation between these putative cell classes (Figure 3.2), we found no differences in modulations (Figure 3.5A, excitatory N = 88, 60.3%, inhibitory N = 58, 39.7%). We next studied response modulations as function of cortical depth. An estimation of 14 (9.6%) neurons were recorded in superficial layers (layers II/III), 29 (19.9%) in layer IV, and 103 (70.5%) in deep layers (layers V/VI). We found that position and reward related modulations were present across all layers (Figure 3.5B). However, we found a tendency for superficial neurons to show stronger position-related modulations and reward modulations (Figure 3.5B) (Position modulation: p = 0.007, 2 sample KS test; superficial = 13.5 ± 1.8%, deep = 8.6 ± 0.7%; reward modulation: p = 5.21e-06, 2 sample KS test; superficial = -28.9 ± 0.7%, deep = -7.6 ± 0.15%; all mean ± sem).

In summary, we found responses of V1 neurons to visual stimuli are influenced by ‘positions’ on the tactile-rich belt. Distinct neurons respond differently at distinct locations in the tactile environment.

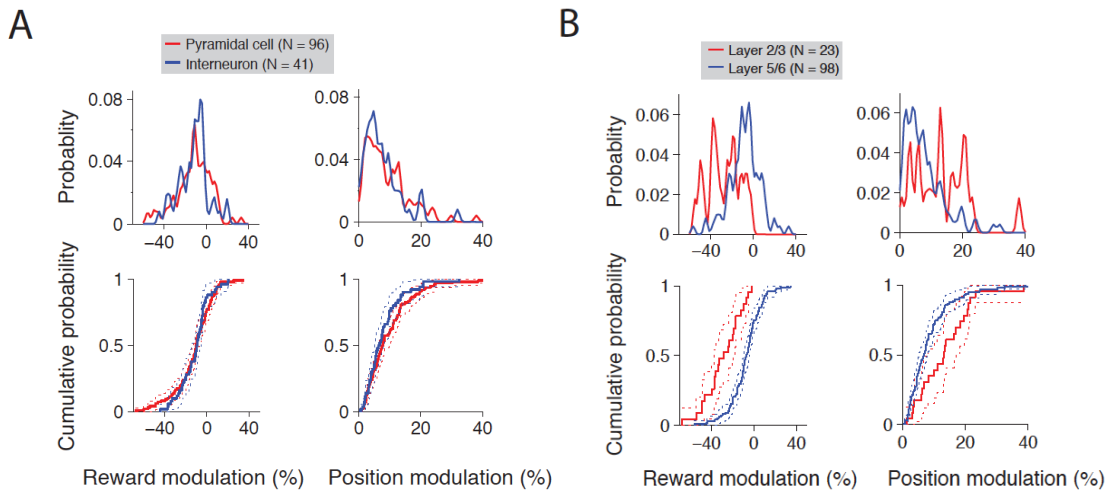

Figure 3.5 Position and reward modulations across cell types and cortical layers
(A) Top, distributions of reward and position modulations for putative pyramidal cells (red) and interneurons (blue); bottom, corresponding cumulative distributions of reward and position modulations. Dashed lines represent 5% and 95% confidence intervals. (B) Same as (A) but for neurons in superficial layers (layer 2/3, red) and deep layers (layer 5/6, blue). Note superficial neurons tended to be more tuned to positions and reward.

3.2.3 V1 Position-related Modulations Are Not Explained by Behavioral Variables

The response modulations we observed could reflect changes in visual inputs and motor outputs that occurred as the animals moved along the treadmill track. The animal’s movement speed varied with position on the virtual track (Figure 3.1B), which could change the responsiveness of V1 activity (Niell & Stryker 2010). It also determined the presentation rate of visual stimulus and hence the neurons’ responsiveness. Eye position and pupil diameter also changed, which can change the drive provided by the visual stimulus. While these task-related variables varied widely across laps, correlations with position could potentially

explain the modulations.

To quantify the effects of changes in visual inputs and motor outputs, we calculated the correlation coefficient between the neurons' firing rates with movement speed, stimulation rate, eye position, and pupil size. Expectedly, V1 neurons showed a strong dependence of responses with movement speed and stimulation rate. Increasing movement speed increased response magnitude (Figure 3.6A) and increasing stimulation rate reduced the strength of response ($r = 0.10 \pm 0.01$, -0.09 ± 0.01, respectively) (Figure 3.6B). While the effects of eye position were varied, we observed no consistent effect of pupil size ($r = 0.01 \pm 0.02$, 0.02 ± 0.01, respectively) (Figures 3.6C and 3.7A).

To assess the link between these task-related variables and V1 modulations, we used a bivariate analysis. If the task-relevant variables underlain V1 modulations, neurons showing stronger task-related correlations should also show stronger modulations. To test this hypothesis, we computed the joint histogram of task-related correlations and modulation indices for the entire neural population ($N = 146$). If the two variables were linked, then the joint histogram would show a slant or other non-separable features otherwise the joint distribution would be separable (Figure 3.6).

We observed a significant link between modulations of responses at the reward position (P1) and movement speed and stimulus history (Figures 3.6A and 3.6B). At the reward position, neurons with strong speed-related correlations showed strong modulations whereas neurons with weak correlations showed weak or no modulation (Figure 3.6A) ($p = 8.1e\text{-}08$, Pearson's r). Similarly,

neurons with positive stimulus rate correlations showed weak or no modulations whereas neurons with negative stimulus rate correlations showed strong modulations (Figure 3.6B) (p = 2.2e-07, Pearson's r). These results indicate that modulations at the reward position can, to a certain degree, be explained by movement speed and stimulation presentation rate.

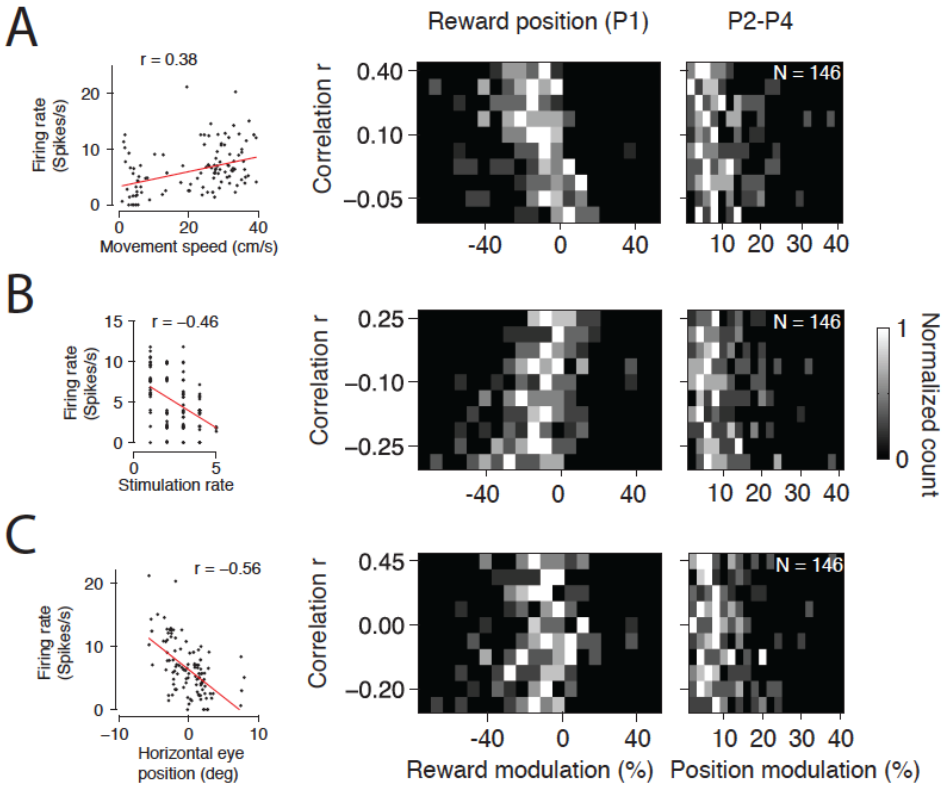

Figure 3.6 Correlations of reward and position modulations with behavioral variables

(A) Effect of movement speed. Left, scatter plot of the firing rate and movement speed of one example neuron. Red line, robust fit to all dots. Right, 2D histograms of the correlation between firing rate and movement speed and reward and position modulations. Grey scale represents normalized count of neurons that fall into each bin.
(B) Effect of stimulation rate (visual adaptation). Left, scatter plot of the firing rate and stimulation rate (number of stimulation in the past 10 seconds) of one example neuron. Red line, robust fit to all dots. Right, 2D histograms of the correlation between firing rate and stimulation rate and reward and position modulations. Grey scale represents normalized count of neurons that fall into each bin.
(C) Effect of eye movement. Left, scatter plot of the firing rate and horizontal eye position (in degree) of one example neuron. Red line, robust fit to all dots. Right, 2D histograms of the correlation between firing rate and eye position and reward and position modulations. Grey scale represents normalized count of neurons that fall into each bin.

By contrast, modulations at other positions (P2-P4) did not show such a link. The joint histograms showed only weak dependence of modulations on the strength of task-related correlations (Figure 3.6). Neither movement speed nor eye position was related with response modulations at P2-P4 ($p = 0.31$ and 0.20, respectively, Pearson's r). Stimulus presentation rate was weakly correlated but could not account for large diversity of observed position-related modulations ($p = 0.14$, Pearson's r).

Motor activity also affects the oscillatory activity in LFPs, which could potentially influence visual responsiveness. Locomotion increases oscillatory activity in the visual cortex (Niell & Stryker 2010) and in the hippocampus (O'Keefe & Recce 1993). Oscillatory activity is linked to changes in responsiveness (Pinto et al). In our assay, movement speed was significantly correlated with oscillatory activity in LFPs of both the hippocampus and the visual cortex (Figure 3.8A). Movement was correlated with increases in power in theta frequency band (5-12 Hz) in the hippocampus and increases in power in the narrow band gamma (55–65 Hz) in the visual cortex (Figure 3.8A). We found no link between hippocampal theta phase and visual cortical gamma amplitude (Figure 3.9).

While visual cortical oscillations were correlated with the animal's position on the track, they were not linked to modulations at non-reward positions (Figures 3.8B and 3.8C). Gamma oscillations were weakest at the reward position and stronger at positions away from the reward position (Figure 3.8B). We assessed

the correlations between gamma oscillations and reward and position modulations. We assigned gamma oscillations within 70-100 Hz as visual stimulus-evoked gamma and 55-65 Hz gamma as movement-evoked oscillations (Figure 3.8B).

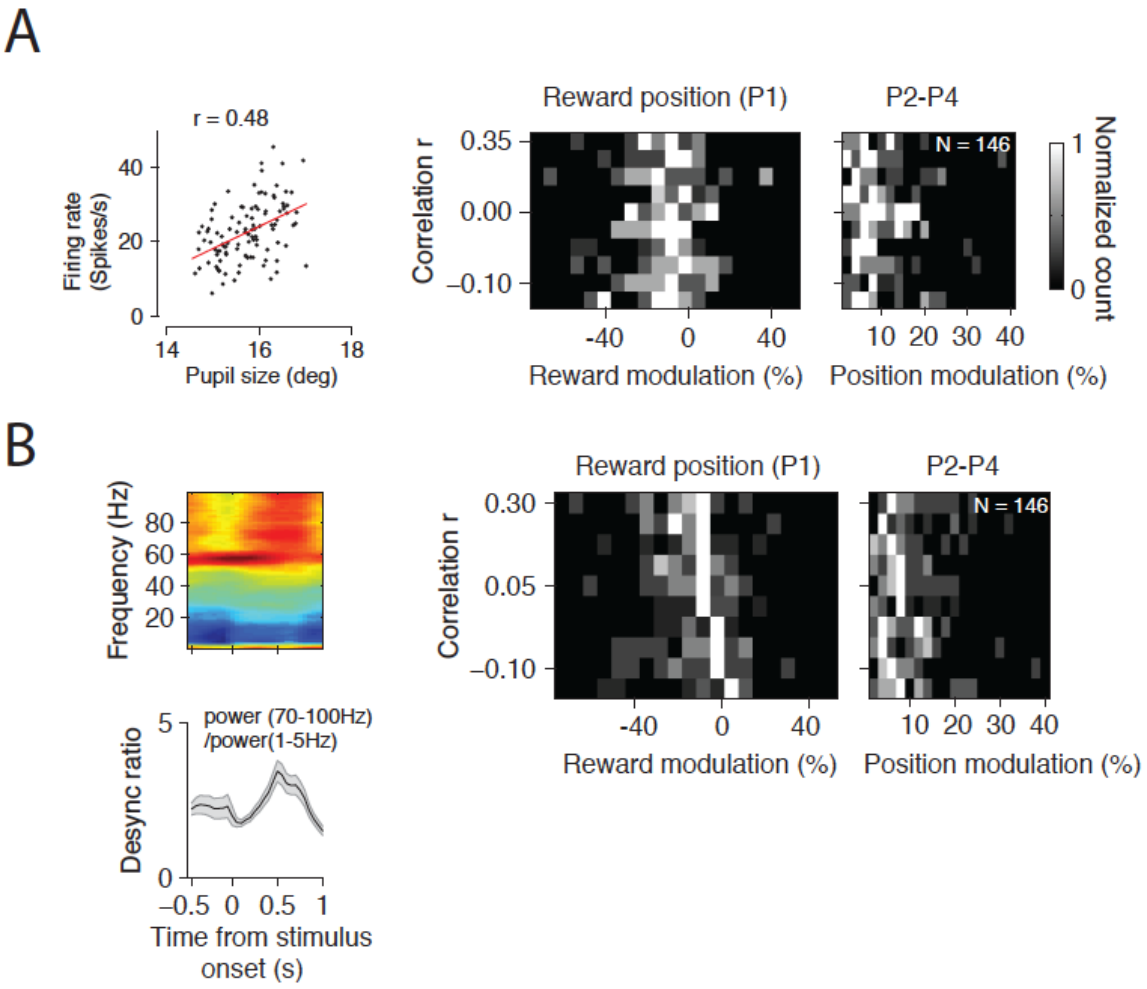

Figure 3.7 Correlations of reward and position modulations with pupil size and cortical oscillations

(A) Effect of pupil size. Left, scatter plot of the firing rate and pupil size of one example neuron. Red line, robust fit to all dots. Right, 2D histograms of the correlation between firing rate and pupil size and reward and position modulations. Grey scale represents normalized count of neurons that fall into each bin.

(B) Effect of desynchronization ratio (desync ratio). Left, top, spectrogram of an example V1 LFP for one stimulation epoch; bottom, desync ratio (ratio between the power in 70-100 Hz and the power in 1-5 Hz), gray shaded area represents s.e.m. 0 is the stimulus onset time. Right, 2D histograms of the correlation between firing rate and desync ratio and reward and position modulations. Grey scale represents normalized count of neurons that fall into each bin.

The gamma oscillations in both bands were correlated with the reward modulation but not the position modulation away from the reward site (Figure 3.8C). We also calculated a desynchronization index (Pinto et al 2013) defined as the ratio of high frequency band power (70-100 Hz) over low frequency band power (1-5 Hz) during the stimulation period (Figure 3.7B). Across all recordings sites, the desynchronization index was 0.83 ± 0.06 at the reward position (P1) and 1.17 ± 0.13 at positions different from reward (P2–P4). The desynchronization ratio did not differ significantly across positions different from reward (P2–P4) ($p = 0.44$, Kruskal-Wallis test). While desynchronization was somewhat slightly correlated with modulations at the reward position ($p = 0.08$, Pearson's r) (Figure 3.7B), we found no link between cortical oscillations and response modulations at other positions in the neural populations (P2-P4, $p = 0.16$, Pearson's r) (Figure 3.7B).

Thus, motor activity, visual adaptation, eye position, and cortical oscillations are linked to modulations at the reward position but not at positions away from reward.

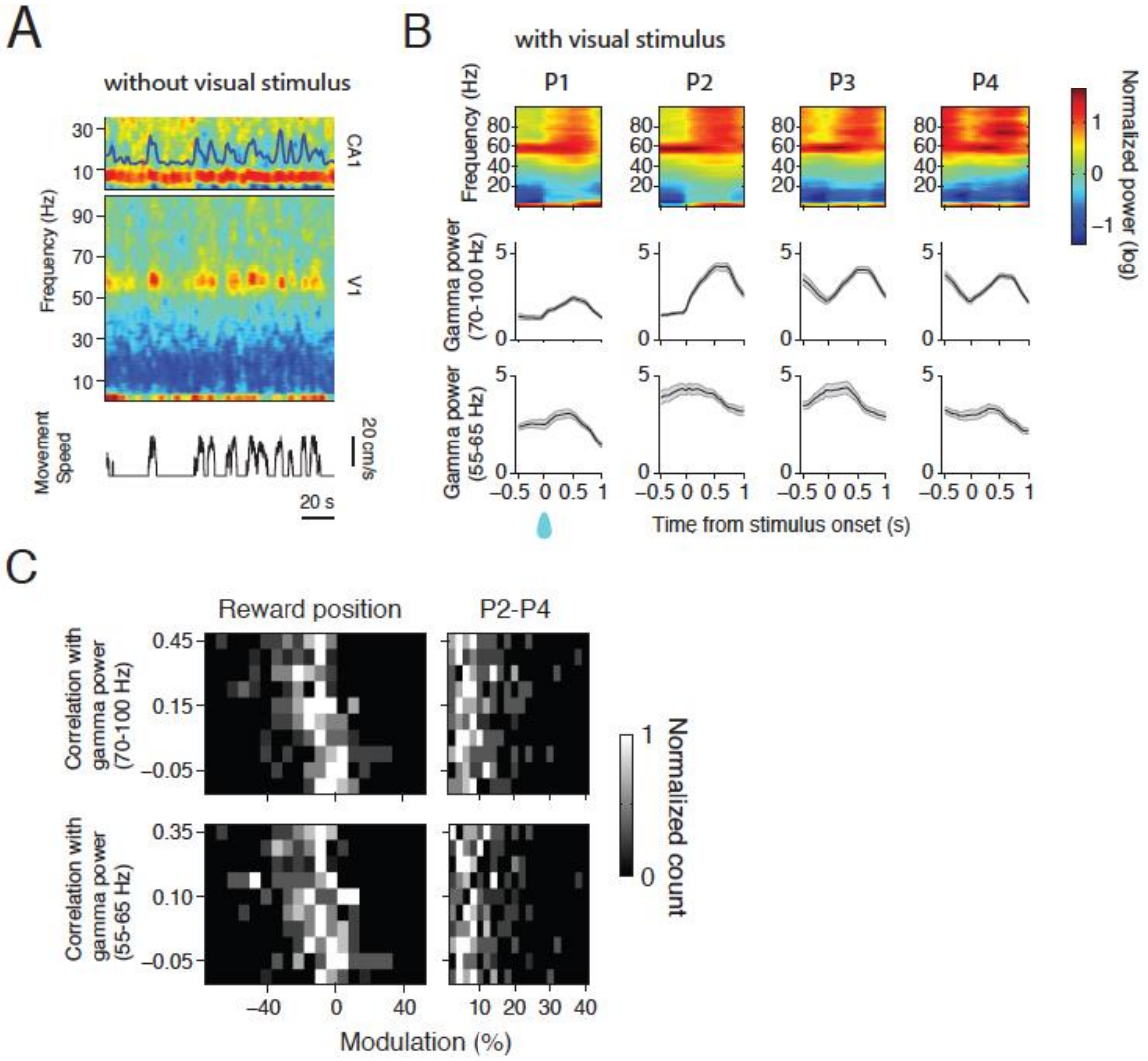

Figure 3.8 Correlations of reward and position modulations with V1 gamma oscillations

(A) Top, example spectrograms of simultaneous LFPs in CA1 and V1 (without visual stimulus). Bottom, movement speed.

(B) Top, V1 spectrograms at the four stimulation positions (P1-P4). Note the movement-related band at 55-65 Hz and stimulus-related band at 70-100 Hz. Middle, gamma power (70-100 Hz) for the four epochs corresponding to the top panel. Bottom, corresponding gamma power at 55-65 Hz. Shaded areas represent s.e.m.

(C) 2D histograms of the correlations between firing rate and gamma powers and reward and position modulations. Grey scale represents normalized count of neurons that fall into each bin.

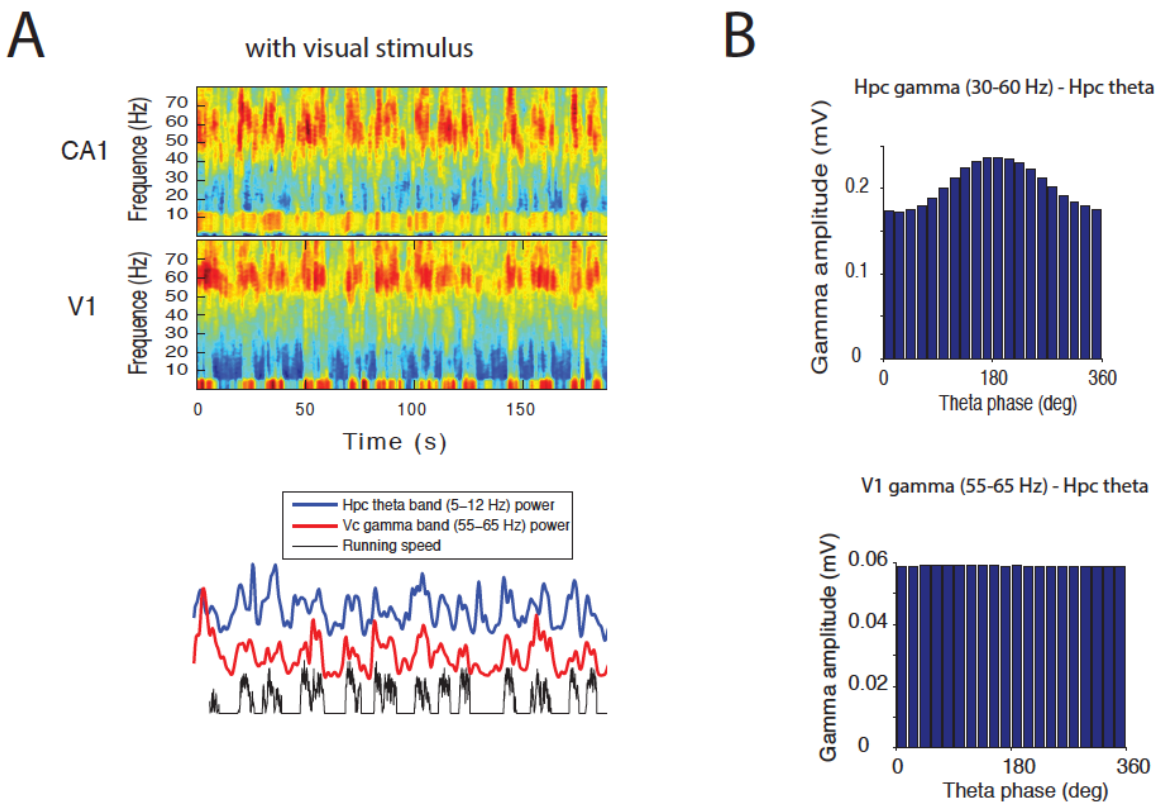

Figure 3.9 No relationship between CA1 theta phase and V1 narrow-band gamma amplitude

(A) Top, example CA1 and V1 spectrograms (with visual stimulus); Bottom, CA1 theta band power (blue), V1 narrow-band gamma power (red), and movement speed (black). (B) Top, distribution of CA1 gamma amplitude relative to CA1 theta phase; bottom, distribution of V1 narrow-band gamma amplitude relative to CA1 theta phase.

3.3. DISCUSSION

We studied the responses of V1 neurons in mice moving on a treadmill belt enriched with tactile cues and found that they exhibit response modulations that are ‘position-related’. These ‘position-related’ V1 response modulations were not explained by behavioural variables, including movement speed, eye movement, visual adaptation, and network oscillatory activity. This treadmill assay also drove reliable spatial representation of the track locations in dorsal hippocampal CA1. Hippocampal population activity was distinct at different locations on the track.

The track belt was also cue-rich, including various tactile and possibly olfactory cues.

Anatomical studies have identified broad hippocampal projections to the neocortex (Cenquizca & Swanson 2007). The neocortex could inherit spatial information from the hippocampus. Hippocampus indexing theory suggests that neocortical coding of hippocampal output could facilitate information association across cortical modalities (Teyler & Rudy 2007). 'Spatial-related' activity in mouse V1 has been reported in previous studies (Fiser et al 2016, Saleem et al 2013). However, these studies failed to rule out the possibility of sensory influences.

On the other hand, cross-modal sensory responses have also been shown and several studies have casted the unimodality of sensory cortices into question (Iurilli et al 2012, Vasconcelos et al 2011). For example, Vasconcelos et al. showed that the firings of some V1 neurons are modulated by tactile inputs. Iurilli et al. reported reduced visual responses during simultaneous audio-visual stimulation due to inhibitory inputs from the auditory cortex to V1. Based on the groundwork presented here, our collaborator, Steffen Kandler has demonstrated that the V1 position-related response modulations originate from whisker-mediated tactile inputs (data not shown in this thesis).

3.4. MATERIALS AND METHODS

Animals and Surgery

All procedures were approved by the ethical research committee of KU Leuven. 5 male C57Bl/6j mice (22–30g, 2–5 months) were injected with dexamethasone

(3.2mg/kg I.M., 4h before surgery), anesthetized with isoflurane (induced: 3%, 0.8L/min O2; sustained: 1-1.5%, 0.5L/min O2), and implanted with a custom-made titanium head plate, centered to the posterior left hemisphere following established procedures (Andermann et al 2011, Glickfeld et al 2013, Goldey et al 2014). Two tiny stainless steel screws were implanted in the skull above the cerebellum to be used as reference and ground electrodes, with the reference electrode touching the brain. Two days prior to electrophysiology experiments, two 1-mm craniotomies were made above the hippocampus (2.0mm posterior to bregma, 1.8mm lateral to midline) and V1 (3.8mm posterior to bregma, 2.5mm to midline). The dura above V1 was left intact, while the dura was slit above the hippocampus. Craniotomies were filled with ACSF, covered with a glass coverslip, and protected with Kwik-cast (WPI). Aseptic conditions were maintained throughout the procedure and body temperature was maintained at 37ºC. Mice received post-operative treatment for 72h (buprenex 0.2mg/kg I.M., cefazolin 15mg/kg I.M.; every 12h) and were given 2–5 days to recover.

Histology

In order to reconstruct the probe track, the probes were dipped in DiI before inserting into the brain. Mice were deeply anesthetized with ketamine and perfused first with 1 × Phosphate Buffered Saline (PBS) followed by 4% Paraformaldehyde (PFA). The brains were left in 4% PFA for 24 hours and then sectioned by a Microtome (Leica, Germany) at 40 µm. The sections were mounted on slides, stained with DAPI, and cover-slipped. The stained sections

were then imaged by NanoZoomer (Hamamatsu, Japan).

Treadmill Apparatus

A linear treadmill preparation was adapted from (Royer et al 2012). The treadmill was equipped with a 1.5m fabric belt with various textures on it. Two custom-printed wheels with 5cm radius and one aluminum platform were used to support the belt and let the animals sit on. Slippery PTFE tape (CS Hyde) was adhered to the platform to minimize friction. An encoder (Avago Tech.) with a resolution of 100 pulses per revolution was attached to the shaft of the wheel to monitor the rotation of the wheel, with which we can estimate the running distance at a precision of 3.14 mm. A photoelectric sensor (Omron) was mounted under the platform and a reflective tape was attached underneath the belt. The photoelectric signal was used as the rewarding trigger (P1) and reset distance estimation for each lap running, with which we can avoid the potential accumulative drifting errors. A pinch valve (MSscientific) was used to control the reward delivery. A custom-assembled PCB board equipped with microcontroller AT89LP52 (Atmel) was used to monitor the photoelectric signal and control the valve. Other mechanic parts were from Thorlabs. The encoder and reward signal were acquired via a data acquisition board (MCC).

Training

Training started earliest 5 days after surgery. Mice were water restricted to 1ml per day. On the first three days, mice were habituated to handling and head fixation. In the following days, mice were head-fixed on the treadmill platform and

were trained to actively move a 130–150cm treadmill belt. Sessions gradually increased to a maximum duration of 2h per day. In case of signs of distress, training sessions were terminated. Mice were rewarded with tap water or a 10% sucrose solution, either after habituation sessions or based on running distance on the belt at a fixed reward position (5–10µl drop size). Reward volume was measured and substituted to 1ml per day.Mice typically showed stable task performance after 2–3 weeks. Once the animals reached good behavioral performance, i.e. ~200 laps in 1h, stereotyped running speed versus position traces, they were prepared for electrophysiology experiments. Mice were trained with a constant gray screen stimulus with 50% luminance was positioned 20cm in front of the right eye. During the training and experiment phase, the animals' body weight was monitored, and in case a drop larger than 15% of the free-feeding weight was observed, training was interrupted and free access to water granted.

Visual Stimulation

A 500–1000ms wavelet noise stimulus was used to drive a diverse V1 population (Bonin et al 2011). A 20'' LED monitor was positioned 20 cm in front of the contralateral eye, covering 120x40 degree in the visual field (0º to 120º central to peripheral, –15º to 25º lower to upper visual field). Noise stimuli were interleaved by a gray screen 'blank' stimulus (50% luminance). Stimulus presentation was triggered by the animals' running distance at four equi-distanced positions along a 150 cm treadmill belt.

Eye Tracking

Eye movements and pupil size of the contralateral eye was monitored at 30fps with an infrared CCD camera (AVT Prosilica GC660; Navitar Zoom 6000). Infrared light was focused on the eye with a far-red LED (735nm) and collimated lens (Thorlabs). Eye parameters were analyzed using custom-written MATLAB routines. Eye motion data was smoothed with a median filter to remove eye blink and whisker artifacts.

Electrophysiology

We used a 256-channel DigiLynx system (Neuralynx) to record electrophysiological signal (32k Hz) and photoelectric signal (reward). On the day of recording, the mice were first put on the treadmill with head fixed, and the belt movement was restricted. The head plate well was cleaned with 70% alcohol. The Kwik-cast silicon elastomer was then removed carefully. The craniotomies were rinsed with ACSF 3 times and the holes were left filled with liquid. Silicon probes (NeuroNexus) were first covered with DiI solution (Life Technologies) and attached to individual adaptors, which were then attached to individual micromanipulators (Scientifica). Then the probes were lowered into the brain surface separately at 1μm precision. A32 probe (4 shanks, 32 sites, 1-3 MΩ impedance) was used for hippocampal recording. The four shanks were positioned 45˚ to the sagittal plane. The tip of the probe was lowered to dorsal hippocampal CA1 pyramidal layer (1.2-1.5 mm), indicated by dense spiking

activity and the polarity inverse of sharp waves across the sites on one shank. A16 linear probe, A2x2 tetrode configuration, or A32 (4 shank, 32 sites) were used for visual cortical recording. The A16 linear probe was positioned in a 70˚ angle and lowered into V1 slowly until the top site was in the brain (700-900 um). This procedure was monitored under a microscope. Once the probes were in position, the craniotomies were covered with 2.5% liquid agar at body temperature. The probe adaptor and the holder were wrapped with an aluminum foil which was grounded. The belt view was blocked. Then the belt was released and the mice were free to run. After waiting 20-30 minutes for the probe to stabilize, recording started. The recording lasted 1-1.5 hours each day, consisting of 2-4 sessions. After recording, the probes were retracted and dipped in enzyme cleaner for 2 hours to remove remaining tissue on the surface. Each mouse was recorded for 2-4 days.

Data Analysis

Electrophysiology

The electrophysiological data was high-passed filtered (0.8-5k Hz) for spike detection and down-sampled to 1250Hz for local field potentials analysis. For data recorded with A32 probe, spike sorting was performed on each individual shank separately. For A16 probe data, all sixteen channels were equally divided into four groups and spike sorting was performed on the four groups separately. For A2x2 tetrode data, spike sorting was performed on each tetrode configuration. Spike waveforms were extracted and stored as 52 samples for

each recording site, with the peak aligned at 26th sample. Then principal components were computed and features were stored for following analysis. We first used KlustaKwik (http://klustakwik.sourceforge.net/) to do automatic clustering. Manual adjustment was followed using Klusters (http://klusters.sourceforge.net/). NeuroScope (http://neuroscope.sourceforge.net/) was used to browse data (Hazan et al 2006). Only stably recorded units with clear refractory period were included in this paper. Putative interneurons and pyramidal cells were separated using established methods (Niell & Stryker 2008). Only putative pyramidal cells were used for place cell analysis.

Place field analysis

The length of the treadmill belt was normalized and divided into 100 equally spaced bins (1.5cm per bin). Occupancy normalized firing rate for each place cell was calculated for each bin. The spikes were not included where the running speed was lower than 3 cm/s. Then the original firing rate vector was smoothed by a Gaussian window with 6 cm σ (4 bins).

For theta phase extraction, LFP was band-pass filtered at 5-12 Hz using a 2-order Butterworth filter. The troughs of the filtered signal were assigned as 0 degree. Then the phase was obtained from linear interpolation for individual spikes.

Hippocampal place cells selection criteria

For each hippocampal CA1 pyramidal cell, we calculated the spatial information per spike in bits/spike (SI) according to the following equation (Skaggs et al

1993):

$$SI = \sum_{i=1}^{N} p_i \frac{f_i}{f} \log_2 \frac{f_i}{f}$$

p_i is the occupancy probability in the i-th bin, f_i is the firing rate in the i-th bin, f is the overall mean firing rate, N is the total number of bins.

For each recording session, spike trains from each neuron were shuffled by a random timestamp between 20 seconds and recording duration minus 20 seconds relative to position information. Herein, relative spike timing was preserved. For each shuffling, SI was calculated. After 1000 times shuffling, we used the 95% percentile of all the SI values we got (n = 1000 × no. of cells). We selected cells with an SI above the 95% percentile as place cells.

Session stability

Hippocampal place cell session stability was calculated as the Pearson correlation coefficient between the firing curve of the first half session and that of the second half session.

Visual responsiveness

For each V1 neuron, pre-stimulus firing rate and within-stimulus firing rate were randomly shuffled 1000 times to get a normally distributed firing rate distribution. Visually responsive neurons were identified if the within-stimulus firing rate was above 97.5% percentile. Visually suppressive neurons were identified if the within-stimulus firing rate was below 2.5% percentile.

Trial-position shuffling

We did 1000 shuffles across the four positions and all trials within the session, and compared the shuffled firing rate and 95% confidence interval with the mean

firing rate to identify significance. If the original firing rate at a specific position is out of the shuffled (mean ± 95%CI) band, we considered the neuron was significantly tuned to that position. A single neuron can be tuned to more than one position.

Correlation analysis

Correlation coefficient between firing rate and task-relevant variables were estimated.

For each task-relevant variable, we grouped the correlation coefficient for all units into 10 groups that contain the same number of samples. We binned the position tuning (%) and reward modulation (%) into 25 equally distributed bins. Then we counted the number of units that fell into the corr-coef and tuning 2-d histogram, and normalized it by the maximum count for each coefficient group for Figures 3 and 4.

Spectral analysis

Multi-taper spectrogram of LFP was computed using the Chronux toolbox (http://www.chronux.org/). 5 tapers, 1 s sliding window were used. We used 50 ms step for Figure 5B. We used 1 s step for Figures 5A and S2. We calculated the desynchronization ratio as the ratio between the average power in frequency band (60-100 Hz) and the average power in frequency band (1-5 Hz) (Pinto et al 2013).

Position tuning and reward modulation

To compute position tuning (%) and reward modulation (%), we used a tetrahedron representation for the four positions, each position as one vertex,

with the center as origin. The responses at each position were represented as a vector pointing from the origin to the corresponding vertex, with the magnitude matching the mean firing rate at that specific position. The summed vector of these four individual vectors in 3-dimensional space was the tuning vector for that neuron. To test the uncertainty of the tuning vector, we first shuffled the firing rate for all trials across all positions (50% randomly selected data was used for each shuffling). We obtained a tuning vector from each shuffling. The results from 1000 shuffling formed a Gaussian-like cloud in multi-dimensional space. We then bootstrapped 50% randomly selected trials for each position (with replacement) and got one tuning vector from each bootstrapping. We did 1000 bootstrapping for each neuron. We then fit the shuffled data and bootstrapped data with a one-component Gaussian mixture model, respectively. The parameters of the models were estimated using Expectation Maximization. For position tuning computation, the firing rate differences between the mean of the bootstrapped and shuffled model along P2, P3, and P4 dimensions were used (P1 not included here). The position tuning vector was then obtained by vectorizing the firing rate difference within the P2-P3-P4 plane, with P2, P3, and P4 representing 0˚, -120˚, and -120˚, respectively. Position tuning (%) was computed as the percentage of the magnitude of the position tuning vector over the mean firing rate. The position tuning angle was the direction the position tuning vector pointed to (-180˚-180˚). For reward modulation, only P1 was taken into consideration. The firing rate difference was calculated between the mean of the bootstrapped and shuffled model along P1 dimension. Then reward modulation (%) was obtained by

computing the percentage of this difference over the mean firing rate. If the firing rate was suppressed at the reward position, then reward modulation (%) was negative. We projected the bootstrapped and shuffled clouds to the dimension of the position tuning vector, and computed the mean and standard deviation for the two collapsed clouds. We used d-prime (d') to measure the discriminability between the two distributions:

$$d' = \frac{\mu_s - \mu_b}{\sqrt{\frac{1}{2}(\sigma_s^2 + \sigma_b^2)}}$$

(μ_s, σ_s) and (μ_b, σ_b) are the mean and standard deviation) for the shuffled and bootstrapped measure, respectively. We compared d' and receiver operating characteristic curves. And they were in perfect agreement.

4. Encoding of Visual Motion Speed in the Retrosplenial Cortex

4.1. ABSTRACT

The ability of perceiving visual motion speed is essential for survival in a dynamic visual world during spatial navigation and escaping behavior. The mouse visual system contains neurons that are sensitive to visual motion speed. However, how visual motion speed is represented beyond the early visual system and the potential pathway that employs this information to guide behavior and navigation remains little known. We combined 2-photon calcium imaging with a treadmill apparatus and studied the neural encoding of visual motion speed in the mouse retrosplenial cortex (RSC) which connects the visual cortex and the hippocampal and parahippocampal regions. We used grating stimuli with different combinations of spatial and temporal frequencies. We identified a subpopulation of RSC neurons with selectivity to the direction, orientation, and speed of the moving gratings. The preferred speeds for anterior-posterior motion and upward motion were highly correlated (only 1/3 of neurons showed speed selectivity to both directions). Similar to the visual cortex, most of the visually responsive neurons in RSC showed enhanced responses during locomotion; however, neurons tuned to the speed of anterior-posterior motion showed the lowest increase by movement. The visual responsiveness differs among different RSC sub-regions, with the agranular part showing the highest fraction of visually responsive neurons. Lastly, these visually responsive neurons formed a separate population from RSC place cells that showed location-specific activity, suggesting RSC may use independent streams for processing allocentric (e.g. spatial) and

egocentric (e.g. visual) information. Combined with its unique anatomical placement, coding of visual motion speed in RSC may underlie an important pathway by which behavioral correlates of visual information transfer to higher cortical and subcortical areas.

4.2. INTRODUCTION

When moving in an environment, animals compute self-motion from various sensory and motor sources, including proprioception, motor efference copy, vestibular inputs, and visual motion. The ability to precisely estimate self-motion is a prerequisite of forming accurate spatial representations in the hippocampal and parahippocampal regions (Chen et al 2013a, Terrazas et al 2005), which can in turn be used to guide behavior. Extensive human and primate studies suggest that optic flow can be a powerful source for sensing self-motion (Kleinschmidt et al 2002, Lappe et al 1999, Mohler et al 2007a, Mohler et al 2007b). Integrating the translational and rotational speed of optic flow over time contributes to the estimation of linear travelling distance and rotation degree, i.e. path integration (Bremmer & Lappe 1999, Etienne & Jeffery 2004, Frenz et al 2003, Frenz & Lappe 2005, Kearns et al 2002, Lappe et al 2007).

Mice studies have shown vision and locomotion are sufficient for the formation of place cell and grid cell representation in the hippocampal formation (Aronov & Tank 2014, Dombeck et al 2010, Domnisoru et al 2013, Harvey et al 2009). Visual motion includes the direction and speed of elements moving in a visual scene. During head-fixed virtual navigation, online feedback of visual motion speed and landmarks during self-motion is helpful for precise estimation

of current location (Chen et al 2013a, Chen et al 2016). In mice, visual motion speed selectivity already occurs in the thalamic lateral geniculate nucleus (LGN), which exhibits direction and orientation selectivity (Piscopo et al 2013, Zhao et al 2013). Downstream of LGN, primary and secondary visual cortices contain neurons that are tuned to the speed of visual motion (Andermann et al 2011, Niell & Stryker 2010, Priebe et al 2003, Priebe et al 2006). How visual motion speed is coded beyond this early visual system has been little studied in mice.

The retrosplenial cortex (RSC) gates information flows between diverse brain areas, including the hippocampal system, the thalamus, and neocortical sensory and motor areas (Cenquizca & Swanson 2007, Czajkowski et al 2013, Miyashita & Rockland 2007, Shibata 1993, van Groen & Wyss 1990, van Groen & Wyss 1992, Van Groen & Wyss 2003, Vogt & Miller 1983, Yamawaki et al 2016). As a major component along the dorsal visual stream and one of the only neocortical regions that receive dense hippocampal projections, RSC is shown to be responsive to visual stimulus and contain place cell-like positional signals (Murakami et al 2015) (Mao et al). However, it is currently unclear how visual motion speed is coded in RSC and how RSC visually responsive neurons interact with RSC place cells. Studying this could potentially contribute to our understanding of the postulated role of RSC in transforming between allocentric (e.g. place) and egocentric (e.g. optic flow) representations (Alexander & Nitz 2015, Burgess et al 2001, Epstein 2008).

We performed cellular imaging in RSC of head-fixed locomoting mice expressing genetically encoded Ca^{2+} indicator GCaMP6. We found that a

subpopulation of RSC neurons is selective for the direction and speed of visual motion. We hypothesize RSC may be particularly important for routing behavioral correlates of sensory information from the visual system to higher cortical areas to guide navigational behavior.

4.3. MATERIALS AND METHODS

Animals and Surgery

All animal procedures were performed in compliance with the protocols approved by the ethical research committee of Katholieke Universiteit of Leuven. Nine male C57BI/6j mice (~22-30 g, ~2-4 months at the time of surgery) were used for this study. Mice were injected with dexamethasone (3.2 mg/kg, intramuscular) minimum 2 hours before surgery. During surgery, mice were anesthetized with isoflurane (1-1.5%, O_2: 0.5-1 L/min) and body temperature was maintained at 37 °C. A custom-made head-plate was attached to the skull using adhesive cement (C&B-metabond, Parkell) and acrylic material (TAB 2000, Kerr). A 3 mm craniotomy was made with a dental drill (600 µm tip) above the left retrosplenial cortex (Kirkcaldie 2012). The craniotomy was rinsed and covered with artificial cerebrospinal fluid (ACSF). Injections of solution containing AAV2.1/Syn.GCaMP6m (Chen et al 2013b) were made with a beveled micropipette at 0.5 mm ML axis and 1 mm from transverse sinus. 1 µL viral solution was mixed with 0.3 µL sulforhodamine SR101 for fluorescent monitoring. Vector solution was injected at 2 depths (750 µm and 250 µm deep). Each site was injected with ~200 nL solution at low speed (9.2 nL/pulse, 15 sec interval) using a nanoliter injector (Nanoject II, Drummond Sci.). A cranial window made of

3 circular (one 5 mm, two 3 mm) coverslips (affixed with optical adhesive NOA71, Norland) was implanted and attached to the skull with Vetbond tissue adhesive (3M) (Goldey et al 2014). For the prism window, a 5 mm circular coverslip, a 3 mm circular coverslip, and a 1 mm right angle prism (the hypotenuse was coated with a thin layer of aluminum) were affixed together. For the implantation of the prism window, a slit in the dura of the right hemisphere was made next to the midline. The prism window was hold by vacuum and slowly pushed down vertically into the midline of the right hemisphere.

Visual Stimulation

A 22'' LED monitor (Samsung 2233RZ, 1680x1050 resolution, 60 Hz refresh rate) was positioned 18 cm in front of the right eye, covering 120 by 80 degree in the right visual field (0–120 deg, central to peripheral and ± 40 deg, lower to upper visual field). Presentation software (Neurobs) was used to control visual stimulation, synchronized to the respective imaging frame rates of the 2-photon (30.9 frames per second) imaging. Visual stimuli were interleaved by a grey screen stimulus (50 % luminance).

Two-photon Imaging

A custom-built 2-photon microscope (Neurolabware) was used. A Ti:Sapphire excitation laser (MaiTai DeepSee, Spectra-Physics) was operated at 920 nm (~20-60 mW laser power at the sample). Laser scanning was controlled by galvo and resonant scanners (Cambridge 6215H and CRS 8K) through a 16x lens (NA = 0.8, Nikon). Green fluorescence from GCaMP6m was collected using a band-pass filter (510/84 nm, Semorock) with a GaAsP photomultiplier tube (PMT,

Hamamatsu). Blackout fabric (Thorlabs) was used to prevent stray light from entering the objective and PMTs. Custom-made software was used to control microscope movement and acquisition. Images were collected at ~30.9 Hz. Imaging sessions normally lasted ~10 min.

Data Analysis

Image pre-processing

Analysis was performed using Matlab (R2014b, Mathworks). Time-series datasets were corrected for motion artifacts using TurboReg (Thevenaz et al 1998). Regions of interest were identified using morphometric filters (Ohki et al 2005). Neurons that were active during the acquisition session were identified by local correlation of 3 x 3 pixels through time. Correlation threshold was set at 0.95 to select all active neurons. The baseline-subtracted dF/F0 was calculated for each ROI using the summed value of all pixels corresponding to that ROI (Bonin et al 2011) by subtracting the summed value of a single layer of pixels that surround the cell body (Chen et al 2013b). The time-courses were deconvolved to infer underlying firing rates (Pnevmatikakis et al 2016, Vogelstein et al 2010).

Visual responsiveness and speed tuning

Visually responsive neurons were identified as the neurons having significantly different activity between within-stimulus (0-2 second) and pre-stimulus responses (-1-0 second, 0 is the stimulus onset) (One-way ANOVA, $p < 0.01$) and the average within-stimulus responses should be at least 5% higher than pre-stimulus responses. In the spatial frequency-temporal frequency (SF-TF) analysis, the average responses were mapped onto the SF-TF space. The

response map was fit by a two-dimensional Gaussian (Priebe et al 2003, Priebe et al 2006):

$$R(sf, tf) = A\, exp\left(\frac{-(log_2 sf - log_2 sf_0)^2}{2(\sigma_{sf})^2}\right) exp\left(\frac{-(log_2 tf - log_2 tf_p(sf))^2}{2(\sigma_{tf})^2}\right)$$

$$log_2 tf_p(sf) = (Q+1)(log_2 sf - log_2 sf_0) + log_2 tf_0$$

and A if the peak response, sf_0 and tf_0 are the neuron's preferred SF and TF. $tf_p(sf)$ is the preferred TF given the corresponding SF. σ_{sf} and σ_{tf} are the tuning widths along the SF and TF dimensions. The dependence between SF and TF is captured by $Q + 1$, which measures the linear relationship between SF and TF in log space. Speed tuned visual neurons must satisfy: 1) Tangent of $Q + 1$ is between 0.5 and 3; 2) Width of the fit ellipse is no more than 4 along the major axis and no more than 1 along the minor axis.

Orientation and direction selectivity

For all visually responsive neurons, orientation selective neurons were identified by one-way ANOVA ($p < 0.01$) comparing responses to the 4 orientations and based on the orientation selectivity index (OSI, > 0.33) (Ohki et al 2005). Direction selective neurons were identified by one-way ANOVA ($p < 0.01$) comparing responses to the 8 directions and based on the direction selectivity index (DSI, > 0.33).

Orientation selectivity index (OSI) was calculated as:

$$OSI = \frac{R_p - R_{or}}{R_p + R_{or}}$$

where R_p is the response to the preferred orientation and R_{or} is the response to the orthogonal orientation.

Direction selectivity index (DSI) was calculated as:

$$DSI = \frac{R_p - R_{null}}{R_p + R_{null}}$$

where R_p is the response to the preferred direction and R_{null} is the response to the 180° direction from the preferred direction.

4.4. RESULTS

We adapted a linear treadmill apparatus in which mice were head-restrained and voluntary to move the track belt (Royer et al 2012). We presented grating stimuli with multiple combinations of spatial and temporal frequencies. We imaged neuronal activity in RSC and studied their correlates with visual stimuli, locomotion, functional organization, as well as RSC place cells.

4.4.1. Visual Motion Speed Selectivity in RSC

To study visual motion speed coding in RSC in a well-controlled manner, we used a treadmill assay combined with visual stimulation. Mice were trained to be head-fixed and voluntarily move or stay still on the treadmill belt. Visual stimulation screen was placed 18 cm in front of the right eye and it covered a visual angle from 0° to 120° in azimuth (Figure 4.1A). We expressed calcium indicator GCaMP6m in RSC (Chen et al 2013b, Goldey et al 2014). We first studied the neuronal activity in the superficial agranular RSC (Figure 4.1A, black

square) (n = 7 animals, 19 sessions), which is adjacent to the medial visual areas (Roth et al 2012, Wang et al 2012).

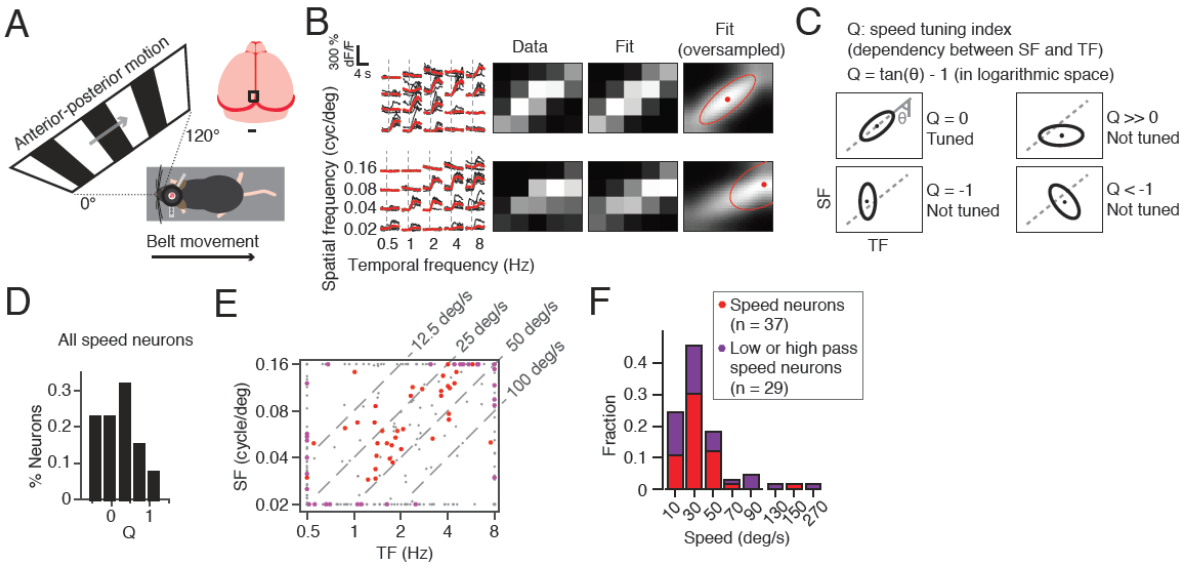

Figure 4.1 Speed tuning to anterior-posterior motion **in RSC**

A, Diagram of the experiment. Vertical gratings with different spatial/temporal frequencies were used to emulate anterior-posterior motion. The moving direction of the grating is indicated as the gray arrow. The mouse was head-fixed and voluntarily moved a treadmill belt. The visual stimulation screen was positioned 18 cm in front of the right eye of the mouse, covering a visual field approximately 0° to 120°. Two-photon calcium imaging was performed in RSC (FOV indicated as the black square in the inset) of the left hemisphere. Scale bar, 1 mm.

B, Spatial-temporal frequency responses of two example RSC neurons. Left, response map to different spatial/temporal frequency combinations for multiple trials (black traces). Red traces indicate the average responses. Dashed lines indicate stimulus onsets. Each stimulus lasted 4 second. Data, normalized color map representation of the average response map. White, high responses; black, low responses. Fit, the response map after a 2-D Gaussian fitting. Fit (oversampled), response map after up-sampling (6 times) and 2-D Gaussian fitting. The red dots represent the centers of the Gaussian fit. The red ellipses represent 68% contours (one standard deviation).

C, Illustration of the quantification of speed tuning. The speed tuning index Q was defined as the tangent function of the angle between the major and minor axes of the fitted Gaussian model (in logarithmic space) minus one. Q = 0 meant perfect speed tuning. Q >> 0 or Q <= -1 meant the neuron is not tuned for visual speed.

D, Distribution of the speed tuning index Q for all RSC neurons that were tuned to the speed of anterior-posterior motion (n = 66).

E, Scatter of the centers of fitted model in the spatial-temporal frequency space. Red dots represent speed neurons of which the fitted centers do not fall on the edge of spatial or temporal axis (n = 37). Magenta dots represent speed neurons of which the fitted centers fall on either spatial or temporal axis (low or high pass in spatial or temporal axis) (n = 29). Gray dots represent other visually responsive neurons. Dashed lines correspond to different speeds of the anterior-posterior motion.

F, Distribution of the preferred speeds of all RSC speed neurons. Note similar distribution between low or high pass speed neurons and other speed neurons.

We emulated anterior-posterior motion by presenting vertical gratings moving from the center to the pheriphery of the visual field with different combinations of spatial frequency (SF) and temporal frequency (TF) (Figures 4.1A and 4.1B). Calcium fluorescence signals of neuronal cell bodies were mapped onto the SF-TF space (Figure 4.1B). The speed of each SF-TF combination was defined as the TF divided by the SF, resulting in the unit of degree per second. Thus, the SF-TF combinations with the same speed constituted 45° lines in our SF-TF space (Figure 4.1E). If a certain neuron exhibits significantly heightened responses along any of the 45° lines, this neuron is selective for the corresponding speed (e.g. Figure 4.1B). We adapted a speed tuning index Q to measure the speed selectivity (Figure 4.1C) (See Materials and Methods) (Priebe et al 2003, Priebe et al 2006). Q measures the dependency between SF and TF. Q was estimated from an orientated two-dimensional Gaussian model fit onto the mean response map in the SF-TF space (Figure 4.1B). If the model shows major axis with 45° orientation (i.e. Q = 0), it indicates a perfect speed tuning (Figure 4.1C). We identified visually responsive neurons with Q between -0.5 and 1.5 and widths along the major and minor axes within certain range as speed tuned neurons (n = 66 speed neurons, 263 visual neurons, 1629 neurons in total; Q = 0.19 ± 0.46, mean ± std) (Figure 4.1D) (see Materials and Methods). The centers of the Gaussian models of speed neurons spread broadly in the SF-TF space, indicating a wide range of tuned speeds across the population (Tuned speed: 4.1 ~ 268.0 deg/s; tuned speed = 11.3, 33.8, 67.9 deg/s; 10, 50, 90 percentiles) (Figures 4.1E and 4.1F). Some speed

neurons showed low or high pass properties in either SF or TF dimension (n = 29/66 speed neurons) (purple dots in Figure 4.1E), likely due to our limited sampling in the SF-TF space. These speed neurons had similar distribution of preferred speeds to other speed neurons (Figure 4.1F). The median of the tuned speeds was ~34 deg/s, which corresponded to a translational speed of ~11 cm/s in our case.

While anterior-posterior motion is mostly encountered during translational or rotational movement, the detection of up and down visual motion is also essential for daily life, for example when detecting predators for rodents. To study how RSC neurons encode visual motion speed in this dimension, we presented upward-moving gratings with rich combinations of SF and TF (Figures 4.2A and 4.2B). We found a subset of RSC neurons are strongly tuned to the speed of upward motion (n = 44 speed neurons, 184 visual neurons, 1205 neurons in total; Q = 0.11 ± 0.40, mean ± std) (Figures 4.2B and 4.2C). The tuned speeds ranged from 9.0 to 177.4 deg/s, with 80% neurons tuned for speeds between 15.1 and 47.2 deg/s. Similarly, some of these speed neurons exhibited low or high pass properties in either SF or TF dimension (n = 22/44 speed neurons) (light blue dots in Figure 4.2D). The speed neurons showed consistent distributions of tuned speeds (Figure 4.2E).

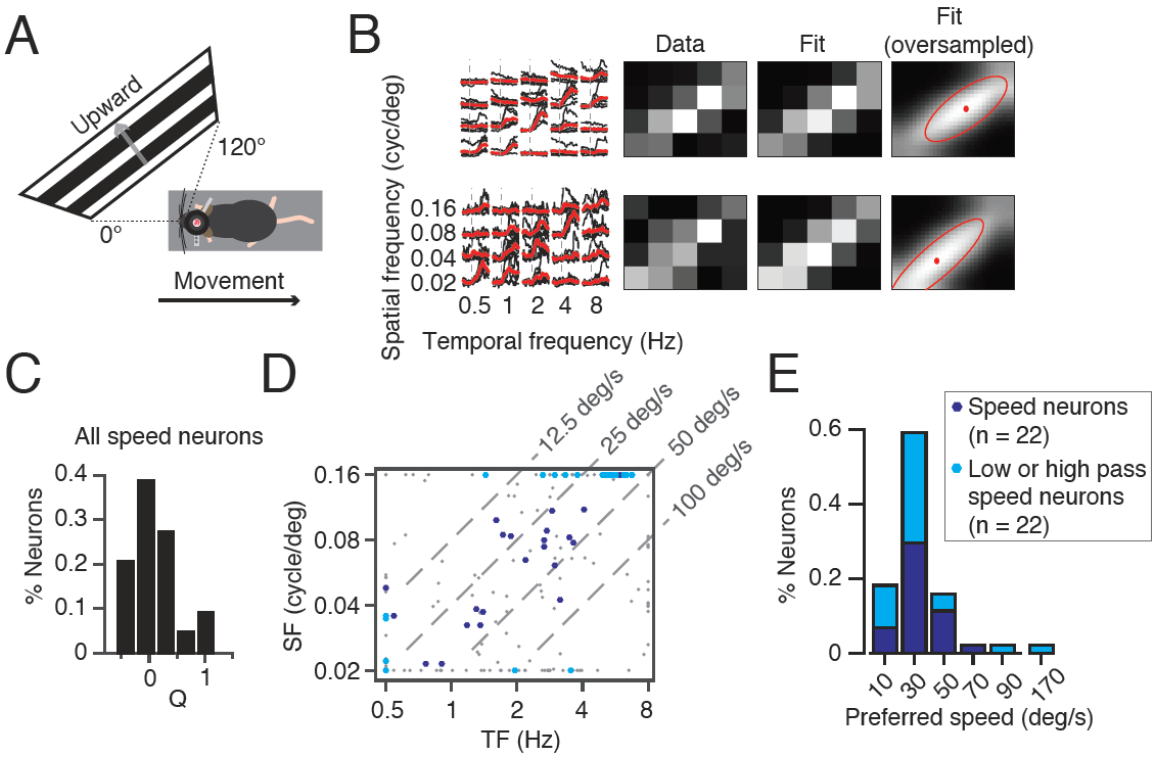

Figure 4.2 Speed tuning to upward motion in RSC

A, Diagram of the experiment. Horizontal gratings with different spatial/temporal frequencies were used to emulate upward motion. The moving direction of the grating is indicated as the gray arrow.

B, Spatial-temporal responses of two example RSC neurons. Left, response map to different spatial/temporal frequency combinations for multiple trials (black traces). Red traces indicate the average responses. Dashed lines indicate stimulus onsets. Each stimulus lasted 4 second. Data, normalized color map representation of the average response map. White, high responses; black, low responses. Fit, the response map after a 2-D Gaussian fitting. Fit (oversampled), response after up-sampling (6 times) and 2-D Gaussian fitting. The red dots represent the centers of the Gaussian fit. The red ellipses represent 68% contours (one standard deviation).

C, Distribution of the speed tuning index Q for all RSC neurons that were tuned to any speed of upward motion (n = 44).

D, Scatter of the centers of fitted model in spatial-temporal frequency space. Dark blue dots represent speed neurons of which the fitted centers do not fall on the edge of spatial or temporal axis (n = 22). Light blue dots represent speed neurons of which the fitted centers fall on either spatial or temporal axis (low or high pass in spatial or temporal axis) (n = 22). Gray dots represent other visually responsive neurons. Dashed lines correspond to different speeds of the upward motion.

E, Distribution of the preferred speeds of all RSC speed neurons. Note similar distribution between low or high pass speed neurons and other speed neurons.

Next we asked if the neurons tuned to the speed of anterior-posterior motion and the neurons tuned to the speed of upward motion are distinct subsets of neuronal populations. To study this, we imaged neurons under the presentation of anterior-posterior motion and upward motion in blocks in a subset of animals (n = 4 animals, 5 sessions, 660 neurons in total) (Figure 4.3A). Within this neuronal population, we identified 21 neurons are selective for the speed of anterior-posterior motion and 22 neurons are selective for the speed of upward motion (n = 119 responsive to anterior-posterior motion; n = 102 responsive to upward stimulus). Twelve neurons were tuned to the speed of both anterior-posterior motion and upward motion (Figure 4.3B). The preferred speeds of these neurons to anterior-posterior motion were significantly correlated with their preferred speeds to upward motion ($r = 0.82$, $p = 0.0012$) (Figure 4.3C).

Together, RSC contains neurons that are tuned to the speed of anterior-posterior motion and/or upward motion. RSC neurons selective for the speeds of both directions have consistent tuned speeds.

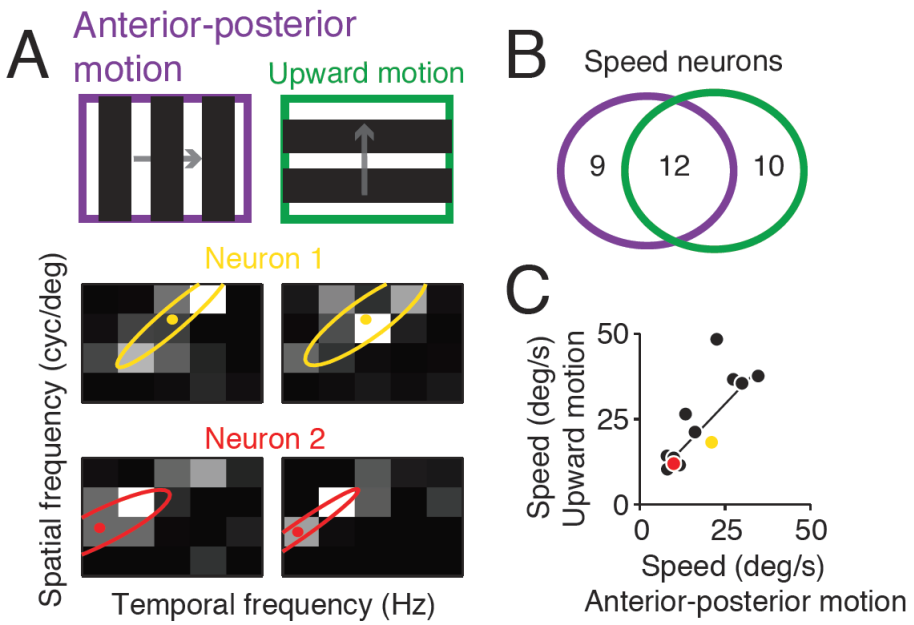

Figure 4.3 Correlated speed tuning to anterior-posterior motion **and upward motion**
A, Response map of two example RSC neurons to anterior-posterior motion (left) and upward motion (right). Ellipses represent 68% contours (one time standard deviation) of 2-D Gaussian fits. Filled dots represent centers of the fits.
B, Set representation of the count of neurons selective to the speed of anterior-posterior motion (within the purple ellipse) and upward motion (within the green ellipse). Twelve neurons (intersection) were selective to the speeds of both anterior-posterior motion and upward motion.
C, Scatter plot of the tuned speeds to anterior-posterior motion and upward motion for the 12 neurons that fall in the intersection in **B**. The red and yellow dots correspond to the example neurons in **A**. The straight line represents robust linear fit ($r = 0.82$, $p = 0.0012$).

4.4.2. The Effect of Locomotion on Visual Responsiveness in RSC

Locomotion significantly enhances visual responses in the primary visual cortex and even the visual thalamus (Erisken et al 2014, Niell & Stryker 2010). The circuit mechanism underlying this effect involves a cholinergic innervation from the basal forebrain which projects widely to cortical and subcortical regions (Pinto et al 2013). To study if RSC visual responsiveness is also influenced by behavioral states, we compared the average visual responses during running and

during stillness. The majority of visually responsive neurons showed increased responses during movement (Figures 4.4A and 4.4B). The mean activity of neurons responsive to anterior-posterior motion increased from 0.58 ± 0.03 during stillness to 0.71 ± 0.04 (all mean ± s.e.m., dF/F(%)/s; p = 7.8e-40, paired t test) during locomotion (n = 180). Neurons responsive to the upward motion exhibited a similar increase (from 0.43 ± 0.02 to 0.61 ± 0.04; all mean ± s.e.m., dF/F(%)/s; n = 148; p = 7.7e-55, paired t test). We then examined if speed-selective RSC visual neurons show the same degree of response enhancement by movement. Interestingly, visual neurons selective for the speed of anterior-posterior motion (n = 37/180) had significantly lower increase than other visual neurons (p = 0.012, unpaired t test; visual neuron = 71 ± 10 % (n = 143, excluding speed neurons), speed neuron = 19 ± 9 % (n = 37); all mean ± s.e.m.; relative increase in response during moving (%)). Visual neurons selective for the speed of upward motion did not exhibit such a property (p = 0.77, unpaired t test; visual neuron = 66 ± 19 % (n = 113, excluding speed neurons), speed neuron = 60 ± 10 (n = 35); all mean ± s.e.m.; relative increase in response during moving (%)) (Figure 4.4C). This may reflect a balanced effect of real locomotion and perceived external motion on the RSC visual responsiveness.

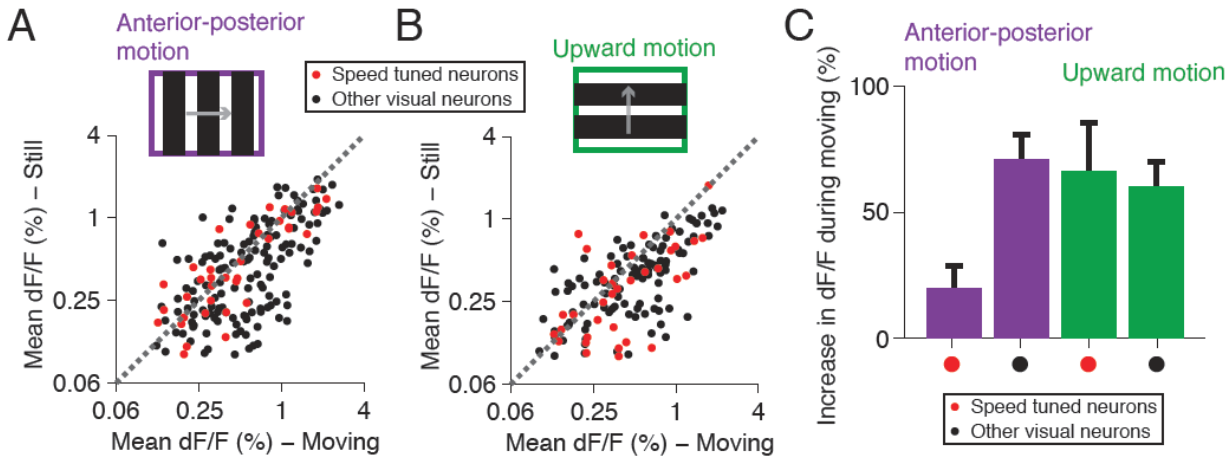

Figure 4.4 The effect of locomotion on RSC visual responses

A, Scatter plot of the mean activity (dF/F/s, %/s) during moving and still epochs for RSC neurons that were responsive to anterior-posterior motion stimuli (n = 180). Red dots indicate speed tuned neurons (n = 37). The dashed line represents unity line. Note the axes are plotted in log scale.

B, Scatter plot of the mean activity (dF/F/s, %/s) during moving and still epochs for RSC neurons that were responsive to upward motion stimuli (n = 148). Red dots indicate speed tuned neurons (n = 35). The dashed line represents unity line. Note the axes are plotted in log scale.

C, Bar plot of the increase in mean activity during moving for all RSC visually responsive neurons (error bars: mean ± s.e.m.). Purple bars correspond to RSC neurons responsive to anterior-posterior motion (19 ± 9 % and 71 ± 10 %); green bars correspond to RSC neurons responsive to upward motion (60 ± 10 % and 66 ± 19 %). The red and black dots in the label of x axis correspond to speed neurons and other visual neurons, respectively.

4.4.3. Functional Organization of RSC Visual Neurons and Speed Cells

RSC is an elongated neocortical region that sits in the posterior medial cerebral cortex. RSC consists of two subregions, agranular and granular parts. Agranular and granular RSC have distinct connections with cortical and subcortical regions (van Groen & Wyss 1992, Van Groen & Wyss 2003). To examine if RSC visual responsiveness is also anatomically different, we correlated the count and ratio of visual neurons and speed cells with their anatomical locations in RSC. First, we examined how RSC visual activity is organized along the anterior-posterior axis in

the superficial agranular RSC (Figure 4.5A). For all the mice, we mapped the imaging planes onto the mouse brain atlas using the superior sagittal sinus and traverse sinus as references (Figure 5.5A). We did not observe a systematic change in the percentage of either visual neurons or speed cells from anterior to posterior RSC (anterior-posterior motion, visual neuron, $r = 0.44$, $p = 0.32$; speed neuron, $r = 0.11$, $p = 0.82$; upward motion, visual neuron, $r = -0.04$, $p = 0.93$; speed neuron, $r = -0.36$, $p = 0.43$; all Pearson's correlation) (Figure 4.5B). The lateral RSC is anatomically more adjacent to the visual cortex than the medial RSC. We then asked if visual neurons in superficial agranular RSC are more prevalent in the lateral portion. We did not observe such a tendency for neurons tuned to the anterior-posterior motion ($r = -0.07$, $p = 0.89$; Pearson's correlation) (Figure 4.5C). However, there was a trend that fewer neurons were responsive to the upward motion in the more medial RSC ($r = -0.83$, $p = 0.0393$; Pearson's correlation), which is in line with its anatomical positioning.

Compared to agranular RSC, the granular RSC positions more closely to the midline and the superficial layers are beneath the superior sagittal sinus. Conventional imaging preparation is difficult to monitor many superficial granular RSC neurons simultaneously (Figure 4.5D). To overcome this, we adapted an imaging window composed of coverslips and a prism (Andermann et al 2013, Chia & Levene 2009) (Figure 4.5E). Visually responsive neurons were more prevalent in the superficial agranular RSC and superficial granular contained the lowest proportion of visual neurons ($p = 9.1718e-04$, One-way ANOVA) (Figure

4.5F). The superficial granular RSC also had the lowest percentage of speed cells out of visual neurons ($p = 0.0156$, One-way ANOVA) (Figure 4.5F).

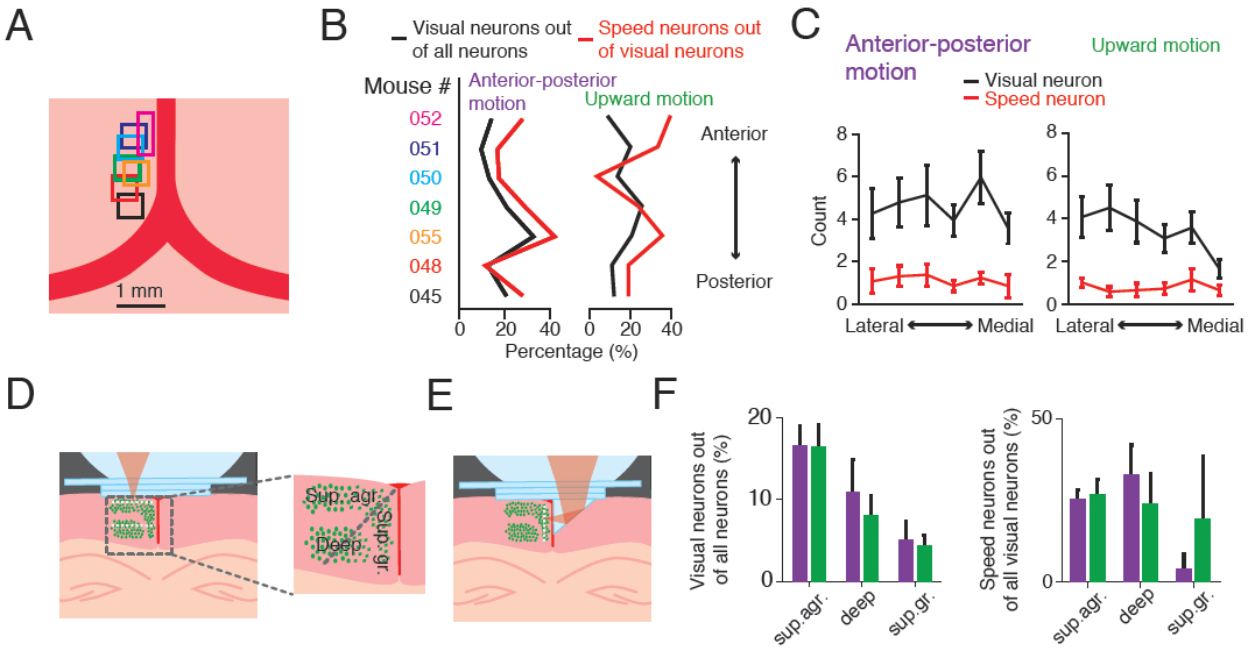

Figure 4.5 Functional organization of RSC spatial and temporal frequency responses

A, Qualitative mapping of imaging planes of different animals (colored rectangles) onto brain atlas. Different colors correspond to different animals. Thick red lines represent superior sagittal and traverse sinuses.

B, Percentage of visual neurons (black) and speed neurons (red) for different animals for both anterior-posterior motion (left) and upward motion (right). Mouse IDs are indicated on the left. Mouse IDs were ordered according to the position of their imaging planes along the anterior to posterior axis.

C, Count of visual neurons (black) and speed neurons (red) for anterior-posterior motion (left) and upward motion (right) stimuli. Note a gradual decrease in the number of visual neurons to upward motion from lateral to medial. Error bars, s.e.m.

D, Diagram of imaging in different subregions in RSC, including superficial agranular (sup. agr.), superficial granular (sup. gr.), and deep subregions. Green dots represent neurons labeled with GCaMP6m. Layer IV neurons were not labeled. White dashed lines indicate imaging planes (axial planes). Light red triangle represents laser beam.

E, Diagram of imaging in superficial granular RSC using a prism. White dashed line indicates imaging plane (sagittal plane). Light red triangles represent laser beam.

F, Bar plots of percentages of visual neurons and speed neurons in all RSC subregions for anterior-posterior motion (purple) and upward motion (green) stimuli. Error bars: s.e.m.

4.4.4. Orientation and Direction Selectivity in RSC

We then studied the orientation and direction selectivity in the superficial agranular RSC. We presented grating stimuli with 8 moving directions with fixed SF and TF. Consistent with a previous study (Murakami et al 2015), ten percent superficial agranular neurons exhibited robust responses to at least one of the stimuli (10.5 ± 2.6 %, mean ± s.e.m.; n = 2489 neurons in total) (Figure 4.6B). We calculated the orientation selectivity and direction selectivity for the visually responsive neurons (see Materials and Methods). We identified orientation selective or direction selective visual neurons (selectivity > 0.33) (Figure 4.6B) (Ohki et al 2005). More than 40% of the orientation selective neurons in the superficial agranular RSC were tuned to the vertical gratings (n = 41/94) (Figure 4.6C).

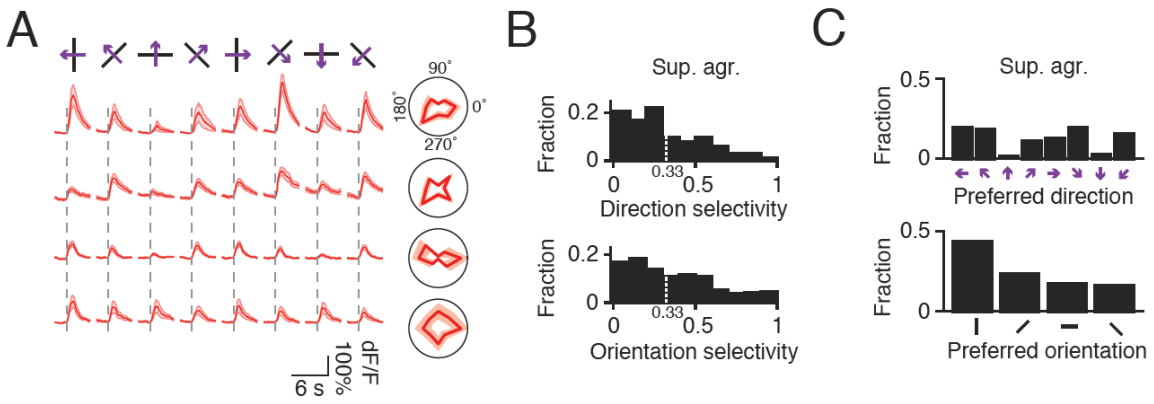

Figure 4.6 Orientation and direction selectivity in RSC

A, Response profiles of 4 example RSC neurons to visual stimuli with 8 moving directions. Dashed lines, stimuli onsets. Right, average responses of the example neurons to the 8 directions in polar plots. Shaded area, s.e.m.

B, Distribution of direction and orientation selectivity for all visually responsive neurons in the superficial agranular RSC (n = 195). Dashed lines correspond to selectivity at 0.33 which was used as the threshold for identifying direction and orientation selective neurons.

C, Distribution of preferred directions and orientations for all direction and orientation selective neurons in the superficial agranular RSC.

4.4.5. Separable Visual Neurons and Place Cells in RSC

RSC contains multiple functional cell types, including head-direction, reward-related, and visual neurons (Chen et al 1994b, Cho & Sharp 2001, Smith et al 2012). We have recently found place cells in RSC, predominantly in superficial layers. It is unclear if RSC visual neurons also exhibit position selectivity or they form functionally independent population from RSC place cells. We asked if RSC visual neurons and place cells were independent populations. RSC place cells exhibited little visual responsiveness while visual neurons did not show pronounced location-locked activity (Figures 4.7A and 4.7B). We used mutual information between neuronal responses and position and visual responsiveness as a measure for position and vision selectivity. The scatter plot demonstrated a separation between place cells and visual neurons (n = 58 place cells; n = 59 visual neurons; n = 643 neurons in total, 5 sessions, 3 mice) (Figure 4.7C). Place cells showed significantly higher position information and much lower visual responsiveness than visual neurons (Position information, p = 1.2603e-09; visual information, p = 4.6136e-13; all unpaired t test) (Figure 4.7C). These two populations make up about 18% of RSC neurons under this paradigm. Thus, RSC contains independent populations encoding visual and position information, reflecting a unique coding of population activity in RSC which connects the hippocampal formation and the visual cortex.

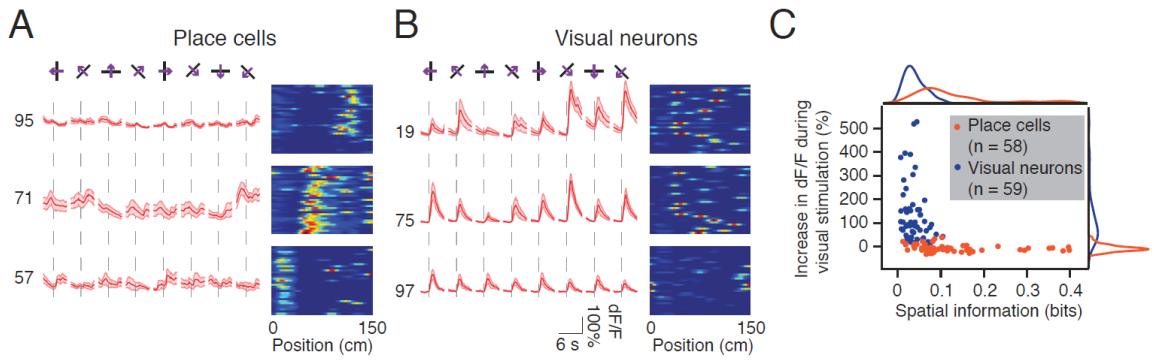

Figure 4.7 RSC visual neurons and place cells form different neuronal populations
A, Left, average response profiles of 3 example RSC place cells synchronized to visual stimuli onsets. Dashed lines indicate stimuli onsets. Shaded area, s.e.m. Neuron IDs are indicated on the left. Right, normalized position activity maps of the neurons shown on the left.
B, Left, average response profiles of 3 example RSC visual neurons synchronized to visual stimuli onsets. Dashed lines indicate stimuli onsets. Shaded area, s.e.m. Neuron IDs are indicated on the left. Right, normalized position activity maps of the neurons shown on the left.
C, Scatter plot of the increase in activity during visual stimulation (relative to pre-stimulus activity) and spatial information (mutual information between neuronal responses and positions) for all RSC place cells (orange dots, n = 58) and visual neurons (blue dots, n = 59). Marginal distributions of the scatter plot are also shown.

4.5. DISCUSSION

We used 2-photon calcium imaging of neurons in the retrosplenial cortex (RSC) of head-fixed behaving mice. We assessed the response properties of RSC neurons to grating stimuli with different combinations of spatial-temporal frequencies, and studied the correlates of the responses with locomotion, functional organization, and RSC place cells. Our main findings are: 1) RSC contained a subpopulation of neurons tuned to the speed of visual motion; 2) a minority of RSC visual neurons were tuned to the speeds of both anterior-posterior motion and upward motion and the tuned speeds were correlated; 3) RSC visual responsiveness was enhanced by running; 4) the agranular RSC

exhibited stronger visual responsiveness than the granular RSC; 5) RSC visual neurons and place cells are distinct neuronal populations. As a transitional region between the neocortex and subcortical regions, RSC is well situated to route the information flow between the hippocampal system and the visual cortex (Cenquizca & Swanson 2007, Sugar et al 2011, van Groen & Wyss 1990, Van Groen & Wyss 2003, Vogt & Miller 1983, Wang et al 2012). Primate and human studies in RSC suggest RSC is a major component in the dorsal visual stream that transmits 'where' and 'how' information (Kravitz et al 2011, Ranganath & Ritchey 2012). Such a link has been lacking in rodent studies. Together with its anatomical placement, we hypothesize that RSC is an important association area that feedforwards behavioral correlates of sensory information to other cortical and subcortical regions. This information flow may be particularly useful for guiding behavior and navigation.

The Similarities and Differences Between Visual Responses in RSC and Visual Cortex

RSC is adjacent to the visual cortex, within which the posteromedial area (PM) provides the major projections to RSC. Our imaging locations are distinct from PM in that PM is about 1.2 mm from the midline while the centers of our imaging windows are typically around 0.5 mm from the midline (Roth et al 2012). Similar as the visual cortex, a recent study shows that RSC exhibits prominent visually evoked activity and direction and orientation selectivity (Murakami et al. 2015). In both the primary visual cortex (V1) and PM, neurons show a preference for

cardinal orientations (Roth et al 2012). We found that RSC neurons show similar preference. More specifically, superficial agranular neurons showed preference for the vertical but not horizontal gratings. Distinct from V1 and PM neurons, RSC neurons showed weaker orientation selectivity (Andermann et al 2011, Roth et al 2012). Consistent with previous studies, we found that RSC contains less than 15% of visually responsive neurons, which is significantly lower than the visual cortex (Murakami et al 2015).

V1 and PM neurons also exhibit selectivity to the speed of visual motion. PM neurons prefer low speed while V1 neurons span a broader range of speed preference (Andermann et al 2011, Marshel et al 2011). Similar as PM but distinct from anterolateral area (AL), our results showed the majority of RSC speed tuned neurons prefer moving speeds in the range of 11 – 68 deg/s (Andermann et al 2011).

Visual responses in the visual cortex are enhanced by locomotion (Andermann et al 2011, Niell & Stryker 2010). We demonstrated that this is also the case for RSC visual neurons. More interestingly, neurons tuned to the speed of vertical gratings had the lowest increase in responses. Optic flow may also evoke illusory feeling of self-motion in the head-fixed animals. Such illusion may interfere with locomotion and this interference may result in different effects of true locomotion on neuronal responses. This may explain our result of lower enhancement by locomotion in neurons tuned to the speed of anterior-posterior motion. This may also reflect a weighted effect on responsiveness between true (internal) and perceived (virtual, external) locomotion speed.

How Could RSC Visual Neurons Relate to Spatial Navigation?

Animals can navigate using external cues (e.g. landmarks) which are independent of animals' movement. They can also navigate using self-motion information, such as vestibular inputs, proprioception, and anterior-posterior motion. Integrating egocentric and allocentric cues gives rise to information about animal's present location. Summing the distance vectors along the outward journey results in a direct route by which animals could return, a process called path integration (Etienne & Jeffery 2004, Mittelstaedt & Mittelstaedt 1982). The hippocampal formation is highly involved in such computation (McNaughton et al 1996). Although neurons in the hippocampal formation show position-locked activity, it is unknown if they are required for successful path integration. Some evidence exists that path integration required for homing task resides outside of the hippocampus (Alyan & McNaughton 1999, Chrastil et al 2015). Consistent with this, RSC lesions impairs performance on both allocentric and egocentric navigation tasks (Pothuizen et al 2008, Ranganath & Ritchey 2012, Vann & Aggleton 2002a, Whishaw et al 2001a). Our findings of visual motion speed tuned neurons in RSC provide a potential mechanism by which path integration could be performed. Integrating the speed of optic flow over time gives rise to travelling distance. A recent study has shown RSC is important for accurate path integration that relies on visual-spatial information (Elduayen & Save 2014). Primate and human studies have also shown evidence for this hypothesis in the posterior cingulate cortex (PCC), that PCC neurons are selective to the motion of

both anterior-posterior motion and vertical movement (Field et al 2015, Fischer et al 2012, Wright et al 2005). And such processing could contribute to distance calculation (Bremmer & Lappe 1999). Detection of visual motion speed contributes to the perception of self-motion, which can be used to control self-movement or heading (Lappe et al 1999). Visual motion speed signals could also travel to the entorhinal cortex, contributing to the generation of speed information and updating the firing of grid cells based on perceived self-motion (Czajkowski et al 2013, Kropff et al 2015, McNaughton et al 2006).

One major role of RSC appears to be transforming egocentric (e.g. anterior-posterior motion) to allocentric (e.g. place code) information (Vann, Aggleton et al. 2009). We showed some evidence that this computation may happen within the local circuit by involving different functional cell types. Besides visual neurons, we observed that a subset of neurons exhibit place-cell like activity. Moreover, RSC visual neurons and place cells are neuronal populations with little overlapping. How these two functional cell types interact within RSC remains to be explored.

Aside from translational visual motion, speed neurons in RSC may also play a role in perceiving rotational motion. Earlier studies in rodent RSC have identified about 10% neurons being head-direction cells, which became active when the animal's head is facing certain directions (Chen et al 1994b, Cho & Sharp 2001). The responsiveness of head direction cells is influenced by how fast the head is passing through that direction. There are several possibilities about how this modulation could happen. One possibility is that there are local

neurons encoding the speed of head rotation, which could exert modulation on head-direction cells. Our results of speed tuned neurons provide evidence for such possibility, in that the anterior-posterior motion (unbalanced between the two sides) might cause illusory feeling of head rotation. Further studies would be required to examine the interactions between RSC head direction cells and RSC visual motion speed neurons.

5. Place Code in the Retrosplenial Cortex

5.1. ABSTRACT

Neurons in retrosplenial cortex (RSC) can convey navigation- or spatial context-related information, but whether they express a population-level place code, such as observed in the hippocampus, is unknown. We combined cellular imaging in RSC with a reward-driven virtual spatial task that reliably drives place cell activity in hippocampal CA1. We identified a subpopulation of RSC neurons, located predominantly in superficial layers, whose activity encodes location in linear environment. These RSC neurons showed firing patterns similar to those observed in CA1 during the same task. As in CA1, they showed highly localized firing and fired in sequences coupled to location during movement. RSC place cell activity was maintained in darkness, and was robust to changes in the reward location. The RSC place code indicates that allocentric representation of the environment is already available in the neocortex, which may be useful for spatially guided behaviour.

5.2. INTRODUCTION

Hippocampal place cell activity is essential for spatial learning and memory, route planning, and navigation (Colgin et al 2008, Eichenbaum et al 1999, O'Keefe & Dostrovsky 1971, Pfeiffer & Foster 2013, Wilson & McNaughton 1994). Although place cell and grid cell activity has been thoroughly described in the hippocampus and the entorhinal cortex, the degree to which place codes are expressed outside the hippocampal formation is unclear, even in its immediately interconnected regions of the neocortex (Knierim 2006). Notably, the retrosplenial cortex (RSC) is densely connected with the hippocampal system (Cenquizca & Swanson 2007, Sugar et al 2011, van Groen & Wyss 1992) and receives direct input from dorsal hippocampal CA1. Lesion and behavioral studies have implicated RSC in spatial processing and contextual memory (Cooper et al 2001a, Hindley et al 2014, Keene & Bucci 2009, Pothuizen et al 2010, Sutherland et al 1988, Vann & Aggleton 2002b, Vann & Aggleton 2005). Inactivating RSC impairs spatial behaviours (Vann & Aggleton 2002b) and path integration in darkness (Elduayen & Save 2014).

Neurons in RSC show rich navigation-related signals including head-direction, speed selective, and goal-related signals (Chen et al 1994a, Cho & Sharp 2001, Smith et al 2012). Recent studies have also shown route encoding in RSC neurons (Alexander & Nitz 2015, Czajkowski et al 2014, Vedder et al 2016) with conjunctive spatial and behavioral correlates (Alexander & Nitz 2015, Cho & Sharp 2001). This activity, however, has limited spatial selectivity and is

unevenly distributed along the route and hence does not meet the essential features of place codes, as observed in the hippocampus.

We performed large-scale calcium imaging of individual neurons across subregions of RSC during a virtual spatial task. We found a subset of RSC neurons that precisely encoded specific locations in a manner that is highly similar to CA1 place cells during the same task. The RSC place code indicates that allocentric representation of the environment is already available in the neocortex, which may be useful for spatially guided behaviour.

5.3. RESULTS

5.3.1. Virtual Spatial Exploration Task and Hippocampal Place Cells

To study spatial encoding in the retrosplenial cortex (RSC) under precise control of sensory inputs, we used a head-fixed, virtual, spatial assay (Royer et al 2012) (Figure 5.2a; see also Materials and Methods). Mice were trained to run laps on a treadmill with local tactile cues and a fixed reward site. The tactile cues, accessible to the paws and the whiskers, were low-profile texture patches attached at multiple locations on the treadmill's surface (Figure 5.1a). To encourage running, a drop of sucrose water was delivered at a fixed location for every completed lap. The animals showed robust locomotor behaviour moving at high speed (18.0 ± 5.6 cm/s, mean ± standard deviation (SD); n = 14 mice, 29 sessions) (Figure 5.2b) with occasional slowdowns or pauses, mostly near the reward site. Experimental sessions lasted 13.0 ± 2.8 minutes (mean ± SD), yielding 36 ± 21 (mean ± SD) laps per session upon which animals encountered precisely the same sequence of cues.

We hypothesized that this combination of sensory, reward and self-motion would engage the animal's navigational system as is observed in freely moving animals. Consistent with this hypothesis, the animals showed highly correlated movement speed patterns across laps (mean trial-to-trial correlation = 0.61 ± 0.17, mean ± SD; n = 14 mice, 29 sessions) and slowed down in approach of the reward location. Hippocampal CA1 neurons showed robust place cell activity during the task (Figure 5.1). Using chronic cellular imaging (Dombeck et al 2010, Goldey et al 2014) (n = 1758 neurons, n = 2 mice, 7 sessions) or

multisite silicon probes recordings (n = 337 neurons, n = 8 mice, 8 sessions), we measured the activity of neuronal populations in dorsal CA1 field of the hippocampus of mice performed the virtual spatial task (Figure 5.1b,e). Consistent with studies in freely-moving animals (Barnes et al 1990), the activity of CA1 neurons was sparse (no. of calcium transients = 0.8, 2.6, 11.3 / min; 10%, 50%, and 90% percentiles, respectively) and the distribution of firing rates was highly skewed (firing rate = 0.6, 1.8, and 4.7 spikes/second; 10%, 50%, and 90% percentiles, respectively). To quantify the spatial modulations of neural activity, responses were expressed as a function of the animal's location on the virtual track, accounting for the time spent at each location. Forty-seven percent (159/337) and 26% (452/1758) of electrically and optically recorded CA1 neurons met established criteria for place cell activity (Figure 5.1c,f) (see Materials and Methods) (Dombeck et al 2010, Mizuseki et al 2012). This was comparable to previous CA1 electrophysiological recordings from the same task (Royer et al 2012) and to findings from CA1 imaging in virtual reality and real environment (Dombeck et al 2010, Ziv et al 2013). In the electrical recordings, CA1 action potentials were locked to low-frequency (5-12 Hz) oscillations in the local-field potential (Figure 5.1c), also similar to previous observations in freely moving animals (O'Keefe & Recce 1993, Skaggs et al 1996). Therefore, CA1 neuronal activity in the task emulated spatially selective activity in freely moving animals.

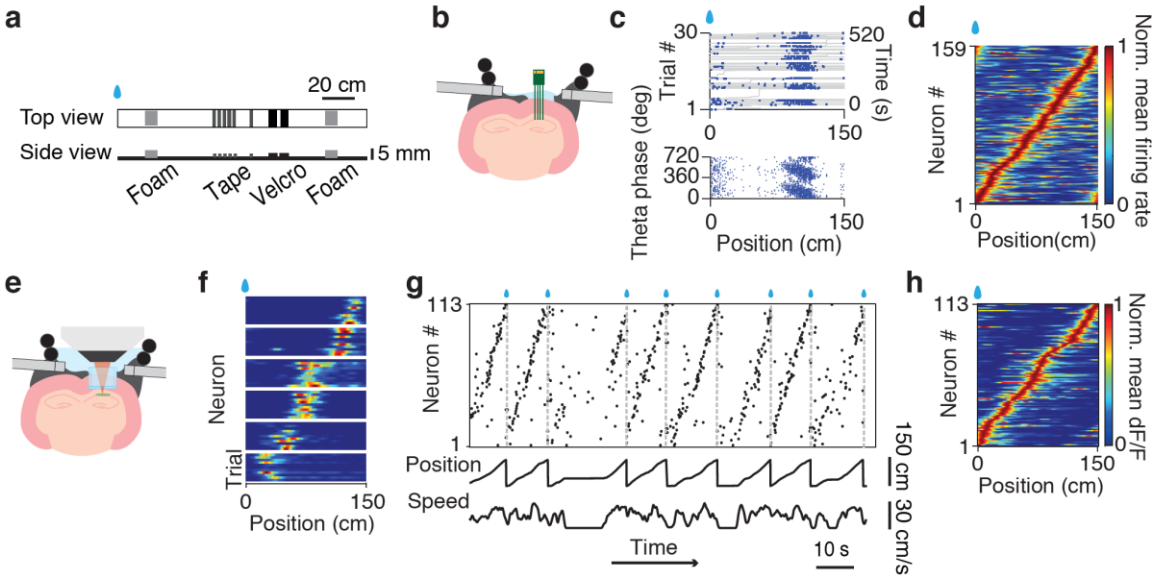

Figure 5.1 Hippocampal place cells during the virtual spatial task

(a) Detailed belt diagram. The treadmill belt was endowed with tactile cues at distinct locations. Blue drop indicates water reward.

(b) Illustration of multi-shank probe recordings in dorsal hippocampus CA1.

(c-d) Electrophysiology results.

(c) Top: raster of an example CA1 place cell in time vs. track position for 30 trials. Blue dots represent spikes. Gray trace indicates locomotion in position and time. Bottom: scatter plot of the example place cell in theta phase and position. Two theta cycles are shown for illustration purposes.

(d) Trial average normalized firing rates for 159 electrophysiologically recorded CA1 place cells from 8 mice ordered by the positions of their peak firing.

(e) Illustration of imaging preparation in dorsal hippocampus CA1 with a glass cannula inserted.

(f-h) Imaging results.

(f) Normalized activity as function of location for 6 example CA1 place cells from one example imaging session, shown for multiple trials.

(g) A section of the raster plot showing activation time points for 113 simultaneously imaged CA1 place cells, for the same session as in (e), together with position and movement speed (bottom). Activation time points were defined as time points of peak response in each lap for each neuron. Cells were ordered by the location that evoked largest responses. Note the repeated activation sequences during movement and lack thereof during stillness.

(h) Trial average normalized activity as a function of location for the 113 place cells in (f).

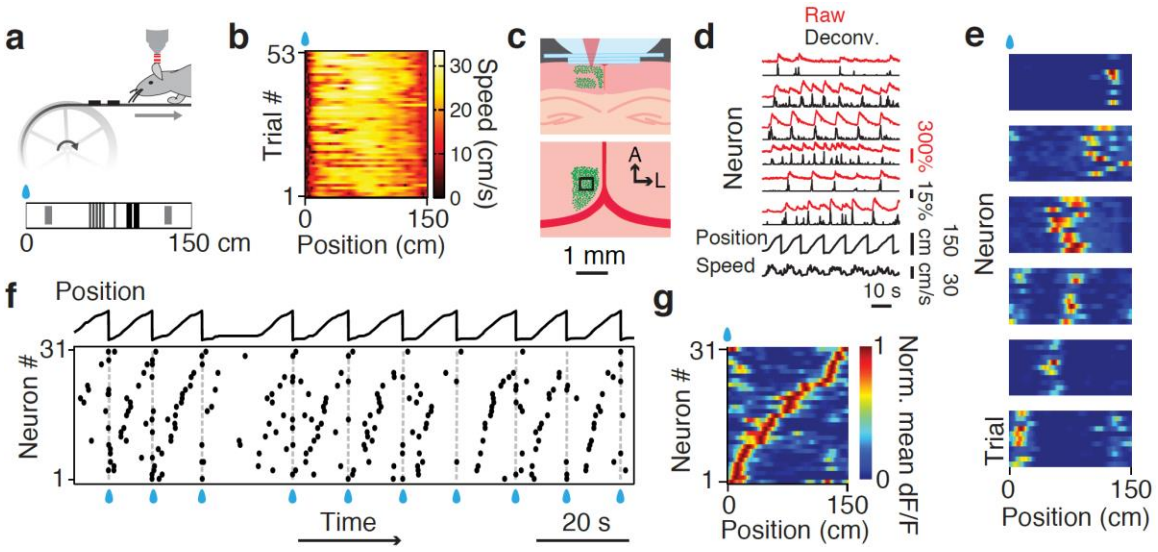

Figure 5.2 Place cells in the retrosplenial cortex

(a) Virtual spatial assay. Mice moved with their heads fixed on a 150 cm linear treadmill (top) with tactile cues (bottom). A sucrose water reward (blue drop) was delivered at a fixed location for every completed lap.

(b) Lap running behaviour. Movement speed as a function of location for 53 laps from one experimental run. The animal moved robustly and slowed down or paused most frequently near the reward (as shown by dark colors on the left).

(c) Cellular imaging of neural activity in the retrosplenial cortex (RSC) during head-fixed navigation. Top: Illustration of superficial and deep RSC neurons labeled with calcium indicator GCaMP6m (green dots). Calcium imaging was performed with a two-photon microscope through a glass window. Bottom: tangential view of the labeled superficial RSC neurons with an example imaging field of view (black square). Red lines indicate superior sagittal sinus and transverse sinuses. Scale bar, 1 mm. A: anterior; L: lateral.

(d) Calcium fluorescence signals (top, red) and inferred neural activity (top, black) of six superficial agranular RSC neurons showing place cell activity, speed, and treadmill position (bottom). Neural activity was inferred using a fast non-negative deconvolution algorithm.

(e) Normalized activity of the six RSC place cells in (d) as a function of location for multiple laps. The y axis in each color map corresponds to trial number. Note how neurons were activated as the animal crossed specific locations. Activity was normalized to the time spent at individual locations.

(f) A section of the raster plot showing activation time points for 31 simultaneously imaged RSC place cells, for the same session as in (e), together with position (top). Activation time points were defined as time points of peak response in each lap for each neuron. Cells were ordered by the location that evoked largest responses. Note the repeated activation sequences during movement and lack of activation when the animal was not moving.

(g) Average normalized activity as a function of location for the 31 RSC place cells shown in (f).

5.3.2. Place Cells in the Retrosplenial Cortex

To study spatial signals in RSC during the same task, we imaged the activity of 2256 superficial agranular RSC neurons (n = 4 mice, 14 sessions, no. of calcium transients = 0.5, 1.6, 8.0 / min; 10%, 50%, and 90% percentiles, respectively) through a cranial glass window implanted over the midline (Goldey et al 2014) (Figure 5.2c). As for CA1 data, calcium fluorescence signals were deconvolved to infer firing rates (Figure 5.2d). A subpopulation of RSC neurons showed robust place cell activity. Thirteen percent (297/2256) of RSC neurons had clear place fields, showing highly selective activity as the animal crossed specific track locations (Figure 5.2e). Similar to CA1 place cells (Figures 5.1d,g,h), the place fields of RSC neurons were distributed over the entire virtual track (Figures 5.2e-g). RSC and CA1 place cells showed sequential activation during movement, with interruptions during epochs of stillness (Figure 5.2f and Figure 5.1g). As CA1, RSC place fields were maintained in darkness (Figure 5.3a–c).

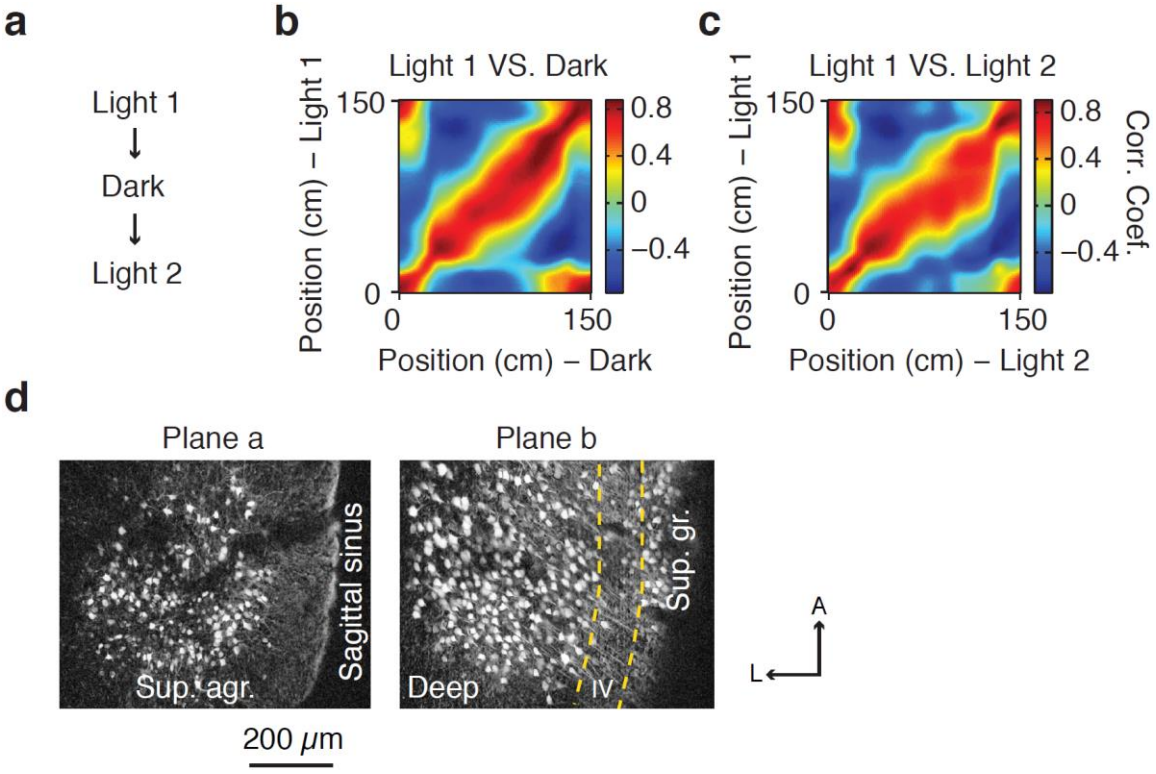

Figure 5.3 Maintenance of RSC position representation in darkness and imaging across RSC subregions

(a) Experiments during light (with a grey screen in front of the mouse during imaging session) and dark conditions. Experiments order: light – dark – light.

(b) Population vector correlation matrix for light (light 1) and dark conditions.

(c) Population vector correlation matrix for light (light 1, before) and light (light 2, after) conditions.

(d) Imaging in dorsal (plane a) RSC yielded superficial agranular (sup. agr.) neurons. White blobs highlight active neurons. Imaging in ventral RSC yielded deep neurons and superficial granular (sup. gr.) neurons. Layer IV (between yellow dashed lines) was not labeled. The midline superior sagittal sinus was visible in the field of view.

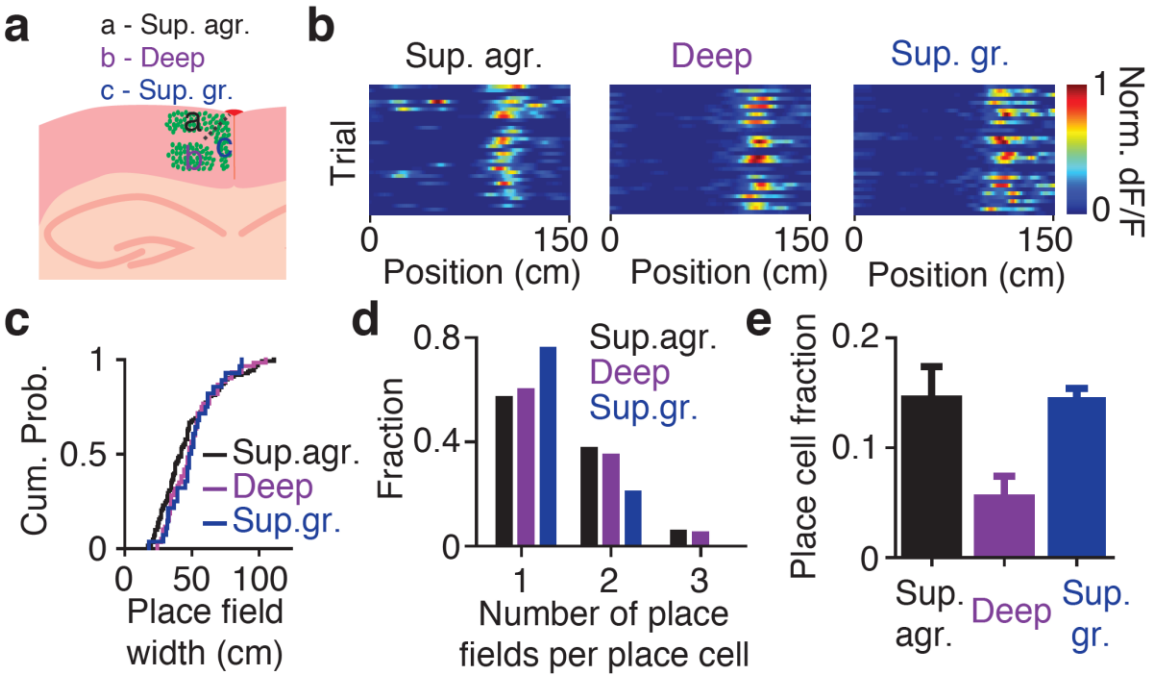

Figure 5.4 RSC place cells are more prevalent in superficial layers

(a) Three RSC sub-regions in the same mouse. Sup. agr.: superficial agranular; Deep: deep agranular and granular; Sup. gr.: superficial granular. Green dots represent GCaMP6m labeled neurons. Imaging at different depths revealed neurons in different sub-regions.

(b) Normalized activity as a function of location for an example superficial agranular place cell (Sup. agr., left panel), an example deep place cell (Deep, middle panel), and an example superficial granular place cell (Sup. gr., right panel). Neurons were imaged in consecutive sessions in the same mouse.

(c) Cumulative probability distributions of place field widths for superficial agranular (black, n = 123), deep (purple, n = 60), and superficial granular (blue, n = 30) RSC place cells.

(d) Distribution of place field count per cell for superficial agranular (black bars), deep (purple bars), and superficial granular (blue bars) RSC place cells.

(e) Place cell fraction in superficial agranular (black bar), deep (purple bar), and superficial granular (blue bar) RSC. Error bars: SEM.

Only the superficial RSC receives direct CA1 output (Cenquizca & Swanson 2007). Consistent with this, we found place cells are mostly in superficial layers of RSC. Place cells were found in the superficial agranular (n = 123/861), superficial granular (n = 31/198), and deep layers (n = 60/1237) of RSC (Figures 5.4a,b and Figure 5.3d). Place cells had similar spatial response properties in the superficial and deep layers of RSC (Figures 5.4c,d); however, there were 2.5 times more place cells in the superficial agranular and superficial granular layers than the deep layers (Superficial agranular: 15 ± 3%; superficial granular: 15 ± 1%; deep layers: 6 ± 2 %; mean ± standard error of the mean (SEM); superficial vs deep, both $p < 0.05$, paired *t* test) (Figure 5.4e). Aside from the laminar preference, we found no evidence of functional organization. Spatial proximity of place fields did not correlate with anatomical proximity ($r = 0.01$, $p = 0.41$, Spearman's correlation), as has been documented in CA1 ($r = -0.01$, $p = 0.14$, Spearman's correlation) (Figure 5.6a) (Dombeck et al 2010, Redish et al 2001).

5.3.3. Similar Properties of Retrosplenial and Hippocampal Place Cells

Place cell activity in RSC and CA1 was similar in several aspects (Figure 5.5a). First, there was a slightly higher density of place fields around the reward location (Figure 5.5b). This is sometimes observed in freely moving animals (Hollup et al 2001). Second, RSC and CA1 place cells had similar spatial response profiles, showing significant activation at mostly one or two locations on the 150-cm track (Figure 5.5d) as well as place fields of similar width (RSC: 39.6 ± 1.2 cm; CA1: 37.0 ± 0.8 cm; both mean ± SEM; $p = 0.57$, two-sample KS test) (Figures 5.5c

and 5.6b). Similarly, the covariance matrix of RSC and CA1 population vectors had a single diagonal structure characteristic of hippocampal activity in linear environments (Figure 5.6c). The width of the covariance matrix diagonals was also similar, indicating that the spatial overlap between pairs of cells is alike (Figure 5.5e).

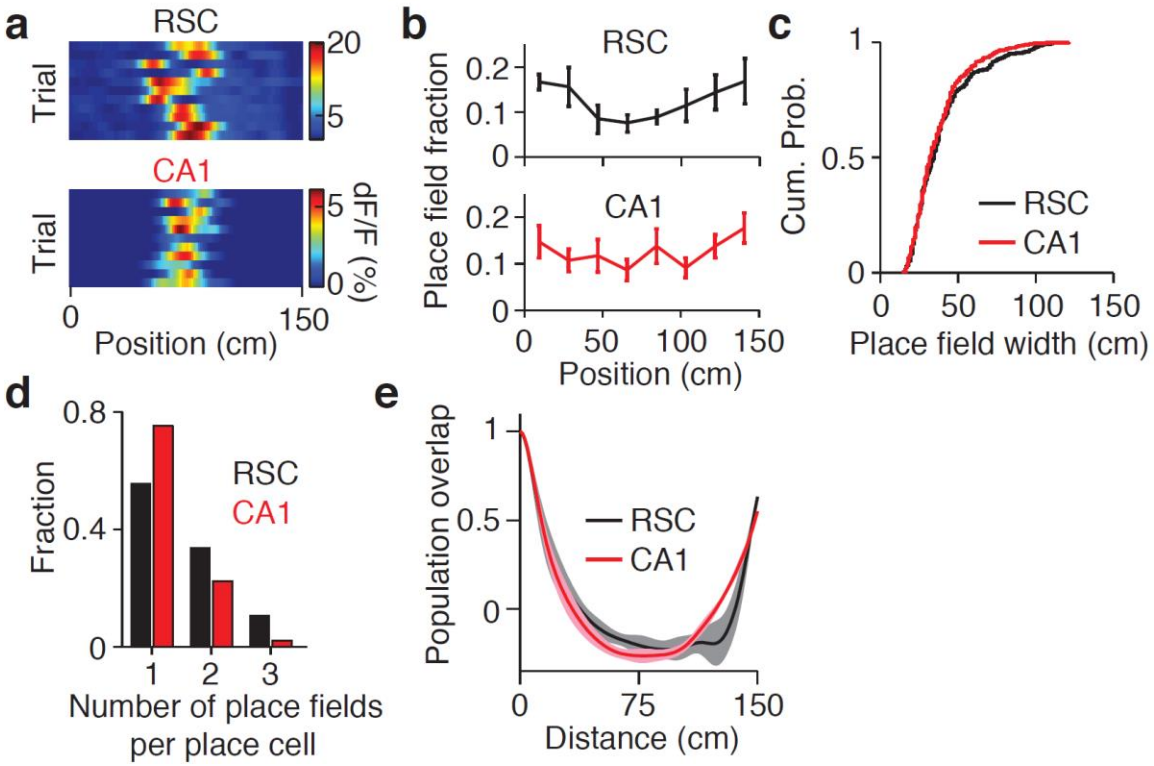

Figure 5.5 Similar spatial response properties between RSC and CA1 place cells
(a) Normalized activity as a function of location for an example RSC place cell (top) and an example CA1 place cell (bottom).
(b) Place field fraction as a function of place field location on the track. Top: RSC place cells (n = 297); bottom: CA1 place cells (n = 159, electrophysiology). Error bars: SEM.
(c) Cumulative probability distributions of place field widths for RSC place cells (black, n = 297) and CA1 place cells (red, n = 452, imaging).
(d) Distribution of place field count per cell for RSC (black bars) and CA1 (red bars) place cells.
(e) Population vector correlation (Pearson correlation coefficient) as a function of distance for RSC (black) and CA1 (red) place cells. Shaded areas represent standard deviation. Note that the periodicity occurred because of the periodicity of the track.

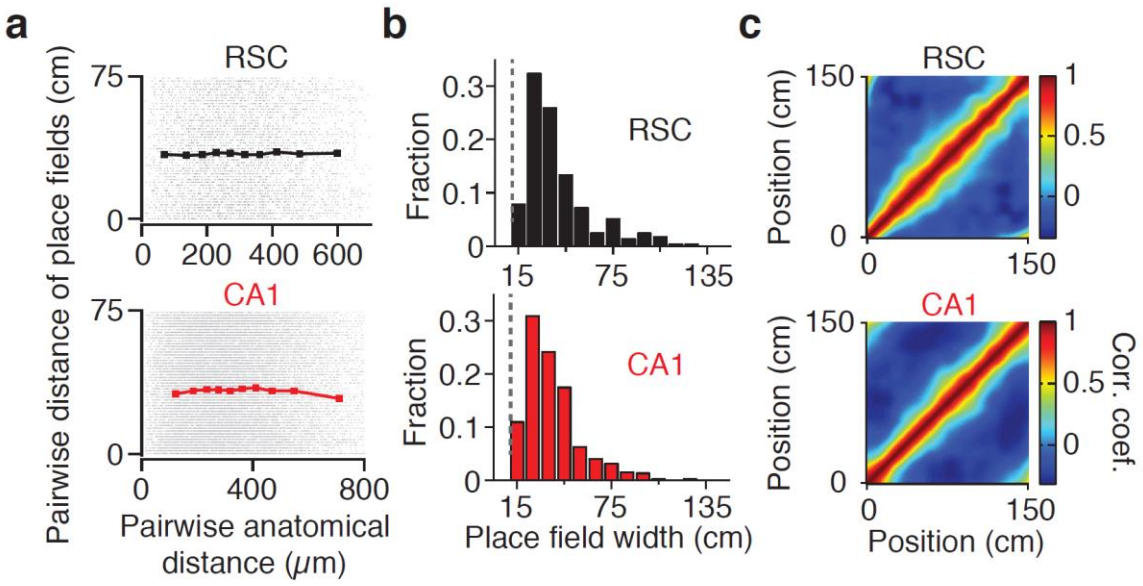

Figure 5.6 Similar place cell properties in RSC and CA1
(a) Gray dots: scatter plot of pairwise distances between place fields as a function of pairwise anatomical distance between cell bodies. Solid lines: mean pairwise field distance as a function of anatomical distance. Error bars: s.e.m. Top: for all RSC place cells; Bottom: for all CA1 place cells.
(b) Distributions of place-field widths for all RSC (top, n = 297 neurons) and CA1 (bottom, n = 452 neurons) place cells. Gray dashed lines indicate minimum field width.
(c) Correlation matrices of population vectors for all RSC (top) and CA1 (bottom) place cells. Bin width: 1.5 cm; Gaussian smoothing standard deviation: 4.5 cm.

5.3.4. Retrosplenial Place Representation is Robust to Change in Reward Location

RSC place cell activity may encode location in the reference frame defined by the tactile cues, or it may encode position relative to the reward site (Gothard et al 1996, Knierim et al 1995). To distinguish between these two possibilities, we examined the impact of changing the reward location on RSC place fields (n = 3 animals, 512 neurons, 63 place cells). Changing the location of the reward site had a limited impact on the RSC place field representation (Figures 5.7 and 5.8). Most RSC place cells showed small changes in peak response location (< 25 cm,

n = 37/63, black dots in Figure 5.7c) (Figures 5.7b,c and Figures 5.8a,b). The cross-correlation between the population vectors indicate the RSC population representations of position are highly correlated before and after reward shift (Figure 5.7d). The RSC place cells whose fields moved with change in reward location (n = 15/63 place cells changed fields' location for less than 25 cm relative to the reward location) had place fields clustered near the reward location (Figure 5.7c). The majority of hippocampal CA1 place fields also stayed when the reward was shifted (< 25 cm, n = 72/91) (Figure 5.7e). We conclude that most RSC place cells, similar to CA1 place cells, encode location in the spatial frame defined by the tactile cues, which are the richest and most stable cues in this experiment.

One important difference between the activity we observed in RSC and CA1 is that, in agreement with previous findings (Murakami et al 2015, Smith et al 2012), there were many active cells in RSC that did not have place-field characteristics. The characteristics of these non-place cells will be reported elsewhere.

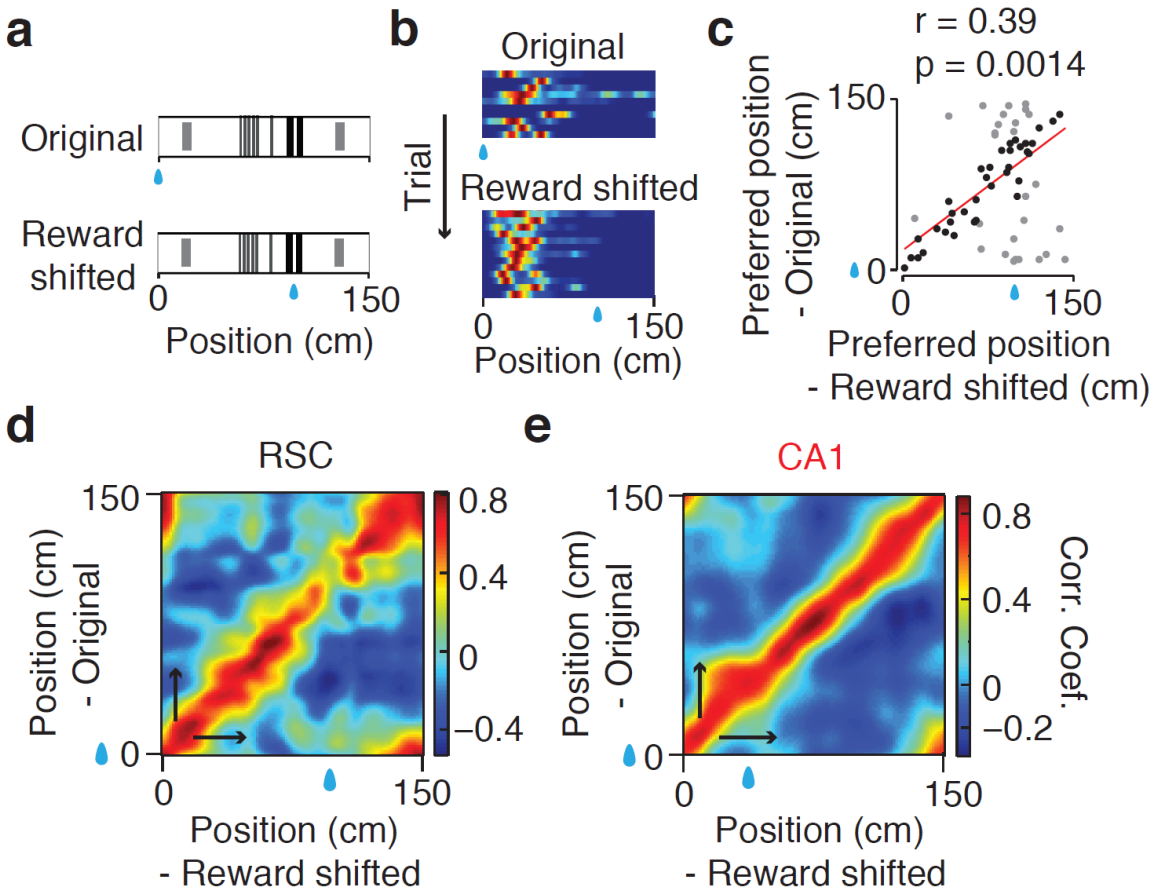

Figure 5.7 RSC place fields encode the absolute position

(a) Illustration of the reward shift experiment. Blue drops indicate reward locations. The reward location was shifted between consecutive sessions.

(b) Normalized activity as a function of location for an example RSC place cell before (original, top) and after reward shift (reward shifted, bottom). Trials were ordered from top to bottom in each color map. Blue drops indicate reward locations.

(c) Scatter plot of the place field locations for all RSC place cells (n = 63) in the reward shift experiment. Black dots correspond to place cells with a change in place field location smaller than 25 cm. Red line represents robust linear fit for all the points.

(d) Population vector correlation (Pearson correlation coefficient) matrix for the RSC place cells with unaltered field location (n = 37/63, black dots in (c)). Blue drops indicate reward locations. Black arrows indicate movement direction.

(e) Population vector correlation (Pearson correlation coefficient) matrix for CA1 place cells in the reward shift experiment (n = 91). Blue drops indicate reward locations. Black arrows indicate movement direction.

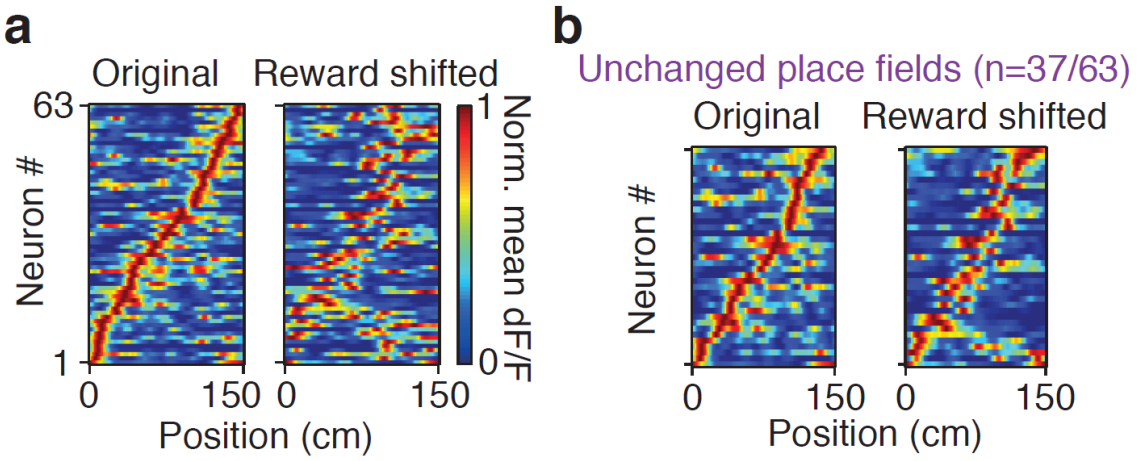

Figure 5.8 Encoding of absolute position in RSC place cells

(a) Trial average normalized activity as a function of location before and after reward shift for the 63 RSC place cells in the reward shift experiment. Place cells were ordered by the locations of their peak activity before reward shift (Original). Blue drops indicate reward location.

(b) Trial average normalized activity as a function of location before and after reward shift for the 37 selected place cells that did not shift field locations relative to the tactile cues.

5.4. DISCUSSION

Thus, neurons in the mouse retrosplenial cortex show spatially selective activity patterns that encode the animal's location during movement in linear environments. Consistent with a place code, these neurons show place fields that closely resemble hippocampal CA1 place fields, with most cells encoding absolute location in the reference frame of the track. CA1 place fields are preserved in the darkness and some fields change position when familiar cues shift (Knierim et al 1995). Similarly, RSC place fields were not affected by illumination and many were not affected by the change in reward location. We observed place cells across layers in RSC, but most frequently in the superficial layers.

The RSC place code indicates that allocentric representation of the environment is employed in the neocortex. Place fields resembling those in the hippocampus have previously been described only in the claustrum (Jankowski & O'Mara 2015). Like RSC, the claustrum receives direct hippocampal input (Cenquizca & Swanson 2007). Positional signals have been observed in the postrhinal, anterior cingulate and visual cortices (Furtak et al 2012, Haggerty & Ji 2015, Ji & Wilson 2007, Weible et al 2009), but these signals have broad spatial selectivity likely reflecting object or sensory responses. In the entorhinal cortex, grid cells also exhibit spatially tuned responses, but this activity is periodic (Hafting et al 2005). The RSC place code may be useful for spatially guided behaviour.

Previous studies of the rodent RSC have reported spatially modulated turn-selective (Smith et al 2012), route-selective (Alexander & Nitz 2015), and head-direction cells (Chen et al 1994a, Cho & Sharp 2001). The place cell activity we observed differs from past observations in that they show clear, isolated place-specific activity with almost no background firing. RSC place cell activity was present in the absence of directional vestibular and visual inputs, therefore is unlikely to involve head direction cells; such a link with head direction was not ruled out in previous studies (Alexander & Nitz 2015, Cho & Sharp 2001, Smith et al 2012).

Place-localized firing patterns in RSC may reflect a path integration mechanism that is referenced to spatial landmarks (Auger et al 2012). Consistent with this, human studies have suggested that RSC is important for path integration with reference to a home location (Chrastil et al 2015). Accurate place cell representations in the hippocampus require integration of self-motion and external cues (Gothard et al 1996, Knierim et al 1998), which appears to occur in RSC place cells. The presence of place cells and egocentric movement-by-place conjunctive cells in RSC is also consistent with a postulated role in translating between external and internal reference frames (Alexander & Nitz 2015).

The question arises as to why place cell-like activity in RSC has not been reported in previous electrophysiological studies (Alexander & Nitz 2015, Smith et al 2012). This may have resulted from the difficulty of measuring the activity from a sufficiently-large sample of superficial RSC neurons in behaving animals, and the fact that RSC ‘place cells’ are intermixed with cells with non-spatial

characteristics; however, it is also possible that the combination of head-fixation and behavioral restriction in the current recording context may have masked more complex responses of these neurons, which might be less similar to hippocampal place cells in a free-behaviour context. These possibilities remain to be investigated.

In addition, the origins of place cell-like activity in RSC remain to be elucidated. Some authors have suggested that RSC may contribute to the spatial selective firing of hippocampal cells and others have shown the existence of RSC projections to the entorhinal cortex (Cooper & Mizumori 2001, Czajkowski et al 2013); however, the striking similarities between location-specific activity in RSC and CA1, and the finding that superficial RSC layers (which receive the bulk of CA1 inputs) have more place cells than deeper layers, suggests the possibility that RSC might inherit its place code from the CA1 region. This hypothesis requires further investigation. The presence of place cells and movement-by-place conjunctive cells in RSC is consistent with its possible role in converting external reference frames to internal reference frames in preparation for spatially directed behaviour (Burgess et al 2001).

5.5. MATERIALS AND METHODS

Animals and Surgery

All animal procedures were performed in compliance with the protocols approved by the ethical research committee of Katholieke Universiteit of Leuven. 14 male C57BI/6J mice (~22-30 g, ~2-4 months old at the time of surgery) were used for

this study (8 mice for hippocampus electrophysiology, 2 mice for hippocampus imaging, 4 mice for retrosplenial cortex imaging). Mice were injected with dexamethasone (3.2 mg/kg, intramuscular) min. 4 hours before surgery. During surgery, mice were anesthetized with isoflurane (1-1.5%, O_2: 0.5-1 L/min) and body temperature was maintained at 37 °C. A custom-made head-plate was attached to the skull using adhesive cement (C&B-metabond, Parkell) and acrylic material (TAB 2000, Kerr). A 3 mm craniotomy was made with a dental drill (600 µm tip) above the left retrosplenial cortex (Kirkcaldie 2012). The craniotomy was rinsed and covered with artificial cerebrospinal fluid (ACSF). A small slit in the dura was made using fine forceps and injections of solution containing AAV2.1/Syn.GCaMP6m (Chen et al 2013b) were made with a beveled micropipette at 0.5 mm ML axis and 1 mm from transverse sinus. 1 µL viral solution was mixed with 0.3 µL sulforhodamine SR101 for fluorescent monitoring. Vector solution was injected at 2 depths (600 µm and 250 µm deep). Each site was injected with ~200 nL solution at low speed (9.2 nL/pulse, 15 sec interval) using a nanoliter injector (Nanoject II, Drummond Sci.). A cranial window made of 3 round coverslips (affixed with optical adhesive NOA71, Norland) was implanted and attached to the skull with Vetbond tissue adhesive (3M) (Goldey et al 2014). For the preparation of hippocampus imaging, a 3 mm craniotomy was made above the left hippocampus. Injections were made 1.5 mm from the surface (2 mm AP, 1.8 mm ML). Then a ~1 mm thick cortex trunk was carefully aspired with vacuum under optical guidance. Aspiration was stopped when the cortical white matter was exposed. The hippocampal cranial window was composed of a 1.5

mm segment of a glass cylinder (3 mm OD, 2.4 mm ID) with a 3 mm coverslip attached to one end. The window was inserted into the craniotomy until it touched the white matter. To minimize motion artefact, the window was slightly pushed against the white matter. The surrounding of the window was sealed with Vetbond and dental acrylic. The top layer was covered with acrylic material mixed with black pigment to shield light during 2-photon imaging. Two rubber rings were attached to the head-plate to form a well to hold water during imaging. Then anesthesia was stopped and the mice were moved to home cage and recovered for min. 5 days. Training started at least 5 days after surgery. Surgeries for electrophysiology were performed after animal performance reached asymptote. A 1mm craniotomy was made above the left hippocampus (2mm AP, 1.8mm ML). Then the craniotomy was covered with a coverslip and then sealed with Kwik-Cast sealant (WPI). Electrophysiological recording followed the next 3 consecutive days.

Treadmill and Training

The mice were trained to be head-fixed and move on a linear treadmill apparatus (Royer et al 2012). The treadmill was equipped with a 150 cm belt made from Velcro material (Country Brook). The belt was covered with patches of tactile cues (hot glue stripes, foam, and velcro loop). Two custom 3D-printed wheels of 5 cm radius made from polyamide were attached to bearings with a steel shaft to guide the movement of the belt. A custom-made aluminum platform was used to support the track and the animal. Teflon tape (CS Hyde) was adhered to the

platform to minimize friction. An optical encoder (Avago Tech.) with a resolution of 100 pulses per revolution was attached to the shaft of the wheel to monitor belt movement at a precision of 3.14 mm. A photoelectric sensor (Omron) was mounted under the platform and a reflective tape was attached underneath the treadmill belt to trigger the opening of an electromagnetic pinch valve. The valve was used to release 10% sugar water reward (~2.5 µl) and to reset track distance after completed laps. A custom-assembled PCB board equipped with a microcontroller (AT89LP52, Atmel) was used to monitor the photoelectric signal and control the opening and closing of the valve. Other mechanic parts were from Thorlabs. The encoder and photoelectric signal were acquired via a USB data acquisition board (Measurement Computing). The signals were recorded with Presentation software (Neurobehavioral Systems) and sampled at 10k Hz.
Mice were water restricted and their weights were recorded daily during training and experiments. They had free access to water on weekends. The mice were introduced to the treadmill and head fixation for a gradually increased duration. Reward was delivered after each lap running. During training, sometimes the reward was given manually to motivate the mice. Reward volume was monitored and free water was given to make sure the mice get at least 1 mL water each day. The mice reached asymptotic performance after ~2-3 weeks of training.

2-photon Imaging

A custom-built 2-photon microscope (Neurolabware) was used. A Ti:Sapphire excitation laser (MaiTai DeepSee, Spectra-Physics) was operated at 920 nm

(~20-60 mW laser power at the sample). Laser scanning was controlled by galvo and resonant scanners (Cambridge 6215H and CRS 8K) through a 16x lens (NA = 0.8, Nikon). Green fluorescence from GCaMP6m was collected using a band-pass filter (510/84 nm, Semorock) with a GaAsP photomultiplier tube (PMT, Hamamatsu). Blackout fabric (Thorlabs) was used to prevent stray light from entering the objective and PMTs. Custom-made software was used to control microscope movement and acquisition. Images were collected at ~30.9 Hz. Imaging sessions normally lasted ~10 min.

Electrophysiology

On the day after surgery, mice were head-fixed and the silicone sealant and coverslip were removed. The craniotomy was rinsed 3 times with ACSF and a small slit was cut in the dura. A 4-shank 32-channel acute silicon probe (NeuroNexus) was attached to a micromanipulator (Scientifica). The shanks were orientated in a ~45º angle (relative to anterior-posterior axis) and lowered into dorsal CA1 (1.2-1.5 mm below pia) at 1 µm steps. The craniotomy was then covered with 2.5% agar at body temperature. A 256-channel DigiLynx system (Neuralynx) was used to record electrophysiological signals (sampling rate 32 kHz). Recording started ~20-30 minutes after insertion. After recording, the probe was retracted slowly and the craniotomy was rinsed with ACSF and covered with coverslip then Kwik-Cast sealant. Recording was performed max 3 times in each mouse.

Data Analysis

Analysis was performed using Matlab (R2014b, Mathworks). Time-series datasets were corrected for motion artifacts using TurboReg (Thevenaz et al 1998). Regions of interest were identified using morphometric filters (Ohki et al 2005). Neurons that were active during the acquisition session were identified by local correlation of 3x3 pixels through time. Correlation threshold was set at 0.95 to select all active neurons. The baseline-subtracted dF/F0 was calculated for each ROI using the average value of all pixels corresponding to that ROI (Bonin et al 2011). The time-courses were deconvolved to infer underlying firing rates (Vogelstein et al 2010). A method based on constrained nonnegative matrix factorization was used to model calcium transients, from which the count of transients was calculated (Pnevmatikakis et al 2016). For electrophysiological data, raw signals were high-pass filtered (0.8-5 kHz) for spike detection. Spike sorting was done semi-automatically for each probe shank using KlustaKwik followed by manual adjustment (Hazan et al 2006). Clusters with clear refractory periods and stable features through time were included for further analysis.

Place field analysis

Place fields were identified based on the deconvolved time-courses. The 150 cm track was binned into 100 position bins. The time-courses were mapped onto the position bins. The interpolated results were normalized by the occupancy (divided by the number of samples) in each position bin. Neurons with mean position activity less than 0.03 $\%dF/F \cdot s^{-1}$ were excluded from following analysis. Then a

Gaussian window with 4.5 cm standard deviation was applied to generate position activity maps. Position activity maps were averaged across trials to get position tuning curves. We implemented two approaches to identify place cells: one was based on place field definition and the other used spatial information. First, criteria for place cell selection were adapted from previous literature (Dombeck et al 2010, Mizuseki et al 2012). Briefly, each place cell had to satisfy the following criteria. (1) Initial threshold was set at 30% of the difference between highest and lowest activity in the position tuning curve. Place fields must be a continuous region with minimum 15 cm width and maximum 120 cm width. (2) The mean in-field activity must be at least 3 times larger than the mean out-field activity. (3) The peaks of the position activity map across trials must be within the potential field for at least one-third of all trials. Neurons met these criteria were selected as potential place cells. We also used spatial information criteria to select place cells (Skaggs, McNaughton et al. 1993). Spatial information (SI) was calculated as follows:

$$SI = \sum_{i=1}^{N} p_i \frac{f_i}{f} \log_2 \frac{f_i}{f}$$

p_i is the occupancy probability in the i-th bin, f_i is the activity (dF/F) in the i-th bin, f is the overall activity, N is the total number of bins. Then the time-courses were circularly shifted for a random time interval. This process was repeated 1000 times and the distribution of the shuffled spatial information was constructed. If the original spatial information was higher than 95 percentile of the shuffled

spatial information, the corresponding neuron was considered as significantly spatially tuned.

The width of place field was calculated from the number of consecutive position bins in which the mean activity was above 20% of the difference between peak and baseline activity from the baseline. Field widths below 15 cm or above 120 cm were discarded. Place field stability was defined as the Pearson correlation coefficient of the trial-averaged mean activity between the first half and second half of all trials.

Population vector analysis

Position maps were normalized so that the position activity of each cell ranged between 0 and 1. For each session, a population vector was constructed using the occupancy-normalized trial-averaged activity of all place cells at each position bin. Population vectors provided a representation of position involving all place cells. The population vector correlation matrix was calculated using the pairwise Pearson's linear correlation coefficient between each pair of columns (population vector at each position bin) in two population vector matrices (Battaglia et al 2004b). The correlation matrix provides a measure of how similar the population representations are at each location under different conditions.

6. The Effect of Hippocampus Lesion on Retrosplenial Place Code

Given the significant CA1 projections in superficial RSC, one outstanding question is whether retrosplenial place cells require intact hippocampal CA1 output. There are several possibilities: 1) CA1 output is always required for the formation and maintenance of RSC place fields; 2) RSC place fields depend on CA1 output only during learning and become independent of CA1 output once RSC place code is established; 3) RSC place code does not require intact CA1 output but MEC output; 4) RSC place code is formed upstream and independently of the hippocampal formation and it may feedforward to MEC to form location-specific firing patterns. We found that unilateral hippocampus lesion does not block RSC place cell activity. The average place cell fraction was not significantly different between the intact and lesioned hemispheres.

6.1. Methods

NMDA lesion of dorsal hippocampus of one hemisphere was used to block ipsilateral CA1 projections to RSC. A cranial window was implanted over the superior sagittal sinus. Cellular imaging was performed in both hemispheres in blocks in a single experimental session, after the animal was well trained (normally 3 weeks after lesion). The field of views was restricted to the same anterior-posterior, dorsal-ventral, and medial-lateral locations in the two hemispheres. Figure 6.1 illustrates the experiment preparation.

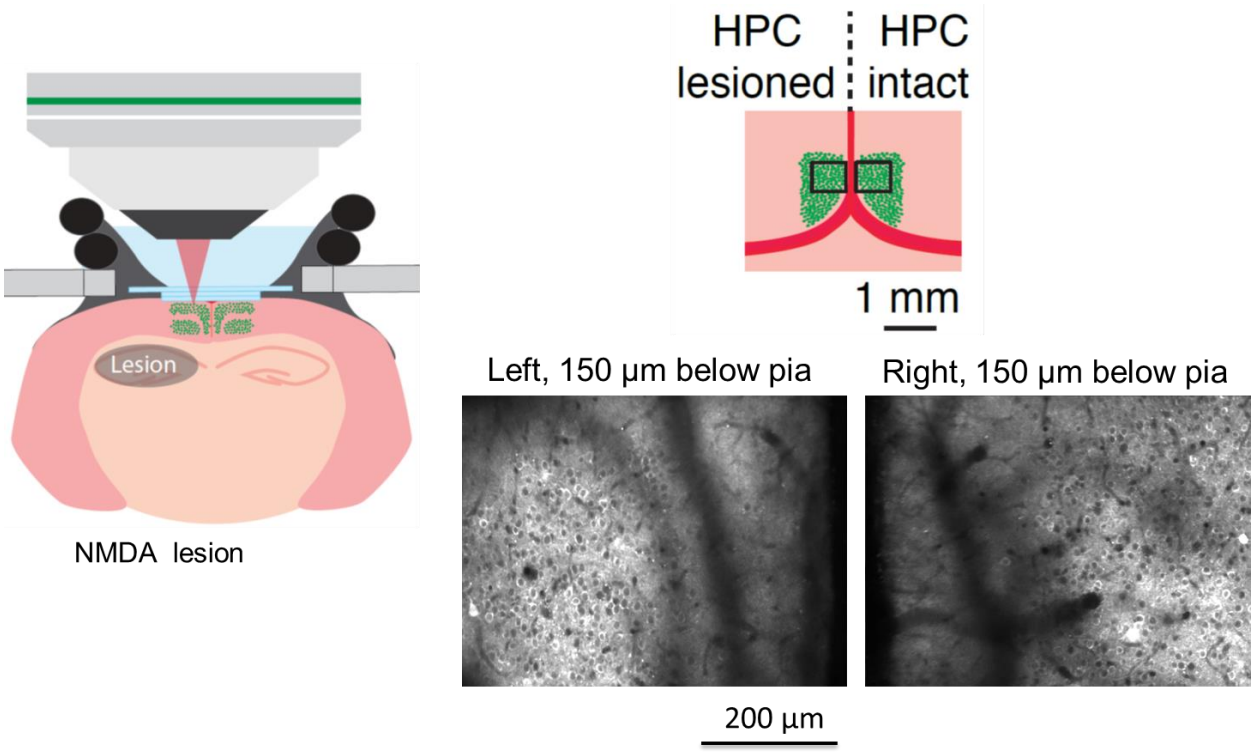

Figure 6.1 Illustration of unilateral hippocampus lesion and bilateral cellular imaging in RSC. Left, coronal view of 2-photon imaging of RSC neurons in both hemispheres, with dorsal hippocampus in one hemisphere lesioned. Top right, diagram of top view of the posterior brain. Green dots represent labelled neurons. Black squares indicate imaging field of views in the 2 hemispheres. Bottom right, example average imaging planes at the same depths in left and right hemispheres. Note the superior sagittal sinus to the medial of the imaging planes.

6.2. Results

Place cell activity was present in RSC in both the hippocampus-lesioned and hippocampus-intact hemispheres (Figure 6.2). We quantified the fraction of place cells in the lesioned and intact hemispheres for 6 mice (4 wildtype mice with GCaMP6m injection, 2 transgenic mice expressing GCaMP6s in excitatory neurons – Thy1 4.3). There was no significant difference in the mean place cell fraction between the lesion and intact hemispheres (Figure 6.3; n = 6; p = 0.46, paired *t* test). We observed a tendency of a much higher place cell fraction in the transgenic mice. This is likely due to: 1) the Thy1 4.3 line only labels excitatory

neurons while GCaMP6 injection labels all neurons within the transfected region. 2) there might be a functional bias in the labeled neuron population in the Thy1 line, which is consistent with what other researchers have seen (personal communications). Although the average place cell fraction did not differ between the intact and lesioned hemispheres, preliminary data suggest that the hippocampus may be related to the experience-dependent dynamics of RSC place cell activity (Figure 6.4).

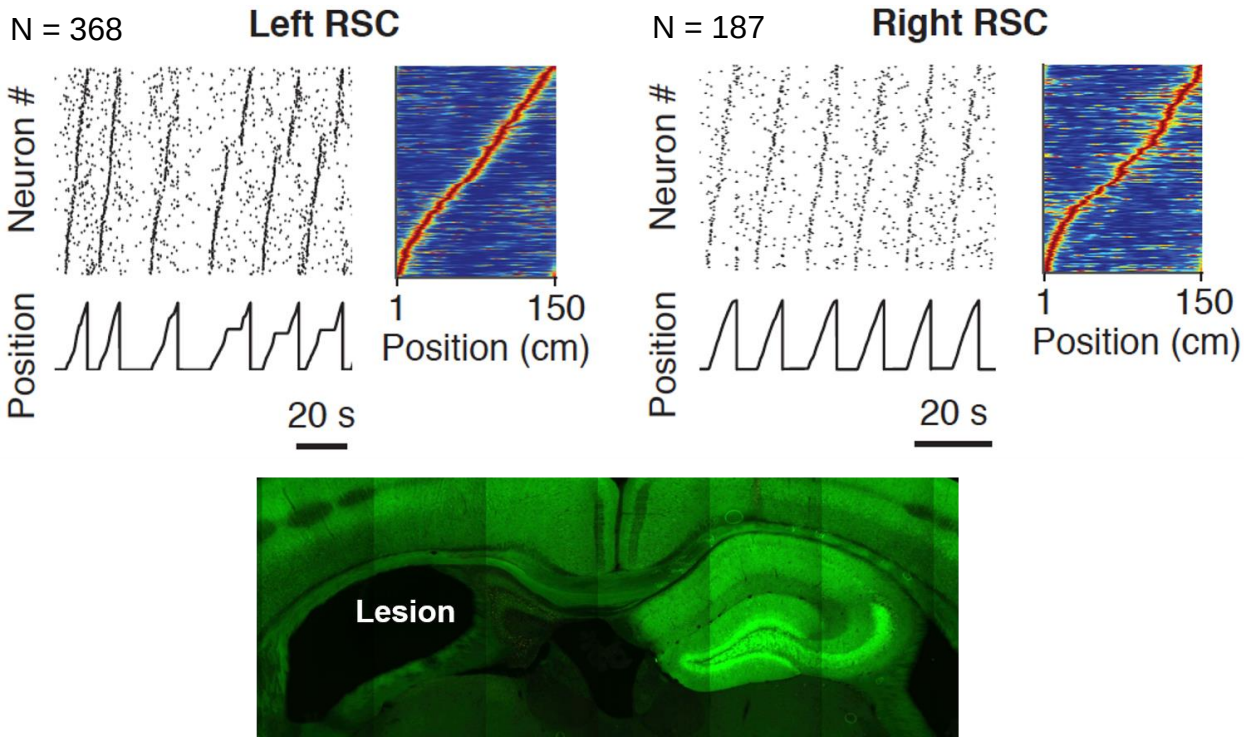

Figure 6.2 RSC place cell activity in both the hippocampus-lesioned and hippocampus-intact hemispheres in an example animal.
Top, raster plots of RSC place cell activation and average position activity maps for the left and right hemispheres. Bottom, example histology showing lesion in the left hippocampus.

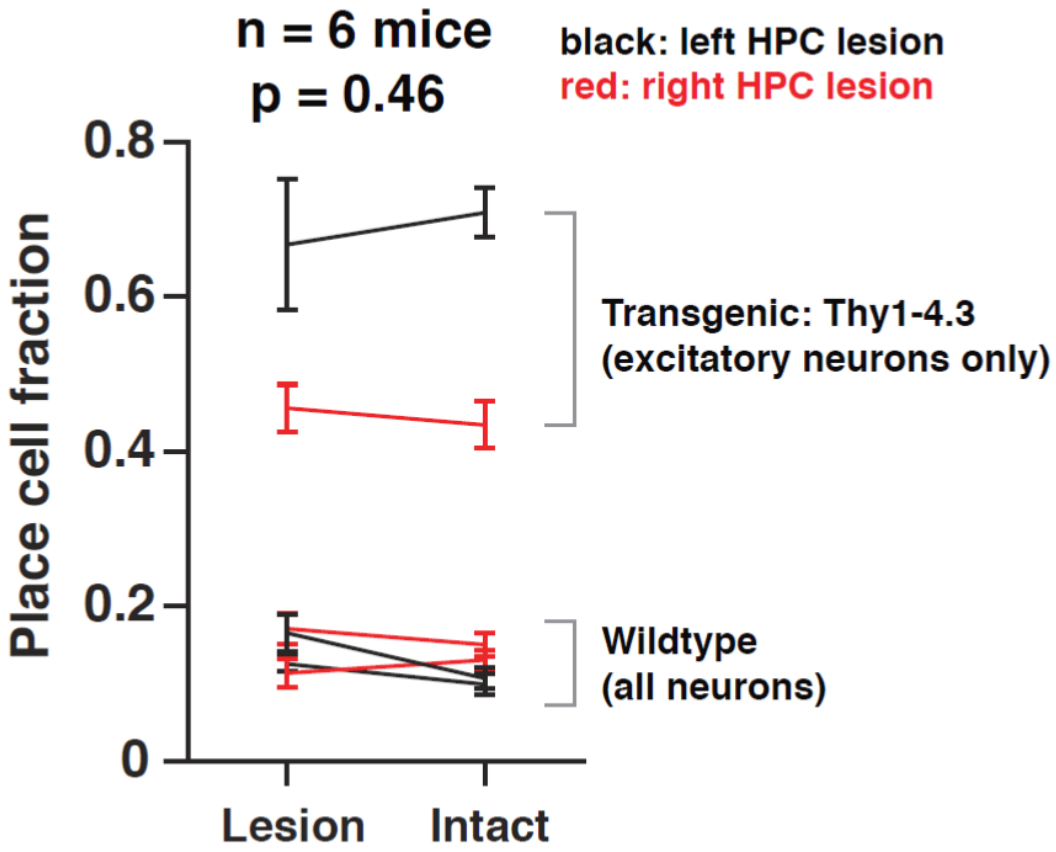

Figure 6.3 Comparison of RSC place cell fraction in hippocampus-lesioned and hippocampus-intact hemispheres for 6 animals.
Each curve corresponds to one animal. Error bars represent standard error of the mean. Black curves indicate animals with left hippocampus lesion. Red curves indicate animals with right hippocampus lesion. Top 2 curves correspond to Thy1-4.3 transgenic GCaMP6s mice. Bottom 4 curves correspond to wildtype mice with GCaMP6m injection.

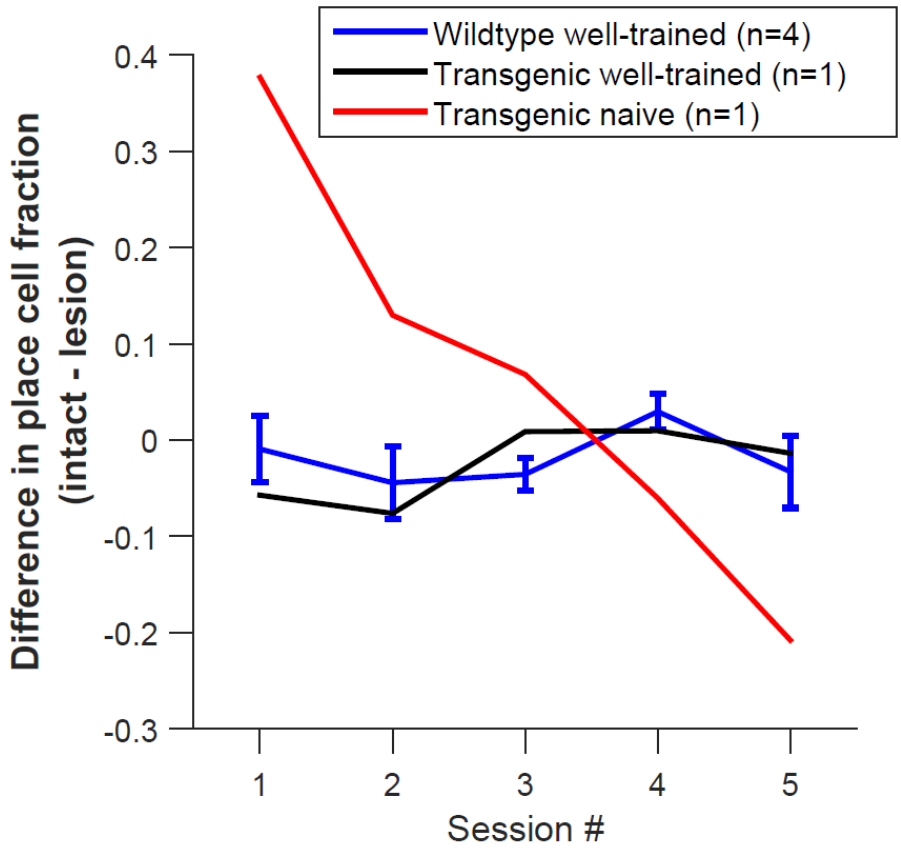

Figure 6.4 Hippocampus may be related to the experience-dependent dynamics of RSC place cell activity.
Difference in place cell fraction between the 2 hemispheres as a function of session #. Blue line: for 4 well-trained wild-type mice with GCaMP6m injections, error bars: S.E.M.; Black line: for one well-trained transgenic Thy1 mouse; Red line: for one naïve transgenic Thy1 mouse who was imaged from the first time on the treadmill belt.

6.3. Discussion

There are several possibilities as why the average RSC place cell fractions did not show a difference between the hippocampus-lesioned and hippocampus-intact hemispheres. First, compensation of functional connections can happen after lesion. Although hippocampal projections in RSC are mostly ipsilateral, there are strong contralateral projections between RSC in both hemispheres,

which likely masks the effect of loss of ipsilateral hippocampal projections. Second, hippocampal output may be required for the formation of RSC place code only during initial learning, after which RSC place cell activity becomes independent of hippocampus. This possibility would result in significant difference in RSC place cell fraction between hemispheres only during learning, and it converges after certain experience. Third, the entorhinal cortex projects widely throughout the entire neocortex mantle, including RSC, which can carry position-specific activity (Zingg et al. 2014). Lastly, given the RSC projections in deep layers of the medial entorhinal cortex (Czajkowski et al. 2013), the hippocampal formation could make use of RSC position signals to help form spatial representation. Further studies are required to test these possibilities.

7. GENERAL DISCUSSION

We started the thesis project with the motivation of testing the hypothesis that the primary visual cortex (V1), the earliest cortical area processing visual information, encodes spatial information. This hypothesis was driven by the hippocampus-indexing theory, in that the hippocampus provides an indexing code that links separate information across the entire cortex (Teyler & DiScenna 1986, Teyler & Rudy 2007). One of the most straightforward representations of this indexing code would be spatial-related, although hippocampal outputs could also be represented in other forms (MacDonald et al 2011, Pastalkova et al 2008). We had some initial observations of position-related modulations in V1 visual responses. Later control experiments studied the origins of these modulations and found that these positional modulations arise from whisker-mediated tactile influences, likely reflecting an effect of somatosensory inputs. Some researchers reported location-related activity in V1 and coordinated activation patterns in the hippocampus and V1 (Haggerty & Ji 2015, Ji & Wilson 2007). They proposed a role of the hippocampus in generating such activity in V1. However, these studies failed to rule out sensory origins of location-specific activity in V1. It is likely it reflects direct sensory inputs.

We then studied the encoding of spatial and visual information in the retrosplenial cortex (RSC), one step closer to the hippocampal formation along the hippocampus-neocortex pathway. RSC is an association cortex that connects the hippocampal and parahippocampal regions with several neocortical areas, including the parietal cortex, the motor cortex, and the visual cortex. Extensive

studies have shown that RSC is important for spatial learning and navigation, memory, and contextual processing. For example, RSC-lesioned rats show deficits in object-location associations and impairments in performance in the Morris water maze. Most previous studies have used lesion and behavior approaches and neurophysiological data are limited. However, understanding the exact functions of RSC requires investigation of the encoding patterns of large RSC neuronal population. We bridged this gap and provided important insights into the functions of RSC by monitoring the activity of thousands of RSC neurons during behavior. First, we demonstrated that some RSC neurons exhibit place cell-like responses. These RSC place cells were comparable to hippocampal CA1 place cells for several aspects. Like CA1 place cells, most RSC place cells were robust to the change of reward location, suggesting that they encode the position in the spatial frame defined by allocentric cues. Second, another subset of RSC neurons was visually responsive and some of them specifically encoded the speed of visual motion. These visually responsive RSC neurons were distinct neuronal populations from the RSC place cells. Altogether, these results posit RSC's role in processing external (sensory) and internal (navigational) information.

7.1. Functional Correlates Between the Hippocampus and RSC

We showed place code in RSC. The RSC place code was similar to CA1 place code during the same task. More importantly, the superficial RSC, which receives the bulk of direct CA1 outputs, showed stronger place encoding than the deep RSC. Electrophysiological recordings in RSC failed to find clear, isolated place

fields likely due to the technical difficulties in recording large population of neurons in superficial agranular and granular RSC (Alexander & Nitz 2015), while the imaging techniques we used could simultaneously monitor hundreds to thousands of superficial cortical neurons.

A remaining question is whether RSC place code arises from CA1 outputs or RSC place code contributes to the formation of CA1 place fields. Previous studies have established a functional interdependency between the hippocampus and RSC (Katche et al 2013b). For example, hippocampal lesions but not entorhinal cortex lesions reduce immediate-early genes expression in RSC (Albasser et al 2007); disconnecting the hippocampus and RSC by inactivating the subiculum alters animal's behavior in an active avoidance task (Gabriel & Sparenborg 1986); Temporarily inactivating RSC changes but does not abolish spatial representation in the hippocampus (Cooper & Mizumori 2001). To answer the question if RSC place code depends on CA1, some causal experiments are needed. It is likely that, in a fixed environment, the initial formation of RSC place cells depends on intact CA1 inputs and RSC place cells gradually become independent of the hippocampus. It is also possible that CA1 inputs are always necessary for providing RSC with day-to-day dynamic representations even for the same environment (Ziv et al 2013). Lesioning dorsal CA1 and then studying the change in RSC place cell activity would be a straightforward way. Our preliminary results showed that unilateral hippocampus lesion does not block RSC place cell activity. Bilateral hippocampus lesion is needed to test the possibility that RSC place cell activity in the lesioned side is compensated from

the other intact hemisphere. Although reorganization of connections and compensation could happen after lesion, lesion does block the effect of learning which would be otherwise less controlled in temporary inactivation methods such as optogenetics and designer receptors exclusively activated by designer drugs (DREADDs) (Boyden et al 2005, López et al 2016). It is not clear yet if DREADDs would block place cell activity in the hippocampus. Powerful imaging techniques allow us to simultaneously monitor presynaptic and postsynaptic structure as well as functional activity using different fluorophores. Given the direct CA1 axonal projections in superficial granular RSC, experiments studying the correlations between presynaptic axonal activity from CA1 and postsynaptic RSC place cells would provide important insights. It would also be interesting to investigate how the functional CA1 inputs are correlated with the columnar organization of the apical dendrites of layer II RSC neurons (Ichinohe 2012). One conjecture is that hippocampal outputs get clustered in RSC before broadcasting to the rest of the neocortex, enabling efficient linking of information across modalities. It would also be very helpful to label the projection neurons of RSC place cells in the hippocampal system with retrograde tracing. A promising retrograde method using the adeno-associated virus (AAV) has recently become available (Tervo et al 2016).

Although RSC and hippocampal place cells are comparable in several aspects, a major difference between the functions of the hippocampus and RSC lies in that RSC functional cell types are more multifaceted. The majority of hippocampal principle cells active during exploration in a certain environment

exhibit place fields. This is not the case for RSC neurons. In addition to RSC place cells, we have shown that a separate population encodes specific visual features but does not show place cell properties. Other prominent functional cell types in RSC include head-direction cells, reward-related cells, and speed-related cells. Thus, we postulate the role of RSC in feedforwarding sensorimotor and contextual signals to as well as routing back-projected information from higher order cortical areas.

7.2. The Role of RSC in Extracting Visual Information

The lateral agranular RSC is adjacent to the higher visual area PM. One previous study shows that PM prefers slow-moving stimuli, which is distinct from another higher visual area AL (Andermann et al 2011). The researchers predict that 1) PM and AL both help guide behaviors by processing slow-moving and fast-moving (e.g. optic flow) stimuli; 2) These two higher visual areas likely form two parallel streams that route and extract complementary visual information in V1. We showed that 80% of RSC visual neurons are tuned to the speed of optic flow from 11 to 68 degree/second, similar to what is reported for PM neurons. Distinct from the visual cortex (Niell & Stryker 2008), the visual responsiveness in RSC is highly laminar specific in that visually responsive neurons are predominantly located in superficial layers. This suggests a specific role of superficial RSC in processing cortical-cortical communication. The encoding of visual landmarks (Auger et al 2012) and sensitivity to visual motion speed may integrate in RSC to contribute to navigational behavior.

RSC projects extensively to the parahippocampal region (PHR), including the presubiculum, the parasubiculum, the medial entorhinal cortex (MEC), and the postrhinal cortex (POR) (Czajkowski et al 2013, Sugar & Witter 2016). However, how these higher order cortical areas make use of visual information routing from RSC remains to be studied. There are several conjectures: 1) visual landmark signals help reset path integration and correct for drifting errors during path integration in MEC; 2) speed tuning in RSC projects to PHR and contributes to path integration from integrating visual motion speed over time; 3) Integration of visual motion speed and landmarks happens within RSC which then feedforwards this information to PHR. An ideal experiment would be to functionally monitor the activity of the projections of these RSC visual neurons in PHR and neuronal activity in PHR. Correlating the presynaptic speed activity with postsynaptic spatial responses would advance our understanding of these computations.

7.3. The Role of RSC in Transforming Between Allocentric and Egocentric Representations

The hippocampal formation (HF) exhibits allocentric representation of space relative to the environment's boundaries. The posterior parietal cortex (PPC) encodes conjunctive egocentric and allocentric reference frames (Wilber et al 2014). Some PPC neurons are also selective to specific behaviors such as left- and right-turning (Burke et al 2005, Whitlock et al 2012). It is possible that these turn-selective responses arise from turn-specific changes in optic flow or vestibular input. Representations across allocentric and egocentric reference

frames must be unified to support successful navigation. For example, subjects have to associate specific behaviors or egocentrically based views of landmarks with distinct positions for successful goal-directed navigation. RSC is well positioned for such processes by virtue of its anatomical placement and functional correlates with both external and internal representations (Alexander & Nitz 2015, Burgess et al 2001). Computational modeling has also suggested such a role for RSC (Byrne et al 2007).

We have demonstrated place encoding in some RSC neurons, presumably reflecting an allocentric representation. We also showed speed-selective RSC visual neurons that are tuned to both optic flow and upward motion. Although the animals were head restrained under the experimental conditions, emulated optic flow and upward motion likely entrains the system that is associated with visual processing during certain actions in more natural conditions. Thus, it is reasonable to argue that these RSC sensory correlates reflect representations in egocentric reference frames. We also showed separable RSC neuronal populations for place and visual encoding. If RSC is required for allocentric and egocentric transformation, how would this computation happen? It remains to be investigated how these two RSC populations interact with each other. It is possible that RSC can perform path integration from optic flow. More studies would be required in freely behaving animals as the head direction system is mostly shut off under head-fixed conditions. The head direction system may be required for an intact and precise transformation between allocentric and egocentric representations.

7.4. Future Directions

We have demonstrated interesting encoding patterns of RSC neurons. However, it also opens the door to more outstanding questions.

First, the mice exhibited stereotyped movement profile along the linear track. While RSC place cells showed sequential activation which was reset by the reward site, the most salient cue in this case, one remaining question is whether RSC is required for such behavior. Temporary inactivation of RSC and study of its effect on behavior would provide some hints.

Second, we have demonstrated that RSC place cells and visually responsive neurons are distinct neuronal populations. As mentioned, anterior-posterior motion can be a powerful source for sensing self-motion. Changing the gain of anterior-posterior motion would alter the sensation of self-motion. Place cell activity arises from integration of self-motion with reference to a salient reset point. A follow-up question would be whether changing the speed of anterior-posterior motion relative to locomotion can exert influence on place cell activity? Would RSC place fields scale corresponding to the speed of anterior-posterior motion? Would they shrink or expand?

Third, the hippocampal place code in mice, even for the same environment, exhibits day-to-day changes with only 20% overlap between days (Ziv et al 2013). While the hippocampus is required for learning new information, the neocortex gradually becomes independent of an intact hippocampus once the new information is consolidated, at least under some conditions. Thus, how the dynamic hippocampal place code influences the dynamics of RSC place code is

a remaining question. Does RSC place code exhibit a dynamic change across days as seen in the hippocampus? If so, does such dynamic RSC place code depend on the hippocampus? Does RSC place code become stabilized after animals become familiar with the environment? How is the spatial representation of a new environment incorporated into old representations of other environments in RSC? These are important questions to be addressed in future studies.

Fourth, place cell activity has been shown to be reactivated in the hippocampus (Wilson & McNaughton 1994). The neuronal activity in the neocortex during learning is also replayed during sleep (Euston et al 2007, Ji & Wilson 2007). Although the reactivations in the hippocampus and the neocortex seem to be coordinated (Ji & Wilson 2007), it is not clear if the reinstatement of neocortical spatial memory depends on the hippocampus (Tanaka et al 2014). It is important for future studies to investigate the role of the hippocampus on the reactivation of place cell activity in RSC (if there is any). The results would provide important insights into hippocampal-neocortical interactions.

8. REFERENCES

Aggleton JP, Neave N, Nagle S, Sahgal A. 1995. A comparison of the effects of medial prefrontal, cingulate cortex, and cingulum bundle lesions on tests of spatial memory: evidence of a double dissociation between frontal and cingulum bundle contributions. *The Journal of Neuroscience* 15: 7270-81

Agster KL, Burwell RD. 2009. Cortical efferents of the perirhinal, postrhinal, and entorhinal cortices of the rat. *Hippocampus* 19: 1159-86

Albasser MM, Poirier GL, Warburton E, Aggleton JP. 2007. Hippocampal lesions halve immediate–early gene protein counts in retrosplenial cortex: distal dysfunctions in a spatial memory system. *European Journal of Neuroscience* 26: 1254-66

Alexander AS, Nitz DA. 2015. Retrosplenial cortex maps the conjunction of internal and external spaces. *Nat Neurosci* 18: 1143-51

Alyan S, McNaughton B. 1999. Hippocampectomized rats are capable of homing by path integration. *Behavioral neuroscience* 113: 19

Andermann ML, Gilfoy NB, Goldey GJ, Sachdev RN, Wölfel M, et al. 2013. Chronic cellular imaging of entire cortical columns in awake mice using microprisms. *Neuron* 80: 900-13

Andermann ML, Kerlin AM, Roumis DK, Glickfeld LL, Reid RC. 2011. Functional specialization of mouse higher visual cortical areas. *Neuron* 72: 1025-39

Aronov D, Tank DW. 2014. Engagement of neural circuits underlying 2D spatial navigation in a rodent virtual reality system. *Neuron* 84: 442-56

Auger SD, Maguire EA. 2013. Assessing the mechanism of response in the retrosplenial cortex of good and poor navigators. *Cortex* 49: 2904-13

Auger SD, Mullally SL, Maguire EA. 2012. Retrosplenial cortex codes for permanent landmarks. *PLoS One* 7: e43620

Auger SD, Zeidman P, Maguire EA. 2015. A central role for the retrosplenial cortex in de novo environmental learning. *eLife* 4: e09031

Barnes CA, McNaughton BL, Mizumori SJ, Leonard BW, Lin LH. 1990. Comparison of spatial and temporal characteristics of neuronal activity in sequential stages of hippocampal processing. *Prog Brain Res* 83: 287-300

Battaglia FP, Sutherland GR, McNaughton BL. 2004a. Hippocampal sharp wave bursts coincide with neocortical “up-state” transitions. *Learning & Memory* 11: 697-704

Battaglia FP, Sutherland GR, McNaughton BL. 2004b. Local sensory cues and place cell directionality: additional evidence of prospective coding in the hippocampus. *J Neurosci* 24: 4541-50

Bonin V, Histed MH, Yurgenson S, Reid RC. 2011. Local diversity and fine-scale organization of receptive fields in mouse visual cortex. *J Neurosci* 31: 18506-21

Bonnevie T, Dunn B, Fyhn M, Hafting T, Derdikman D, et al. 2013. Grid cells require excitatory drive from the hippocampus. *Nature neuroscience* 16: 309-17

Bouton ME, Todd TP. 2014. A fundamental role for context in instrumental learning and extinction. *Behavioural processes* 104: 13-19

Boyden ES, Zhang F, Bamberg E, Nagel G, Deisseroth K. 2005. Millisecond-timescale, genetically targeted optical control of neural activity. *Nature neuroscience* 8: 1263-68

Bremmer F, Lappe M. 1999. The use of optical velocities for distance discrimination and reproduction during visually simulated self motion. *Experimental Brain Research* 127: 33-42

Bucci DJ, Robinson S. 2014. Toward a conceptualization of retrohippocampal contributions to learning and memory. *Neurobiology of learning and memory* 116: 197-207

Burgess N, Becker S, King JA, O'Keefe J. 2001. Memory for events and their spatial context: models and experiments. *Philos Trans R Soc Lond B Biol Sci* 356: 1493-503

Burke SN, Chawla MK, Penner MR, Crowell BE, Worley PF, et al. 2005. Differential encoding of behavior and spatial context in deep and superficial layers of the neocortex. *Neuron* 45: 667-74

Burwell RD, Amaral DG. 1998. Cortical afferents of the perirhinal, postrhinal, and entorhinal cortices of the rat. *The Journal of comparative neurology* 398: 179-205

Burwell RD, Hafeman DM. 2003. Positional firing properties of postrhinal cortex neurons. *Neuroscience* 119: 577-88

Buxhoeveden DP, Casanova MF. 2002. The minicolumn hypothesis in neuroscience. *Brain* 125: 935-51

Byrne P, Becker S, Burgess N. 2007. Remembering the past and imagining the future: a neural model of spatial memory and imagery. *Psychological review* 114: 340

Carr MF, Jadhav SP, Frank LM. 2011. Hippocampal replay in the awake state: a potential substrate for memory consolidation and retrieval. *Nature neuroscience* 14: 147-53

Cenquizca LA, Swanson LW. 2007. Spatial organization of direct hippocampal field CA1 axonal projections to the rest of the cerebral cortex. *Brain Res Rev* 56: 1-26

Chen G, King JA, Burgess N, O'Keefe J. 2013a. How vision and movement combine in the hippocampal place code. *Proceedings of the National Academy of Sciences* 110: 378-83

Chen G, Manson D, Cacucci F, Wills TJ. 2016. Absence of Visual Input Results in the Disruption of Grid Cell Firing in the Mouse. *Current Biology* 26: 2335-42

Chen LL, Lin L-H, Barnes CA, McNaughton BL. 1994a. Head-direction cells in the rat posterior cortex. *Experimental Brain Research* 101: 24-34

Chen LL, Lin L-H, Green EJ, Barnes CA, McNaughton BL. 1994b. Head-direction cells in the rat posterior cortex. *Experimental Brain Research* 101: 8-23

Chen TW, Wardill TJ, Sun Y, Pulver SR, Renninger SL, et al. 2013b. Ultrasensitive fluorescent proteins for imaging neuronal activity. *Nature* 499: 295-300

Chia TH, Levene MJ. 2009. Microprisms for in vivo multilayer cortical imaging. *Journal of neurophysiology* 102: 1310-14

Cho J, Sharp PE. 2001. Head direction, place, and movement correlates for cells in the rat retrosplenial cortex. *Behav Neurosci* 115: 3-25

Chrastil ER, Sherrill KR, Hasselmo ME, Stern CE. 2015. There and Back Again: Hippocampus and Retrosplenial Cortex Track Homing Distance during Human Path Integration. *J Neurosci* 35: 15442-52

Clark BJ, Bassett JP, Wang SS, Taube JS. 2010. Impaired head direction cell representation in the anterodorsal thalamus after lesions of the retrosplenial cortex. *J Neurosci* 30: 5289-302

Colgin LL, Moser EI, Moser MB. 2008. Understanding memory through hippocampal remapping. *Trends Neurosci* 31: 469-77

Cooper BG, Manka TF, Mizumori SJ. 2001a. Finding your way in the dark: the retrosplenial cortex contributes to spatial memory and navigation without visual cues. *Behav Neurosci* 115: 1012-28

Cooper BG, Manka TF, Mizumori SJ. 2001b. Finding your way in the dark: the retrosplenial cortex contributes to spatial memory and navigation without visual cues. *Behavioral neuroscience* 115: 1012

Cooper BG, Mizumori SJ. 2001. Temporary inactivation of the retrosplenial cortex causes a transient reorganization of spatial coding in the hippocampus. *J Neurosci* 21: 3986-4001

Corcoran KA, Donnan MD, Tronson NC, Guzman YF, Gao C, et al. 2011. NMDA receptors in retrosplenial cortex are necessary for retrieval of recent and remote context fear memory. *J Neurosci* 31: 11655-9

Cowansage KK, Shuman T, Dillingham BC, Chang A, Golshani P, Mayford M. 2014. Direct reactivation of a coherent neocortical memory of context. *Neuron* 84: 432-41

Czajkowski R, Jayaprakash B, Wiltgen B, Rogerson T, Guzman-Karlsson MC, et al. 2014. Encoding and storage of spatial information in the retrosplenial cortex. *Proc Natl Acad Sci U S A* 111: 8661-6

Czajkowski R, Sugar J, Zhang SJ, Couey JJ, Ye J, Witter MP. 2013. Superficially projecting principal neurons in layer V of medial entorhinal cortex in the rat receive excitatory retrosplenial input. *J Neurosci* 33: 15779-92

Dana H, Chen T-W, Hu A, Shields BC, Guo C, et al. 2014. Thy1-GCaMP6 transgenic mice for neuronal population imaging in vivo. *PLoS One* 9: e108697

Dombeck DA, Harvey CD, Tian L, Looger LL, Tank DW. 2010. Functional imaging of hippocampal place cells at cellular resolution during virtual navigation. *Nat Neurosci* 13: 1433-40

Domnisoru C, Kinkhabwala AA, Tank DW. 2013. Membrane potential dynamics of grid cells. *Nature* 495: 199-204

Eichenbaum H, Dudchenko P, Wood E, Shapiro M, Tanila H. 1999. The hippocampus, memory, and place cells: is it spatial memory or a memory space? *Neuron* 23: 209-26

Elduayen C, Save E. 2014. The retrosplenial cortex is necessary for path integration in the dark. *Behav Brain Res* 272: 303-7

Epstein RA. 2008. Parahippocampal and retrosplenial contributions to human spatial navigation. *Trends Cogn Sci* 12: 388-96

Erisken S, Vaiceliunaite A, Jurjut O, Fiorini M, Katzner S, Busse L. 2014. Effects of locomotion extend throughout the mouse early visual system. *Current Biology* 24: 2899-907

Etienne AS, Jeffery KJ. 2004. Path integration in mammals. *Hippocampus* 14: 180-92

Euston DR, Tatsuno M, McNaughton BL. 2007. Fast-forward playback of recent memory sequences in prefrontal cortex during sleep. *science* 318: 1147-50

Field DT, Inman LA, Li L. 2015. Visual processing of optic flow and motor control in the human posterior cingulate sulcus. *Cortex* 71: 377-89

Finch DM, Derian EL, Babb TL. 1984. Afferent fibers to rat cingulate cortex. *Experimental neurology* 83: 468-85

Fischer E, Bulthoff HH, Logothetis NK, Bartels A. 2012. Visual motion responses in the posterior cingulate sulcus: a comparison to V5/MT and MST. *Cereb Cortex* 22: 865-76

Fiser A, Mahringer D, Oyibo HK, Petersen AV, Leinweber M, Keller GB. 2016. Experience-dependent spatial expectations in mouse visual cortex. *Nat Neurosci* 19: 1658-64

Frenz H, Bremmer F, Lappe M. 2003. Discrimination of travel distances from 'situated'optic flow. *Vision Research* 43: 2173-83

Frenz H, Lappe M. 2005. Absolute travel distance from optic flow. *Vision research* 45: 1679-92

Fu Y, Tucciarone JM, Espinosa JS, Sheng N, Darcy DP, et al. 2014. A cortical circuit for gain control by behavioral state. *Cell* 156: 1139-52

Furtak SC, Ahmed OJ, Burwell RD. 2012. Single neuron activity and theta modulation in postrhinal cortex during visual object discrimination. *Neuron* 76: 976-88

Gabriel M, Sparenborg S. 1986. Anterior thalamic discriminative neuronal responses enhanced during learning in rabbits with subicular and cingulate cortical lesions. *Brain research* 384: 195-98

Glickfeld LL, Andermann ML, Bonin V, Reid RC. 2013. Cortico-cortical projections in mouse visual cortex are functionally target specific. *Nature neuroscience* 16: 219-26

Goldey GJ, Roumis DK, Glickfeld LL, Kerlin AM, Reid RC, et al. 2014. Removable cranial windows for long-term imaging in awake mice. *Nat Protoc* 9: 2515-38

Gothard KM, Skaggs WE, McNaughton BL. 1996. Dynamics of mismatch correction in the hippocampal ensemble code for space: interaction between path integration and environmental cues. *J Neurosci* 16: 8027-40

Hafting T, Fyhn M, Molden S, Moser MB, Moser EI. 2005. Microstructure of a spatial map in the entorhinal cortex. *Nature* 436: 801-6

Haggerty DC, Ji D. 2015. Activities of visual cortical and hippocampal neurons co-fluctuate in freely moving rats during spatial behavior. *Elife* 4

Harker KT, Whishaw IQ. 2002. Impaired spatial performance in rats with retrosplenial lesions: importance of the spatial problem and the rat strain in identifying lesion effects in a swimming pool. *J Neurosci* 22: 1155-64

Harker KT, Whishaw IQ. 2004. A reaffirmation of the retrosplenial contribution to rodent navigation: reviewing the influences of lesion, strain, and task. *Neurosci Biobehav Rev* 28: 485-96

Harvey CD, Collman F, Dombeck DA, Tank DW. 2009. Intracellular dynamics of hippocampal place cells during virtual navigation. *Nature* 461: 941-46

Hazan L, Zugaro M, Buzsaki G. 2006. Klusters, NeuroScope, NDManager: a free software suite for neurophysiological data processing and visualization. *J Neurosci Methods* 155: 207-16

Hindley EL, Nelson AJ, Aggleton JP, Vann SD. 2014. The rat retrosplenial cortex is required when visual cues are used flexibly to determine location. *Behav Brain Res* 263: 98-107

Hollup SA, Molden S, Donnett JG, Moser MB, Moser EI. 2001. Accumulation of hippocampal place fields at the goal location in an annular watermaze task. *J Neurosci* 21: 1635-44

Hubel DH, Wiesel TN. 1962. Receptive fields, binocular interaction and functional architecture in the cat's visual cortex. *The Journal of physiology* 160: 106-54

Iaria G, Chen JK, Guariglia C, Ptito A, Petrides M. 2007. Retrosplenial and hippocampal brain regions in human navigation: complementary functional contributions to the formation and use of cognitive maps. *Eur J Neurosci* 25: 890-9

Ichinohe N. 2012. Small-scale module of the rat granular retrosplenial cortex: an example of the minicolumn-like structure of the cerebral cortex. *Front Neuroanat* 5: 69

Ichinohe N, Rockland KS. 2002. Parvalbumin positive dendrites co-localize with apical dendritic bundles in rat retrosplenial cortex. *Neuroreport* 13: 757-61

Iordanova MD, Good M, Honey RC. 2011. Retrieval-mediated learning involving episodes requires synaptic plasticity in the hippocampus. *The Journal of Neuroscience* 31: 7156-62

Itaya S, Van Hoesen G, Jenq C-B. 1981. Direct retinal input to the limbic system of the rat. *Brain research* 226: 33-42

Iurilli G, Ghezzi D, Olcese U, Lassi G, Nazzaro C, et al. 2012. Sound-driven synaptic inhibition in primary visual cortex. *Neuron* 73: 814-28

Jankowski MM, O'Mara SM. 2015. Dynamics of place, boundary and object encoding in rat anterior claustrum. *Front Behav Neurosci* 9: 250

Ji D, Wilson MA. 2007. Coordinated memory replay in the visual cortex and hippocampus during sleep. *Nat Neurosci* 10: 100-7

Jinno S. 2009. Structural organization of long-range GABAergic projection system of the hippocampus. *Front Neuroanat* 3: 13

Jones BF, Groenewegen HJ, Witter MP. 2005. Intrinsic connections of the cingulate cortex in the rat suggest the existence of multiple functionally segregated networks. *Neuroscience* 133: 193-207

Jones BF, Witter MP. 2007. Cingulate cortex projections to the parahippocampal region and hippocampal formation in the rat. *Hippocampus* 17: 957-76

Karlsson MP, Frank LM. 2009. Awake replay of remote experiences in the hippocampus. *Nature neuroscience* 12: 913-18

Katche C, Dorman G, Gonzalez C, Kramar CP, Slipczuk L, et al. 2013a. On the role of retrosplenial cortex in long-lasting memory storage. *Hippocampus* 23: 295-302

Katche C, Dorman G, Slipczuk L, Cammarota M, Medina JH. 2013b. Functional integrity of the retrosplenial cortex is essential for rapid consolidation and recall of fear memory. *Learn Mem* 20: 170-3

Kearns MJ, Warren WH, Duchon AP, Tarr MJ. 2002. Path integration from optic flow and body senses in a homing task. *Perception* 31: 349-74

Keene CS, Bucci DJ. 2008a. Contributions of the retrosplenial and posterior parietal cortices to cue-specific and contextual fear conditioning. *Behavioral neuroscience* 122: 89

Keene CS, Bucci DJ. 2008b. Neurotoxic lesions of retrosplenial cortex disrupt signaled and unsignaled contextual fear conditioning. *Behavioral neuroscience* 122: 1070

Keene CS, Bucci DJ. 2009. Damage to the retrosplenial cortex produces specific impairments in spatial working memory. *Neurobiol Learn Mem* 91: 408-14

Keller GB, Bonhoeffer T, Hübener M. 2012. Sensorimotor mismatch signals in primary visual cortex of the behaving mouse. *Neuron* 74: 809-15

Kimchi T, Etienne AS, Terkel J. 2004. A subterranean mammal uses the magnetic compass for path integration. *Proceedings of the National Academy of Sciences of the United States of America* 101: 1105-09

Kirkcaldie M. 2012. Neocortex. In *The Mouse Nervous System*, pp. 52-111: Elsevier

Kleinschmidt A, Thilo KV, Büchel C, Gresty MA, Bronstein AM, Frackowiak RS. 2002. Neural correlates of visual-motion perception as object-or self-motion. *Neuroimage* 16: 873-82

Knierim JJ. 2006. Neural representations of location outside the hippocampus. *Learn Mem* 13: 405-15

Knierim JJ, Kudrimoti HS, McNaughton BL. 1995. Place cells, head direction cells, and the learning of landmark stability. *J Neurosci* 15: 1648-59

Knierim JJ, Kudrimoti HS, McNaughton BL. 1998. Interactions between idiothetic cues and external landmarks in the control of place cells and head direction cells. *J Neurophysiol* 80: 425-46

Kononenko NL, Witter MP. 2012. Presubiculum layer III conveys retrosplenial input to the medial entorhinal cortex. *Hippocampus* 22: 881-95

Kravitz DJ, Saleem KS, Baker CI, Mishkin M. 2011. A new neural framework for visuospatial processing. *Nat Rev Neurosci* 12: 217-30

Kropff E, Carmichael JE, Moser M-B, Moser EI. 2015. Speed cells in the medial entorhinal cortex. *Nature*

Lappe M, Bremmer F, van den Berg AV. 1999. Perception of self-motion from visual flow. *Trends Cogn Sci* 3: 329-36

Lappe M, Jenkin M, Harris LR. 2007. Travel distance estimation from visual motion by leaky path integration. *Experimental Brain Research* 180: 35-48

Lever C, Burton S, Jeewajee A, O'Keefe J, Burgess N. 2009. Boundary vector cells in the subiculum of the hippocampal formation. *The journal of neuroscience* 29: 9771-77

López AJ, Kramár E, Matheos DP, White AO, Kwapis J, et al. 2016. Promoter-Specific Effects of DREADD Modulation on Hippocampal Synaptic Plasticity and Memory Formation. *The Journal of Neuroscience* 36: 3588-99

MacDonald CJ, Lepage KQ, Eden UT, Eichenbaum H. 2011. Hippocampal “time cells” bridge the gap in memory for discontiguous events. *Neuron* 71: 737-49

Maguire EA. 2001. The retrosplenial contribution to human navigation: a review of lesion and neuroimaging findings. *Scand J Psychol* 42: 225-38

Marr D, Willshaw D, McNaughton B. 1991. Simple memory: a theory for archicortex In *From the Retina to the Neocortex*, pp. 59-128: Springer

Marshel JH, Garrett ME, Nauhaus I, Callaway EM. 2011. Functional specialization of seven mouse visual cortical areas. *Neuron* 72: 1040-54

McClelland JL, McNaughton BL, O'Reilly RC. 1995. Why there are complementary learning systems in the hippocampus and neocortex: insights from the successes and failures of connectionist models of learning and memory. *Psychological review* 102: 419

McNaughton B, Barnes C, Gerrard J, Gothard K, Jung M, et al. 1996. Deciphering the hippocampal polyglot: the hippocampus as a path integration system. *Journal of Experimental Biology* 199: 173-85

McNaughton BL, Battaglia FP, Jensen O, Moser EI, Moser MB. 2006. Path integration and the neural basis of the 'cognitive map'. *Nat Rev Neurosci* 7: 663-78

Michael JW, Van Groen T, Sripanidkulchai K. 1990. Dendritic bundling in layer I of granular retrosplenial cortex: intracellular labeling and selectivity of innervation. *Journal of Comparative Neurology* 295: 33-42

Minoshima S, Giordani B, Berent S, Frey KA, Foster NL, Kuhl DE. 1997. Metabolic reduction in the posterior cingulate cortex in very early Alzheimer's disease. *Ann Neurol* 42: 85-94

Mittelstaedt H, Mittelstaedt M-L. 1982. Homing by path integration In *Avian navigation*, pp. 290-97: Springer

Mittelstaedt M-L, Mittelstaedt H. 1980. Homing by path integration in a mammal. *Naturwissenschaften* 67: 566-67

Miyashita T, Rockland KS. 2007. GABAergic projections from the hippocampus to the retrosplenial cortex in the rat. *European Journal of Neuroscience* 26: 1193-204

Mizuseki K, Royer S, Diba K, Buzsaki G. 2012. Activity dynamics and behavioral correlates of CA3 and CA1 hippocampal pyramidal neurons. *Hippocampus* 22: 1659-80

Mohler BJ, Thompson WB, Creem-Regehr SH, Pick HL, Jr., Warren WH, Jr. 2007a. Visual flow influences gait transition speed and preferred walking speed. *Exp Brain Res* 181: 221-8

Mohler BJ, Thompson WB, Creem-Regehr SH, Willemsen P, Pick Jr HL, Rieser JJ. 2007b. Calibration of locomotion resulting from visual motion in a treadmill-based virtual environment. *ACM Transactions on Applied Perception (TAP)* 4: 4

Mountcastle VB. 1997. The columnar organization of the neocortex. *Brain* 120: 701-22

Murakami T, Yoshida T, Matsui T, Ohki K. 2015. Wide-field Ca(2+) imaging reveals visually evoked activity in the retrosplenial area. *Front Mol Neurosci* 8: 20

Naber P, Witter M. 1998. Subicular efferents are organized mostly as parallel projections: A double-labeling, retrograde-tracing study in the rat. *Journal of comparative neurology* 393: 284-97

Neave N, Lloyd S, Sahgal A, Aggleton JP. 1994. Lack of effect of lesions in the anterior cingulate cortex and retrosplenial cortex on certain tests of spatial memory in the rat. *Behav Brain Res* 65: 89-101

Nestor PJ, Fryer TD, Ikeda M, Hodges JR. 2003. Retrosplenial cortex (BA 29/30) hypometabolism in mild cognitive impairment (prodromal Alzheimer's disease). *Eur J Neurosci* 18: 2663-7

Niell CM, Stryker MP. 2008. Highly selective receptive fields in mouse visual cortex. *The Journal of Neuroscience* 28: 7520-36

Niell CM, Stryker MP. 2010. Modulation of visual responses by behavioral state in mouse visual cortex. *Neuron* 65: 472-79

O'Keefe J, Dostrovsky J. 1971. The hippocampus as a spatial map. Preliminary evidence from unit activity in the freely-moving rat. *Brain Res* 34: 171-5

O'Keefe J, Recce ML. 1993. Phase relationship between hippocampal place units and the EEG theta rhythm. *Hippocampus* 3: 317-30

Ohki K, Chung S, Ch'ng YH, Kara P, Reid RC. 2005. Functional imaging with cellular resolution reveals precise micro-architecture in visual cortex. *Nature* 433: 597-603

Pastalkova E, Itskov V, Amarasingham A, Buzsáki G. 2008. Internally generated cell assembly sequences in the rat hippocampus. *Science* 321: 1322-27

Pfeiffer BE, Foster DJ. 2013. Hippocampal place-cell sequences depict future paths to remembered goals. *Nature* 497: 74-9

Pinto L, Goard MJ, Estandian D, Xu M, Kwan AC, et al. 2013. Fast modulation of visual perception by basal forebrain cholinergic neurons. *Nature neuroscience* 16: 1857-63

Piscopo DM, El-Danaf RN, Huberman AD, Niell CM. 2013. Diverse visual features encoded in mouse lateral geniculate nucleus. *The Journal of neuroscience* 33: 4642-56

Pnevmatikakis EA, Soudry D, Gao Y, Machado TA, Merel J, et al. 2016. Simultaneous Denoising, Deconvolution, and Demixing of Calcium Imaging Data. *Neuron* 89: 285-99

Pothuizen HH, Aggleton JP, Vann SD. 2008. Do rats with retrosplenial cortex lesions lack direction? *Eur J Neurosci* 28: 2486-98

Pothuizen HH, Davies M, Aggleton JP, Vann SD. 2010. Effects of selective granular retrosplenial cortex lesions on spatial working memory in rats. *Behav Brain Res* 208: 566-75

Priebe NJ, Cassanello CR, Lisberger SG. 2003. The neural representation of speed in macaque area MT/V5. *The Journal of neuroscience* 23: 5650-61

Priebe NJ, Lisberger SG, Movshon JA. 2006. Tuning for spatiotemporal frequency and speed in directionally selective neurons of macaque striate cortex. *The Journal of Neuroscience* 26: 2941-50

Ranck Jr J. *Soc Neurosci Abstr1984,* 10.

Ranganath C, Ritchey M. 2012. Two cortical systems for memory-guided behaviour. *Nat Rev Neurosci* 13: 713-26

Redish AD, Battaglia FP, Chawla MK, Ekstrom AD, Gerrard JL, et al. 2001. Independence of firing correlates of anatomically proximate hippocampal pyramidal cells. *J Neurosci* 21: RC134

Ringach DL, Shapley RM, Hawken MJ. 2002. Orientation selectivity in macaque V1: diversity and laminar dependence. *The Journal of neuroscience* 22: 5639-51

Robinson S, Keene CS, Iaccarino HF, Duan D, Bucci DJ. 2011. Involvement of retrosplenial cortex in forming associations between multiple sensory stimuli. *Behavioral neuroscience* 125: 578

Roth MM, Helmchen F, Kampa BM. 2012. Distinct functional properties of primary and posteromedial visual area of mouse neocortex. *J Neurosci* 32: 9716-26

Royer S, Zemelman BV, Losonczy A, Kim J, Chance F, et al. 2012. Control of timing, rate and bursts of hippocampal place cells by dendritic and somatic inhibition. *Nat Neurosci* 15: 769-75

Saleem AB, Ayaz A, Jeffery KJ, Harris KD, Carandini M. 2013. Integration of visual motion and locomotion in mouse visual cortex. *Nat Neurosci* 16: 1864-9

Samsonovich A, McNaughton BL. 1997. Path integration and cognitive mapping in a continuous attractor neural network model. *The Journal of neuroscience* 17: 5900-20

Sargolini F, Fyhn M, Hafting T, McNaughton BL, Witter MP, et al. 2006. Conjunctive representation of position, direction, and velocity in entorhinal cortex. *Science* 312: 758-62

Schwindel CD, McNaughton BL. 2011. Hippocampal-cortical interactions and the dynamics of memory trace reactivation. *Prog. Brain Res* 193: 163-77

Sharp PE, Green C. 1994. Spatial correlates of firing patterns of single cells in the subiculum of the freely moving rat. *The Journal of Neuroscience* 14: 2339-56

Shibata H. 1993. Efferent projections from the anterior thalamic nuclei to the cingulate cortex in the rat. *J Comp Neurol* 330: 533-42

Shibata H. 1994. Terminal distribution of projections from the retrosplenial area to the retrohippocampal region in the rat, as studied by anterograde transport of biotinylated dextran amine. *Neuroscience research* 20: 331-36

Shibata H, Honda Y, Sasaki H, Naito J. 2009. Organization of intrinsic connections of the retrosplenial cortex in the rat. *Anat Sci Int* 84: 280-92

Shibata H, Naito J. 2008. Organization of anterior cingulate and frontal cortical projections to the retrosplenial cortex in the rat. *Journal of Comparative Neurology* 506: 30-45

Shuler MG, Bear MF. 2006. Reward timing in the primary visual cortex. *Science* 311: 1606-09

Skaggs WE, McNaughton BL, Gothard KM, Markus EJ. *In1993*. Citeseer.

Skaggs WE, McNaughton BL, Wilson MA, Barnes CA. 1996. Theta phase precession in hippocampal neuronal populations and the compression of temporal sequences. *Hippocampus* 6: 149-72

Smith DM, Barredo J, Mizumori SJ. 2012. Complimentary roles of the hippocampus and retrosplenial cortex in behavioral context discrimination. *Hippocampus* 22: 1121-33

Smith DM, Wakeman D, Patel J, Gabriel M. 2004. Fornix lesions impair context-related cingulothalamic neuronal patterns and concurrent discrimination learning in rabbits (Oryctolagus cuniculus). *Behavioral neuroscience* 118: 1225

Solstad T, Boccara CN, Kropff E, Moser M-B, Moser EI. 2008. Representation of geometric borders in the entorhinal cortex. *Science* 322: 1865-68

Stensola H, Stensola T, Solstad T, Frøland K, Moser M-B, Moser EI. 2012. The entorhinal grid map is discretized. *Nature* 492: 72-78

Sugar J, Witter MP. 2016. Postnatal development of retrosplenial projections to the parahippocampal region of the rat. *Elife* 5

Sugar J, Witter MP, van Strien NM, Cappaert NL. 2011. The retrosplenial cortex: intrinsic connectivity and connections with the (para)hippocampal region in the rat. An interactive connectome. *Front Neuroinform* 5: 7

Sutherland RJ, Whishaw IQ, Kolb B. 1988. Contributions of cingulate cortex to two forms of spatial learning and memory. *J Neurosci* 8: 1863-72

Tanaka KZ, Pevzner A, Hamidi AB, Nakazawa Y, Graham J, Wiltgen BJ. 2014. Cortical representations are reinstated by the hippocampus during memory retrieval. *Neuron* 84: 347-54

Taube JS, Muller RU, Ranck JB. 1990a. Head-direction cells recorded from the postsubiculum in freely moving rats. I. Description and quantitative analysis. *The Journal of neuroscience* 10: 420-35

Taube JS, Muller RU, Ranck JB. 1990b. Head-direction cells recorded from the postsubiculum in freely moving rats. II. Effects of environmental manipulations. *The Journal of Neuroscience* 10: 436-47

Terrazas A, Krause M, Lipa P, Gothard KM, Barnes CA, McNaughton BL. 2005. Self-motion and the hippocampal spatial metric. *The Journal of neuroscience* 25: 8085-96

Tervo DGR, Hwang B-Y, Viswanathan S, Gaj T, Lavzin M, et al. 2016. A Designer AAV Variant Permits Efficient Retrograde Access to Projection Neurons. *Neuron*

Teyler TJ, DiScenna P. 1986. The hippocampal memory indexing theory. *Behavioral neuroscience* 100: 147

Teyler TJ, Rudy JW. 2007. The hippocampal indexing theory and episodic memory: updating the index. *Hippocampus* 17: 1158-69

Thevenaz P, Ruttimann UE, Unser M. 1998. A pyramid approach to subpixel registration based on intensity. *IEEE Trans Image Process* 7: 27-41

van Groen T, Wyss JM. 1990. Connections of the retrosplenial granular a cortex in the rat. *J Comp Neurol* 300: 593-606

van Groen T, Wyss JM. 1992. Connections of the retrosplenial dysgranular cortex in the rat. *J Comp Neurol* 315: 200-16

Van Groen T, Wyss JM. 2003. Connections of the retrosplenial granular b cortex in the rat. *J Comp Neurol* 463: 249-63

Vann SD, Aggleton JP. 2002a. Extensive cytotoxic lesions of the rat retrosplenial cortex reveal consistent deficits on tasks that tax allocentric spatial memory. *Behav Neurosci* 116: 85-94

Vann SD, Aggleton JP. 2002b. Extensive cytotoxic lesions of the rat retrosplenial cortex revel consistent deficits on tasks that tax allocentric spatial memory. *Behavioral Neuroscience* 116: 85-94

Vann SD, Aggleton JP. 2005. Selective dysgranular retrosplenial cortex lesions in rats disrupt allocentric performance of the radial-arm maze task. *Behav Neurosci* 119: 1682-6

Vann SD, Aggleton JP, Maguire EA. 2009. What does the retrosplenial cortex do? *Nat Rev Neurosci* 10: 792-802

Vann SD, Albasser MM. 2009. Hippocampal, retrosplenial, and prefrontal hypoactivity in a model of diencephalic amnesia: Evidence towards an interdependent subcortical-cortical memory network. *Hippocampus* 19: 1090-102

Vasconcelos N, Pantoja J, Belchior H, Caixeta FV, Faber J, et al. 2011. Cross-modal responses in the primary visual cortex encode complex objects and correlate with tactile discrimination. *Proceedings of the National Academy of Sciences* 108: 15408-13

Vedder LC, Miller AM, Harrison MB, Smith DM. 2016. Retrosplenial Cortical Neurons Encode Navigational Cues, Trajectories and Reward Locations During Goal Directed Navigation. *Cereb Cortex*

Villette V, Malvache A, Tressard T, Dupuy N, Cossart R. 2015. Internally Recurring Hippocampal Sequences as a Population Template of Spatiotemporal Information. *Neuron* 88: 357-66

Vogelstein JT, Packer AM, Machado TA, Sippy T, Babadi B, et al. 2010. Fast nonnegative deconvolution for spike train inference from population calcium imaging. *J Neurophysiol* 104: 3691-704

Vogt BA, Miller MW. 1983. Cortical connections between rat cingulate cortex and visual, motor, and postsubicular cortices. *J Comp Neurol* 216: 192-210

Vogt BA, Peters A. 1981. Form and distribution of neurons in rat cingulate cortex: areas 32, 24, and 29. *J Comp Neurol* 195: 603-25

Wang Q, Sporns O, Burkhalter A. 2012. Network analysis of corticocortical connections reveals ventral and dorsal processing streams in mouse visual cortex. *The Journal of Neuroscience* 32: 4386-99

Warburton E, Aggleton J, Muir J. 1998. Comparing the effects of selective cingulate cortex lesions and cingulum bundle lesions on water maze performance by rats. *European Journal of Neuroscience* 10: 622-34

Weible AP, Rowland DC, Pang R, Kentros C. 2009. Neural correlates of novel object and novel location recognition behavior in the mouse anterior cingulate cortex. *J Neurophysiol* 102: 2055-68

Whishaw IQ, Maaswinkel H, Gonzalez CL, Kolb B. 2001a. Deficits in allothetic and idiothetic spatial behavior in rats with posterior cingulate cortex lesions. *Behav Brain Res* 118: 67-76

Whishaw IQ, Maaswinkel H, Gonzalez CL, Kolb B. 2001b. Deficits in allothetic and idiothetic spatial behavior in rats with posterior cingulate cortex lesions. *Behavioural brain research* 118: 67-76

Whitlock JR, Pfuhl G, Dagslott N, Moser M-B, Moser EI. 2012. Functional split between parietal and entorhinal cortices in the rat. *Neuron* 73: 789-802

Wilber AA, Clark BJ, Forster TC, Tatsuno M, McNaughton BL. 2014. Interaction of egocentric and world-centered reference frames in the rat posterior parietal cortex. *The Journal of Neuroscience* 34: 5431-46

Wilson MA, McNaughton BL. 1994. Reactivation of hippocampal ensemble memories during sleep. *Science* 265: 676-9

Wimmer GE, Shohamy D. 2012. Preference by association: how memory mechanisms in the hippocampus bias decisions. *Science* 338: 270-73

Winter SS, Clark BJ, Taube JS. 2015. Disruption of the head direction cell network impairs the parahippocampal grid cell signal. *Science* 347: 870-74

Witter MP, Ostendorf RH, Groenewegen HJ. 1990. Heterogeneity in the dorsal subiculum of the rat. Distinct neuronal zones project to different cortical and subcortical targets. *European Journal of Neuroscience* 2: 718-25

Wright W, DiZio P, Lackner J. 2005. Vertical linear self-motion perception during visual and inertial motion: more than weighted summation of sensory inputs. *Journal of Vestibular Research* 15: 185-95

Yamawaki N, Radulovic J, Shepherd GM. 2016. A Corticocortical Circuit Directly Links Retrosplenial Cortex to M2 in the Mouse. *J Neurosci* 36: 9365-74

Zhao X, Chen H, Liu X, Cang J. 2013. Orientation-selective responses in the mouse lateral geniculate nucleus. *The Journal of Neuroscience* 33: 12751-63

Ziv Y, Burns LD, Cocker ED, Hamel EO, Ghosh KK, et al. 2013. Long-term dynamics of CA1 hippocampal place codes. *Nat Neurosci* 16: 264-6